

Copyright Undertaking

This thesis is protected by copyright, with all rights reserved.

By reading and using the thesis, the reader understands and agrees to the following terms:

1. The reader will abide by the rules and legal ordinances governing copyright regarding the use of the thesis.
2. The reader will use the thesis for the purpose of research or private study only and not for distribution or further reproduction or any other purpose.
3. The reader agrees to indemnify and hold the University harmless from and against any loss, damage, cost, liability or expenses arising from copyright infringement or unauthorized usage.

IMPORTANT

If you have reasons to believe that any materials in this thesis are deemed not suitable to be distributed in this form, or a copyright owner having difficulty with the material being included in our database, please contact lbsys@polyu.edu.hk providing details. The Library will look into your claim and consider taking remedial action upon receipt of the written requests.

**ENHANCING THE DEHUMIDIFICATION
PERFORMANCE OF PLATE LIQUID DESICCANT
DEHUMIDIFIER WITH SUPER-HYDROPHILIC
COATING CONSIDERING THE SOLID-LIQUID
INTERACTION EFFECT**

DONG CHUANSHUAI

PhD

The Hong Kong Polytechnic University

2018

The Hong Kong Polytechnic University

Department of Building Services Engineering

**Enhancing the Dehumidification Performance of Plate
Liquid Desiccant Dehumidifier with Super-hydrophilic
Coating Considering the Solid-liquid Interaction Effect**

DONG CHUANSHUAI

**A thesis submitted in partial fulfillment of the requirements for the
Degree of Doctor of Philosophy**

June 2018

Certificate of Originality

I hereby declare that this thesis is my own work and that, to the best of my knowledge and belief, it reproduces no material previously published or written, nor material that has been accepted for the award of any other degree or diploma, except where due acknowledgement has been made in the text.

_____ (Signed)

Dong Chuanshuai (Name of student)

Abstract

Humidity control of indoor air is very important for both indoor occupants and indoor building materials, especially in hot and humid regions. Falling film liquid desiccant air dehumidification is a promising alternative to traditional vapor compression air-conditioning system due to its lower energy consumption and less pollution. Besides, falling film is widely used in other engineering fields, such as falling film heat exchangers, evaporators and cooling towers, for simple structure and high efficiency. However, the incomplete wetting condition of falling film deteriorates the operating performance and limits the wide application of falling film devices. Therefore, this thesis aims to study the effect of plate surface properties on flow characteristics and heat/mass transfer performance and then try to develop a novel super-hydrophilic coating using nanoscale anatase TiO_2 particles to improve the surface wettability and enhance the operating performance of falling film liquid desiccant dehumidifiers accordingly. The principles of the dehumidification performance enhancement are investigated experimentally and theoretically in this thesis.

Firstly, to investigate the surface properties on flow and heat/mass transfer characteristics in falling film dehumidifiers, three commonly-used types of falling film dehumidifiers, i.e., stainless plate dehumidifier, titanium plate dehumidifier and polytetrafluoroethylene (PTFE) plate dehumidifier, with distinctive surface properties but same geometrical size are chosen for study. The surface properties of plate

dehumidifiers are investigated through FESEM test of microstructures and contact angle test of surface wettability. The surface free energy of Titanium plate, Stainless plate and PTFE plate is calculated to be 50.61 mJ/m², 36.98 mJ/m² and 30.34 mJ/m², respectively, indicating that Titanium plate possesses the superior wettability compared with the other plates. It is observed that the falling film shrinks seriously along the flow direction in PTFE plate dehumidifier while a little shrinkage occurs in Titanium plate dehumidifier due to the strong adhesion between solid surface and desiccant solution. The effect of surface properties on heat/mass transfer characteristics in falling film dehumidifiers are experimentally investigated. The experimental results prove that surface wettability demonstrates positive effect on dehumidification performance. Therefore, it is very important to improve the surface wettability of falling film dehumidifiers.

Based on this research, a novel super-hydrophilic coating is developed using nanoscale anatase TiO₂ particles to improve the surface wettability of liquid desiccant plate dehumidifiers. The microstructures of the new coating on substrates are investigated through XRD, FESEM and HRTEM test. The test results indicate that pure and highly-dispersed TiO₂ paste is well developed. Then, the thin TiO₂ film is well coated on substrates with high hardness and durability. The surface wettability of TiO₂ film before and after UV illumination is investigated through surface free energy test and the super-hydrophilicity of TiO₂ coating is effectively activated by UV illumination.

Then, the highly-dispersed TiO_2 paste is successfully coated onto dehumidifier plates to enhance the heat and mass transfer performance. The contact angle test shows that the surface wettability of plate dehumidifier is significantly improved by TiO_2 super-hydrophilic coating with the contact angle decreasing from 84.6° to 8.8° . The flow characteristics of falling film in coated plate dehumidifier are also investigated. Little shrinkage occurs along the flow direction in coated plate dehumidifier, while severe shrinkage occurs in the uncoated plate dehumidifier. The maximum wetting ratio increased from 75% to 100% by super-hydrophilic coating. The effect of surface wettability on falling film thickness and its fluctuation is also investigated. A novel and simplified correlation of falling film wave is developed to estimate the actual interfacial area between liquid desiccant and processed air. With more than 200 experimental conditions, the experimental results indicate that the dehumidification performance is significantly improved by surface treatment with the average performance enhancing ratio of 60%. The dehumidification performance enhancement is mainly attributed to the increasing of wetting area and decreasing of falling film thickness. Based on the experimental results, a novel empirical correlation of mass transfer coefficient is developed using non-linear regression. The surface wettability is considered in the correlation to account for the effect of surface wettability on dehumidification performance.

Based on the experimental analysis, an improved heat and mass transfer model

considering the solid-liquid interaction effect is developed to simulate the heat and mass transfer process in an internally-cold falling film dehumidifier. A shrinkage model of falling film is proposed to accurately estimate the actual wetting area of liquid desiccant solution in falling film dehumidifiers with different surface wettability. Then, the effect of surface wettability on dehumidification performance is investigated theoretically. As the contact angle decreases from 85° to 5° , the moisture removal rate increases from 2.0 g/kg to 2.56 g/kg, i.e., by a performance enhancing factor of 28 %. The performance enhancement is attributed to the increase of the wetting area and the decrease of the falling film thickness. The total wetting area increases significantly from 0.145 m² to 0.176 m² with the enhancing ratio of 21.4%, while the mean falling film thickness decreases from 0.952 mm to 0.889 mm.

Finally, a dynamic model of solar-assisted liquid desiccant air-conditioning system is developed using C++ to investigate the effect of solid-liquid interaction effect on energy consumption. Three iteration loops, i.e. iteration loop of liquid desiccant solution, iteration loop of cooling water and iteration loop of heating water, are proposed in the dynamic model. The effect of surface properties for falling film dehumidifiers on energy consumption is also analyzed. Improving the surface wettability of falling film dehumidifiers could reduce the energy consumption effectively. Around 9.1% (100 MW · h) of total energy consumption could be saved for solar-assisted liquid desiccant air-conditioning system with the surface contact

angle reducing from 110° to 10° . The energy saving is attributed to the dehumidification performance enhancement by higher surface wettability of falling film dehumidifiers. Besides, the introduction of solar energy could save around 15.4 % (200 MW · h) of electricity consumption for liquid desiccant air-conditioning system.

In summary, this thesis develops a novel TiO_2 super-hydrophilic coating to improve the surface wettability and investigate the effect of solid-liquid interaction on dehumidification performance of falling film dehumidifiers. As the incomplete wetting problem is encountered in other falling film applications, such as heat exchangers, evaporators and cooling towers, the findings in this research is very useful to improve the efficiency of falling film devices by improving the surface wettability. The correlation of falling film wave can be adopted in other falling film devices to accurately estimate the actual interfacial area between liquid and gas. Besides, the newly-developed model in this research is also salutary to the theoretical investigation of other falling film applications.

Publications during PhD study

Journal papers

- [1] **Chuanshuai Dong**, Lin Lu, Tao Wen. (2017). Experimental study on dehumidification performance enhancement by TiO₂ superhydrophilic coating for liquid desiccant plate dehumidifiers. *Building and Environment*, 124: 219-231.
- [2] **Chuanshuai Dong**, Lin Lu, Ronghui Qi. (2017). Model Development of Heat/Mass Transfer for Internally Cooled Dehumidifier Concerning Liquid Film Shrinkage Shape and Contact Angles. *Building and Environment*, 114: 11-22.
- [3] **Chuanshuai Dong**, Ronghui Qi, Lu Lin, Yalin Wang, Lingshi Wang. (2016). Comparative Performance Study on Liquid Desiccant Dehumidification with Different Packing Types for Built Environment. *Science and Technology for the Built Environment (formerly HVAC&R Research Journal)*, 23 (1): 1-11.
- [4] **Chuanshuai Dong**, Lin Lu, Tao Wen. (2018). Comparative performance analysis of internally-cooled liquid desiccant dehumidifiers with different working plates for built environment. *Energy*. (Revised)
- [5] **Chuanshuai Dong**, Takashi Hibiki. (2018). Heat transfer correlation for two-component two-phase slug flow in horizontal pipes. *Applied Thermal Engineering*,

141: 866-876.

[6] **Chuanshuai Dong**, Takashi Hibiki. (2018). Correlation of heat transfer coefficient for two component two-phase slug flow in a vertical pipe. *International Journal of Multiphase Flow*. (Revised)

[7] **Chuanshuai Dong**, Lin Lu, Wang Xin. (2018). Experimental investigation on non-boiling heat transfer of gas-oil and gas-water two-phase slug flow in horizontal pipes. *Experimental Thermal and Fluid Science*. (Revised)

[8] Tao Wen, Lin Lu, **Chuanshuai Dong**, Yimo Luo. (2018). Development and experimental study of a novel plate dehumidifier made of anodized aluminium. *Energy*. 144:169-177.

[9] Tao Wen, Lin Lu, **Chuanshuai Dong**, Yimo Luo. (2018). Investigation on the regeneration performance of liquid desiccant by adding surfactant PVP-K30. *International Journal of Heat and Mass Transfer*. 123: 445-454.

[10] Tao Wen, Lin Lu, **Chuanshuai Dong**. (2018). Enhancing the dehumidification performance of LiCl solution with surfactant PVP-K30. *Energy and Buildings*. 171: 183-195.

Conference papers

[1] **Chuanshuai Dong**, Lin Lu, Tao Wen. (2017). Enhancing the Heat/mass Transfer Performance of Plate Liquid Desiccant Dehumidifier with Super-hydrophilic Coating. The 12th Conference on Sustainable Development of Energy, Water and Environment Systems (SDEWES Conference 2017), Dubrovnik, Croatia.

[2] **Chuanshuai Dong**, Lin Lu, Tao Wen. (2017). Comparative study on dehumidification performance and energy consumption of plate liquid desiccant dehumidifier with different surface-treated plates. The 3rd International Symposium of Fluids & Thermal Engineering 17-19 December, Ningbo, China.

[3] **Chuanshuai Dong**, Lin Lu. (2018). Enhancing the dehumidification efficiency of solar-assisted liquid desiccant air dehumidifiers using nanoscale TiO₂ super-hydrophilic coating 10th International Conference on Applied Energy (ICAE2018), 22-25 August 2018, Hong Kong, China.

[4] Tao Wen, Lin Lu, **Chuanshuai Dong**. (2017). Experimental study on the regeneration performance of an anodized aluminum plate regenerator. The 12th Conference on Sustainable Development of Energy, Water and Environment Systems (SDEWES Conference 2017), Dubrovnik, Croatia.

[5] Tao Wen, Lin Lu, **Chuanshuai Dong**. (2017). Experimental and numerical study on the regeneration performance of LiCl solutions with surfactant and nanoparticle. The 3rd International Symposium of Fluids & Thermal Engineering 17-19 December, Ningbo, China.

Other Publications

Lin Lu, **Chuanshuai Dong**. Handbook of Energy Efficiency in Buildings: A Life Cycle Approach. Elsevier. 2018. ISBN: 9780128128176.

Acknowledgements

First and foremost, I would like to express my deepest appreciation and gratitude to my chief supervisor, Prof. Lu Lin. During my pursuing of the doctoral degree, she always gave me valuable advices, continuous encouragement, patient guidance and generous support. Without her, it is impossible for me to complete the thesis on time. What's more, her optimism and friendly personality also set an example for my life-long learning.

My special appreciation is also devoted to Prof. Yang Hongxing, for his insightful view and valuable suggestions on my research work.

I also wish to express sincerest gratitude to Prof. Takashi Hibiki of Purdue University, USA, for providing me the opportunity to study in his research group at Purdue University.

Furthermore, I would like to express my thanks to all the members in the Renewable Energy Research Group for their help and company during the PhD study. I'm deeply indebted to Dr. Qi Ronghui, who is already an associate professor in South China University of Technology, for her kind guidance, especially at the beginning of my PhD study.

My special thanks go to the Research Grant Council (RGC) of Hong Kong and the Hong Kong Polytechnic University for financially supporting this research work.

My heartfelt appreciation goes to my beloved parents, Mr. Dong Xiaozhong and Ms. Lu yuqin for their love and sacrifice without expecting any return.

Finally, I would like to express thanks to my wife, Ms. Jia Shaoting for her support and encouragement. Without her, I would never make it so far.

Table of Contents

Certificate of Originality	i
Abstract	ii
Publications during PhD study	vii
Acknowledgements	xi
Table of Contents	xiii
List of Figures	xix
List of Tables	xxvii
Nomenclature	xxix
CHAPTER 1	1
INTRODUCTION	1
1.1 Introduction of liquid desiccant dehumidification	1
1.2 Research objectives of the thesis	5
1.3 Organization of the thesis	7
CHAPTER 2	12
LITERATURE REVIEW AND RESEARCH METHODOLOGY	12
2.1 Background of liquid desiccant dehumidification	12
2.1.1 Principles and features	12
2.1.2 Types of liquid desiccant	16
2.2 Structures of falling film liquid desiccant dehumidifiers	19

2.3 Simulation models of falling film dehumidifier	22
2.3.1 Finite difference model	23
2.3.2 Effectiveness <i>NTU</i> model	30
2.3.3 Simplified simulation models	31
2.4 Investigation on wetting characteristics in falling film applications	37
2.5 Investigation on performance enhancing methods for falling film applications	41
2.5.1 Surface modification	42
2.5.2 Addition of surfactant	45
2.5.3 Optimization of the absorber structure	48
2.5.4 Addition of nanofluid	50
2.6 Investigation on surface wettability and super-hydrophilic surfaces	51
2.6.1 Wetting models	53
2.6.2 Preparation of super-hydrophilic surfaces	56
2.6.3 Application of super-hydrophilic surfaces	58
2.7 Research gaps and methodology	62
CHAPTER 3	68
ANALYSIS OF SURFACE PROPERTIES ON FLOW AND HEAT/MASS	
TRANSFER PERFORMANCE FOR FALLING FILM LIQUID DESICCANT	
DEHUMIDIFIERS	68
3.1 Introduction	68

4.5 Summary	124
CHAPTER 5	127
EXPERIMENTAL STUDY ON DEHUMIDIFICATION PERFORMANCE ENHANCEMENT BY APPLYING TiO₂ SUPER-HYDROPHILIC COATING	127
5.1 Introduction	127
5.2 Description of experimental test rig	129
5.3 Performance indices and uncertainty analysis	133
5.4 Results and discussion	135
5.4.1 Energy conservation and results validation analysis	135
5.4.2 Flow characteristics of falling film	139
5.4.3 Dehumidification performance enhancement	150
5.4.4 Influencing factors analysis of dehumidification performance	151
5.4.5 Development of mass transfer coefficient considering solid-liquid interaction effect	162
5.5 Summary	166
CHAPTER 6	169
ANALYTICAL MODEL OF HEAT AND MASS TRANSFER PERFORMANCE CONSIDERING THE SOLID-LIQUID INTERACTION EFFECT	169
6.1 Introduction	169
6.2 Numerical model development	170

6.2.1 Model development of falling film shrinkage with different contact angles	170
6.2.2 Model development of heat and mass transfer with variable film thickness	174
6.2.3 Discretization and calculation of the new model	177
6.3 Model validation and uncertainty analysis	180
6.3.1 Model validation	180
6.3.2 Uncertainty analysis	182
6.4 Results and discussion	184
6.4.1 Effect of surface wettability on wetting area	184
6.4.2 Effect of surface wettability on film thickness	187
6.4.3 Effect of surface wettability on dehumidification performance	189
6.5 Summary	193
CHAPTER 7	196
ENERGY CONSUMPTION ANALYSIS OF SOLAR-ASSISTED LIQUID DESICCANT AIR-CONDITIONING SYSTEM CONSIDERING SOLID-LIQUID INTERACTION EFFECT	196
7.1 Introduction	196
7.2 Model development of solar-assisted liquid desiccant air-conditioning system considering solid-liquid interaction effect	198
7.2.1 Description of solar-assisted liquid desiccant air-conditioning	

system	198
7.2.2 Models of individual components	200
7.2.3 Model iterations	207
7.2.4 Description of the case building	211
7.3 Results and discussion	212
7.3.1 Model validation	212
7.3.2 Energy consumption of solar-assisted liquid desiccant air- conditioning system	213
7.3.3 Effect of surface wettability on energy consumption	214
7.4 Summary	217
CHAPTER 8	219
CONCLUSIONS AND RECOMMENDATIONS FOR FUTURE WORK	219
8.1 Conclusions	219
8.2 Recommendations for Future Work	223
References	226

List of Figures

		Pages
Chapter 1		
Fig. 1.1	Hong Kong energy consumption analysis (2016)	2
Chapter 2		
Fig. 2.1	Schematic diagram of liquid-desiccant dehumidification air-conditioning system	12
Fig. 2.2	Schematic of the typical cycle of liquid desiccant solution	14
Fig. 2.3	The structure diagram of two dehumidifiers	19
Fig. 2.4	Control volume for liquid desiccant dehumidifier	25
Fig. 2.5	Control volume for liquid desiccant regenerator	28
Fig. 2.6	Pictures of working surfaces incompletely wetted by the liquid desiccant	37
Fig. 2.7	Schematic diagram of different types of tubes	43
Fig. 2.8	Schematic of micro-hatched tube	44
Fig. 2.9	Schematic of four low ribs enhanced tubes	45
Fig. 2.10	Images of Marangoni convection using holographic interferometer	47
Fig. 2.11	Schematic diagram of the film-inverting absorbers	49
Fig. 2.12	Schematic diagram of plate falling film absorber with the	50

film-inverting configuration

Fig. 2.13	Water droplets on different wetting surfaces	52
Fig. 2.14	Contact angle of the liquid droplet on the solid surface	54
Fig. 2.15	Models for rough surface	56
Fig. 2.16	Comparison of the condensation and optical clarity of polyester films under high relative humidity	59
Fig. 2.17	A boiling curve correlating the heat flux with wall superheat	60
Fig. 2.18	Research flow chart of the thesis	64
Chapter 3		
Fig. 3.1	Schematic diagram of the experimental setup	70
Fig. 3.2	Schematic diagram of the solution distributor	73
Fig. 3.3	Main devices in the experimental setup	74
Fig. 3.4	Measuring devices in the experimental setup	76
Fig. 3.5	Schematic diagram of falling film measuring system	78
Fig. 3.6	Calibration curves of the Capacitance micrometer	80
Fig. 3.7	Energy conservation of air, liquid desiccant and cooling water	85
Fig. 3.8	FESEM images of different plate dehumidifiers	86
Fig. 3.9	Contact angles of diiodomethane and deionized water in	89

different plate dehumidifiers

Fig. 3.10	Thermal images of falling film in different plate dehumidifiers	92
Fig. 3.11	Effect of solution flow rates on wetting ratios on coated and uncoated plates	94
Fig. 3.12	Mean falling film thickness in different plate dehumidifiers	97
Fig. 3.13	Comparison of dehumidification performance in different plate dehumidifiers	98
Fig. 3.14	Influence of air temperature on dehumidification capacity in different plate dehumidifiers	100
Fig. 3.15	Influence of air humidity on dehumidification performance in different plate dehumidifiers	102
Fig. 3.16	Influence of air flow rates on dehumidification performance in different plate dehumidifiers	104
Fig. 3.17	Influence of liquid desiccant temperature on dehumidification performance in different plate dehumidifiers	106
Fig. 3.18	Influence of liquid desiccant flow rates on dehumidification performance in different plate	107

dehumidifiers

Fig. 3.19	Influence of cooling water temperature on dehumidification performance in different plate dehumidifiers	109
-----------	---	-----

Chapter 4

Fig. 4.1	Structure of Titanium ethoxide	113
Fig. 4.2	Picture of nanoscale TiO ₂ super-hydrophilic paste	114
Fig. 4.3	Fabrication process of TiO ₂ super-hydrophilic film	115
Fig. 4.4	XRD test of TiO ₂ nanocrystals	115
Fig. 4.5	HRTEM test of nanoscale TiO ₂ colloid solvent	116
Fig. 4.6	HRTEM test of nanoscale TiO ₂ super-hydrophilic particles	117
Fig. 4.7	Contact angles of different liquid reagents on coated substrate before and after UV activation	121
Fig. 4.8	Mechanism of the UV-induced super-hydrophilicity of TiO ₂ coating	124
Fig. 4.9	Schematic of the UV-induced super-hydrophilicity of TiO ₂ coating	124
Fig. 4.10	Contact angles of different liquid reagents on coated substrate plates	125

Chapter 5

Fig. 5.1	Schematic of the experimental setup	128
Fig. 5.2	Photographs of the experimental setup	129
Fig. 5.3	Photograph of the working channels	130
Fig. 5.4	Energy conservation of the experimental results	137
Fig. 5.5	Contact angles of LiCl aqueous solution on coated and uncoated plates	138
Fig. 5.6	Contact angles of coated plates under one-time and periodical activation	139
Fig. 5.7	Thermal images of falling film on coated and uncoated plate dehumidifiers	140
Fig. 5.8	Effect of solution flow rates on wetting ratios on coated and uncoated plates	142
Fig. 5.9	Mean falling film thickness in coated and uncoated plate dehumidifiers	143
Fig. 5.10	Comparison between measured and calculated falling film thickness for both coated and uncoated plate dehumidifier	145
Fig. 5.11	Instantaneous falling film thickness at both lower and upper test point for both coated and uncoated plate dehumidifier ($Re_s=57.9$, $T_s=25^{\circ}\text{C}$)	147

Fig. 5.12	Probability density of the performance enhancing ratio for the coated plate dehumidifier	149
Fig. 5.13	Effect of air temperature on dehumidification performance of coated and uncoated plate dehumidifiers	151
Fig. 5.14	Effect of air humidity on dehumidification performance of coated and uncoated plate dehumidifiers.	153
Fig. 5.15	Effect of air flow rate on dehumidification performance of coated and uncoated plate dehumidifiers	155
Fig. 5.16	Effect of desiccant solution flow rate on dehumidification performance of coated and uncoated plate dehumidifiers	157
Fig. 5.17	Effect of cooling water temperature on dehumidification performance of coated and uncoated plate dehumidifiers	159
Fig. 5.18	Condensation of vapor on exposed surfaces	160
Fig. 5.19	Comparison between calculated and experimental mass transfer coefficient	163
Fig. 5.20	Comparison between calculated and experimental mass transfer coefficient	164
Chapter 6		
Fig. 6.1	Schematic of (a) falling film and (b) rim part	169
Fig. 6.2	Schematic of the internally cooled plate dehumidifier	172

Fig. 6.3	Numerical model of plate dehumidifier with variable wetting length	175
Fig. 6.4	Flow chart of calculation process	177
Fig. 6.5	Comparison of the simulation results with the experimental data	179
Fig. 6.6	Comparison of the simulated and experimental film boundaries with different contact angles	180
Fig. 6.7	Shrinkage of the falling film with different contact angles	183
Fig. 6.8	Effect of desiccant solution temperature on wetting area with different contact angles	184
Fig. 6.9	Effect of desiccant solution temperature on wetting area with different contact angles	185
Fig. 6.10	Variation of the falling film thickness with different contact angles	187
Fig. 6.11	Effect of desiccant solution temperature on wetting area with different contact angles	189
Fig. 6.12	Effect of desiccant solution temperature on wetting area with different contact angles	190
Fig. 6.13	Effect of desiccant solution temperature on wetting area with different contact angles	191

Chapter 7

Fig. 7.1	Schematic diagram of solar-assisted liquid desiccant air-conditioning system	196
Fig. 7.2	Schematic diagram of input and output parameters of each component	205
Fig. 7.3	Layout of the typical commercial building in Hong Kong	209
Fig. 7.4	Comparison between simulated and experimental results	211
Fig. 7.5	Comparison of electricity consumption between different systems	212
Fig. 7.6	Comparison of electricity consumption of SLDACS	214
Fig. 7.7	Monthly electricity consumption of chillers	215

List of Tables

		Pages
Chapter 2		
Table 2.1	Comparison between LDDS and CACS	16
Table 2.2	Weighing factors and figures of merit for desiccant selection	18
Table 2.3	Summary of internally-cold falling film liquid desiccant dehumidifiers	20
Table 2.4	Summary of simulation models for falling film liquid desiccant dehumidifiers	35
Table 2.5	Wettability and contact angels	53
Chapter 3		
Table 3.1	Specifications of different measuring devices	77
Table 3.2	Ranges of the inlet experimental parameters	83
Table 3.3	Part of the experimental conditions	84
Table 3.4	Surface free energy and its components of different liquid reagents	
Table 3.5	Surface free energy of different plate dehumidifiers	90
Table 3.6	Physical properties of different plate dehumidifiers	91

Table 3.7	Correlations of mean film thickness for tubes	95
-----------	---	----

Chapter 4

Table 4.1	Surface free energy and its components of different liquid reagents	120
-----------	---	-----

Table 4.2	Contact angles of deionized water, glycerol and ethanol on TiO ₂ film	122
-----------	--	-----

Table 4.3	Surface free energy and its components of TiO ₂ coating	123
-----------	--	-----

Chapter 5

Table 5.1	Ranges of the inlet experimental parameters	134
-----------	---	-----

Table 5.2	Part of the experimental conditions	135
-----------	-------------------------------------	-----

Table 5.3	Summary of mass transfer correlations	161
-----------	---------------------------------------	-----

Table 5.4	Summary of coefficients in the new mass transfer correlation	162
-----------	--	-----

Chapter 6

Table 6.1	Uncertainty and sensitivity analysis of present model	181
-----------	---	-----

Chapter 7

Table 7.1	Specifications of main equipment	204
-----------	----------------------------------	-----

Table 7.2	Assumed initial values of the parameters	208
-----------	--	-----

Nomenclature

A	Area	m^2
c_p	Specific heat capacity	$\text{kJ}/(\text{kg} \cdot ^\circ\text{C})$
d	Width of the air channel	m
D	Width of the rim part	m
D_a	Diffusion coefficient	m^2/s
f	Friction factor	
F	Wetting factor	
G, m	Mass flow rate	kg/s
h	enthalpy	kJ/kg
h_c	Heat transfer coefficient between air and desiccant	$\text{W}/(\text{m}^2 \cdot \text{K})$
h_d	Mass transfer coefficient	$\text{kg}/(\text{m}^2 \cdot \text{s})$
h_f	Heat transfer coefficient between cooling water and desiccant	$\text{W}/(\text{m}^2 \cdot \text{K})$
H	Height	m
J	Colburn J factor	
K	Thermal conductivity	$\text{W}/(\text{m} \cdot \text{K})$

Le	Lewis number	
NTU	Number of transfer unit	
n	Element number	
Nu	Nusselt number	
P	Pressure	Pa
Pr	Prandtl number	
Q	Heat	W
Re	Reynolds number	
Sc	Schmidt number	
SC	Sensitivity coefficient	
Sh	Sherwood number	
T	Temperature	°C
V	Velocity	m/s
U	Uncertainty	
W	Width or air humidity	m or g/kg
Δx	Shrinkage distance	m
X	Concentration	%
<i>Greek letters</i>		
α	Contact angle	°
β	Shrinkage angle	°

γ	Latent heat	kJ/kg
ω	Humidity ratio	g/kg
$\Delta\omega$	Moisture removal rate	g/kg
σ	Surface tension	N/m
ε	Deformation factor	
ρ	Density	kg/m ³
δ	Film thickness	mm
μ	Dynamic viscosity	Pa · s

Subscripts

a	Air
ave	Average
cen	Central part
eff	effective
equ	equilibrium
f	Cooling water
g, G	air
in	Inlet
L	Liquid
m	Maximum
Out	Outlet

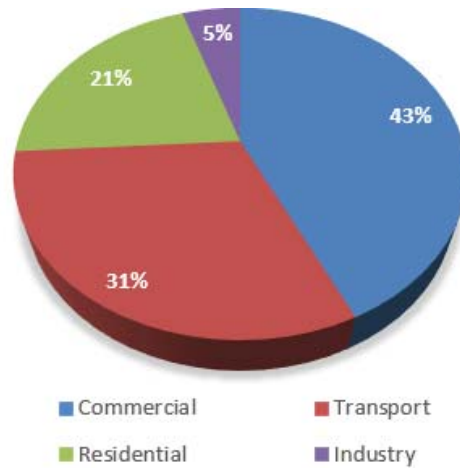
s	Desiccant solution
S	Solid
v	vapor
x	x coordinate
y	y coordinate
z	z coordinate

CHAPTER 1

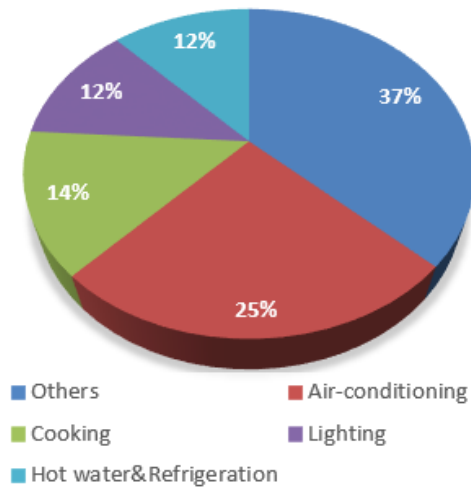
INTRODUCTION

1.1 Introduction of liquid desiccant dehumidification

The building energy consumption has increased rapidly during the past decades [1]. In developed countries, the global contribution from buildings towards energy consumption, both residential and commercial, had steadily increased reaching figures between 20% and 40% and exceeded the major sectors: industry and transportation [2]. Among the building energy services, the Heating, Ventilation and Air-Conditioning (HVAC) systems are the most energy consuming devices, accounting for more than 50% of the total building energy consumption. It was reported that the energy consumed by air-conditioning systems took up 54% and 23% of the total building energy consumption for the typical official and residential buildings, respectively, in hot and humid regions [3]. In Hong Kong, the commercial building sector accounts for 43% of the whole energy consumption, among which air-conditioning systems occupy around 25% [3], as shown in Fig. 1. Therefore, it is important to develop highly-efficient air-conditioning systems and to reduce the building energy consumption accordingly.



(a) Breakdown of total energy consumption



(b) Breakdown of energy consumption in commercial sector

Fig.1.1 Hong Kong energy consumption analysis (2016)

In air-conditioning systems, air dehumidification is one of the key component. Moisture affects building materials, thermal comfort of building occupants and the work performed by them [4]. Excess moisture can lead to mold and mildew, affecting indoor air quality. Therefore, humidity control is very important.

The air dehumidification has been investigated for several years and many air dehumidification technologies have been developed, such as condensation dehumidification technology, compression dehumidification technology, electrostatic dehumidification technology, solid adsorption dehumidification technology and liquid absorption dehumidification [5]. Amongst these dehumidification technologies, liquid absorption dehumidification is promising for its lower energy consumption, less pollution and more flexible humidity control.

By handling extra air humidity with desiccant absorption, liquid desiccant dehumidifier is an energy-efficient and eco-friendly alternative to traditional air dehumidification approaches. More than 30% of energy use of traditional air-conditioning system and even up to 50% if solar energy or waste heat is utilized for desiccant regeneration can be saved with liquid desiccant air dehumidification system (LDACS) [6]. In LDAC systems, the extra moisture is removed by liquid desiccant absorption and the sensible and latent heat can be handled separately.

The dehumidifier is one of the core components in LDAC systems. The liquid desiccant dehumidifier is mainly categorized into two types, i.e., packing dehumidifiers and plate dehumidifiers. The packing liquid desiccant dehumidifier is famous for large contact area. However, the latent heat released during the dehumidification process cannot be removed in packing dehumidifier, which might

increase the temperature of desiccant solution and deteriorate the dehumidification performance [7]. Therefore, the internally-cold liquid desiccant plate dehumidifier is developed to solve the problem and improve the dehumidification efficiency [8,9]. In internally-cold liquid desiccant plate dehumidifier, the desiccant solution flow on the working plates and interact with the humid air. The moisture is removed from the humid air to the desiccant solution. Meanwhile, the latent heat released during the dehumidification process is removed by the cooling fluid, which helps to maintain the solution temperature and improve the dehumidification performance.

The enhancement of heat/mass transfer between liquid desiccant and humid air in dehumidifier is an important research area of internally-cold liquid desiccant plate dehumidifier [10]. The falling film type is promising due to the larger liquid/gas contact area and lower pressure drop [11] compared to the packing type dehumidifier. However, the insufficient wetting condition and film area contraction of practical liquid desiccant systems have been commonly reported in previous studies [12,13], which seriously deteriorates the dehumidification performance. In addition, the carryover of solution droplets in the air stream is also a big problem in desiccant cooling systems as the solution droplets may lead to the corrosion of ventilation system and potential pollution to indoor air [14, 15]. The droplets usually occur when falling film breaks down, which is determined by the solid/fluid properties and cooling

conditions [16].

To date, several approaches of enhancing the heat/mass transfer performance of falling films have been investigated such as modification of the working surface [17,18], addition of surfactant [19], optimization of plate structure [20,21] and addition of nano-fluids [22,23]. The essence of these approaches is to improve the wetting area and enhance the flow turbulence of the falling film. Recent findings indicate that reducing the contact angle of the liquid on solid plate surface could effectively enlarge the wetting area and therefore improve the dehumidification performance.

1.2 Research objectives of the thesis

The falling film liquid desiccant plate dehumidifier is a promising alternative to traditional air dehumidification technologies for lower energy consumption, environment-friendly and more flexible humidity control. Besides, the liquid desiccant plate dehumidifier possesses some other advantages, such as lower possibility of droplet carryover and lower pressure drop. However, there exist some obstacles preventing the development of the falling film liquid desiccant plate dehumidifier. One of the main problems is the incomplete wetting conditions of desiccant solution on working plates. The incomplete wetting conditions mainly results from the hydrophobic properties of working plates, which seriously deteriorates the heat and mas transfer between desiccant solution and humid air. The effect of surface properties,

such as contact angle, surface free energy, of working plates on dehumidification performance is seldom investigated. In addition, the existing theoretical models do not consider the incomplete wetting conditions. This thesis aims to resolve these existing problems and promote the wide application of falling film liquid desiccant plate dehumidifiers. The main research objectives of this thesis are summarized as follows.

1) To investigate the surface properties such as surface free energy on dehumidification performance. Three commonly-used plate dehumidifiers, i.e., stainless plate dehumidifier, titanium plate dehumidifier and polytetrafluoroethylene (PTFE) plate dehumidifier, with distinctive surface properties are adopted in this project to experimentally investigate the surface properties on dehumidification performance. The effect of surface wettability on both flow characteristics and dehumidification performance are investigated.

2) To develop a novel TiO_2 super-hydrophilic coating, which can significantly improve the surface wettability and the wetting area as well. The TiO_2 super-hydrophilic coating is characterized in terms of microscopic surface structure, contact angle and surface free energy.

3) To experimentally investigate the heat and mass transfer performance of surface-modified liquid desiccant plate dehumidifier with TiO_2 super-hydrophilic coating and

investigate the principles of dehumidification performance enhancement. Besides, the effect of operating parameters, including the flow rates, temperature and concentration of liquid desiccant solution, flow rates, temperature and humidity of processed air as well as the flow rates and temperature of the cooling fluid, on dehumidification performance are comprehensively analysed.

4) To develop an improved heat and mass transfer model of the internally-cold liquid desiccant plate dehumidifier considering the actual wetting area. The contact angles of desiccant solution on working plates are considered in the newly-developed model to account for the effect of surface properties on dehumidification performance.

5) To develop a dynamic energy consumption model of solar-assisted liquid desiccant air-conditioning system regarding surface wettability. A typical commercial building in Hong Kong is selected for case study to analyse the effect of surface properties on energy consumption of the whole air-conditioning system.

1.3 Organization of the thesis

The overall structure of this thesis takes the form of eight chapters, including Chapter 1 Introduction, Chapter 2 Literature review and research methodology, Chapter 3 Analysis of surface properties on flow and heat/mass transfer performance for falling film liquid desiccant dehumidifiers, Chapter 4 Fabrication and characterization of

TiO₂ super-hydrophilic coating, Chapter 5 Experimental study on dehumidification performance enhancement TiO₂ super-hydrophilic coating, Chapter 6 Analytical model development of heat and mass transfer considering solid-liquid interaction effect, Chapter 7 Energy consumption analysis of solar-assisted liquid desiccant air-conditioning system considering solid-liquid interaction effect, and Chapter 8 Conclusions and recommendations for future work.

Chapter 1 gives a brief introduction of liquid desiccant dehumidification air-conditioning system. The liquid desiccant air dehumidification technology, handling the latent and sensible load separately, is a promising alternative to traditional air dehumidification technologies. The research objectives of this project are also summarized in Chapter 1.

Chapter 2 provides a comprehensive literature review of both experimental and theoretical investigation on liquid desiccant air dehumidification technologies. Firstly, a detailed introduction of liquid desiccant dehumidification technology, including basic principles, desiccant types and dehumidifier structures. Then, the experimental investigation on liquid desiccant dehumidification technologies are summarized. Thirdly, the theoretical investigation and existing models of liquid desiccant dehumidifier are reviewed. Fourthly, the investigation of the wetting area in plate dehumidifiers are also concluded. Fifthly, the existing performance enhancing

methods of liquid desiccant dehumidifiers are reviewed. Besides, a brief introduction about surface wettability and super-hydrophilic coating is present. Finally, the research gaps of liquid desiccant air dehumidification technologies are summarized based on the literature review and the research methodology adopted in this thesis is present briefly.

Chapter 3 aims to investigate the effect of surface properties on dehumidification performance. Three common plate dehumidifiers, i.e., Stainless steel plate dehumidifier, Titanium plate dehumidifier and Polytetrafluoroethylene (PTFE) plate dehumidifier, with distinctive surface properties are adopted in this chapter to experimentally investigate the surface properties on dehumidification performance. The microscopic surface structures of different working plates are investigated with FESEM test. Besides, the contact angle of desiccant solution and surface free energy are also identified to characterize the working plates. The flow characteristics of falling film in different plate dehumidifiers are investigated in detail. The results indicates that the Titanium plate dehumidifier demonstrates the superior dehumidification performance compared with the other plate dehumidifiers.

Based on the findings in Chapter 4, a novel super-hydrophilic formula using nanoscale anatase TiO_2 particles is successfully coated on the plate surface to improve the surface wettability and thus enhance the dehumidification performance. The detailed

development procedure of the TiO_2 super-hydrophilic coating is demonstrated. Then, the microstructures of the TiO_2 super-hydrophilic coating is investigated through XRD, FESEM and HRTEM test. Finally, the preliminary research about the effect of TiO_2 super-hydrophilic coating on wetting area is conducted in this section.

Chapter 5 mainly investigates the heat/mass transfer performance of internally-cold liquid desiccant plate dehumidifier modified by TiO_2 super-hydrophilic coating. Firstly, the experimental setup is reconstructed with two single-channel internally-cold liquid desiccant plate dehumidifiers. One plate dehumidifier is fabricated with TiO_2 super-hydrophilic coating, while the other plate dehumidifier is just cleaned by ethanol. The comparative investigation on dehumidification performance between the coated and uncoated plate dehumidifiers is conducted comprehensively. The flow characteristics including wetting area and flow fluctuation of falling film in surface-modified plate dehumidifier are investigated. The effect of operating parameters, including the flow rates, temperature and concentration of liquid desiccant solution, flow rates, temperature and humidity of processed air as well as the flow rates and temperature of the cooling fluid, on dehumidification performance are comprehensively analysed. Finally, a novel empirical mass transfer correlation is developed based on the experimental results, in which solid-liquid interaction effect is considered to account for its effect on dehumidification performance.

Chapter 6 develops an improved heat and mass transfer model of internally-cold liquid desiccant plate dehumidifier considering solid-liquid interaction effect based on the experimental investigation above. The shrinkage of the falling film in liquid desiccant plate dehumidifier is theoretically investigated and a shrinkage model is developed to accurately estimate the actual wetting area of desiccant solution on working plate. The model is well validated by the experimental results and the effect of contact angles on dehumidification performance is investigated theoretically with the newly-developed model. The distribution of air parameters along the flow direction is also simulated.

Chapter 7 proposes a dynamic energy consumption model of solar-assisted liquid desiccant air-conditioning system considering dehumidifier surface properties. A typical commercial building in Hong Kong is selected as a case building to analyse the effect of surface properties on energy consumption of the whole air-conditioning system. Besides, the effect of solar collection system on the whole energy consumption is also investigated.

Chapter 8 summarizes the major conclusions and achievements of this dissertation and proposes several recommendations for the future research.

CHAPTER 2

LITERATURE REVIEW AND RESEARCH

METHODOLOGY

2.1 Background of liquid desiccant dehumidification

2.1.1 Principles and features

Fig. 2-1 presents the schematic diagram of a basic liquid-desiccant dehumidification air-conditioning system [24]. The whole system is composed of four sub-systems, i.e., a dehumidification system, a regeneration system, a liquid desiccant storage system and an air cooling system.

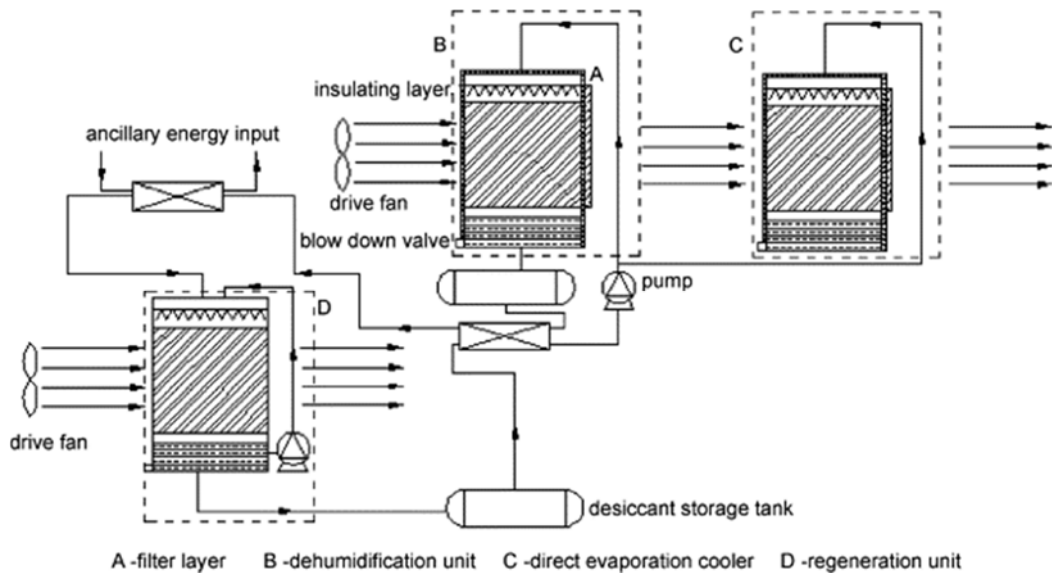


Fig. 2.1 Schematic diagram of liquid-desiccant dehumidification air-conditioning system [24]

The task of dehumidification system is to remove the extra moisture of air through absorption process. The moisture exchange from the humid air to liquid desiccant solution is driven by vapour pressure difference between liquid-desiccant solution and humid air. In liquid desiccant dehumidification system, the vapor pressure of air which is in equilibrium with the desiccant solution is lower than that of the humid air. Therefore, the moisture of humid air is absorbed by the liquid desiccant solution and the air is dehumidified. In addition, the latent heat released during the dehumidification process may increase the temperature of liquid desiccant solution and the equilibrium vapor pressure accordingly. To maintain the low surface equilibrium vapor pressure, new dehumidification systems, such as internally-cold liquid desiccant dehumidification system, were developed [8, 9]. In internally-cold liquid desiccant dehumidification system, the latent heat can be removed by the cooling fluid, which could effectively prevent the temperature increase of desiccant solution.

The liquid desiccant solution is recycled in liquid desiccant dehumidification system. The typical cycle of liquid desiccant solution is present in Fig. 2.2 [25].

A-B. The liquid desiccant solution at Stage A is cold and concentrated. As the equilibrium surface vapor pressure is lower than that of humid air, the extra moisture

of the air is absorbed by desiccant solution. Therefore, the concentration of desiccant solution decreases and the desiccant moisture content increases.

B-C. The liquid desiccant solution at Stage B is weak and need to be re-concentrated. The weak desiccant solution is firstly heated to improve the equilibrium surface vapor pressure. Then, the moisture content of the weak desiccant solution is removed by processed air and the desiccant solution is regenerated.

C-A. The liquid desiccant solution at Stage C is concentrated but hot. Thus, the desiccant solution is pre-cooled before being supplied to the dehumidifier. Finally, the desiccant solution returns to Stage A.

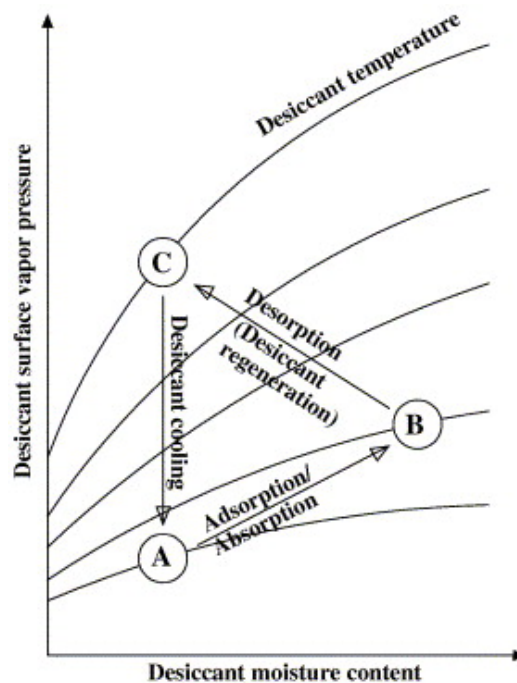


Fig. 2.2 Schematic of the typical cycle of liquid desiccant solution [25]

The air cooling system is to handle the rest of sensible load and cool the air temperature to the required values. Then, the comfortable (cool and dry) air is supplied to the air-conditioned rooms.

Compared with traditional air dehumidification technologies, such as air-condensation dehumidification technology, liquid desiccant air dehumidification has many advantages: 1) lower energy consumption. As the latent heat and sensible heat are handled separately, the energy consumption of the air-conditioning system is reduced. Besides, the use of low-grade thermal energy also contributes to the lower energy consumption of air-conditioning system; 2) more environment-friendly. CFCs and HCFCs, which may have serious impacts on the ozone layer, are no longer required in liquid desiccant air-conditioning system; 3) easier maintenance. As the whole system is operated under atmospheric pressure or near atmospheric pressure, the maintenance of the system is simplified. Therefore, the liquid desiccant dehumidification system (LDDS) is a promising alternative to conventional air conditioning system (CACS). The comparison between LDDS and CACS is summarized in Table 1 [26,27].

Table 2.1 Comparison between LDDS and CACS

Types	CACS	LDDS
System initial investment	Similar	
Operation cost	High	Save around 40% of cost
Driving energy source	Electricity, natural gas	Low-grade energy
Control over humidity	Average	Accurate
Indoor air quality	Average	Good
System instalment	Average	Slightly complicate
Energy storage capacity	Bad	Good

2.1.2 Types of liquid desiccant

The liquid desiccant is one of the key components in liquid desiccant dehumidification system. As the properties of liquid desiccant can affect the dehumidification performance directly, the type selection of liquid desiccant is critical. The liquid desiccant solution absorbs the extra moisture due to the vapour pressure difference. Therefore, an ideal liquid desiccant should possess the following properties: low surface vapour pressure, high solubility, low viscosity, low regeneration temperature, high energy storage density, non-volatile, non-toxic, stable and inexpensive, etc. [28].

The types of liquid desiccant have been investigated for several years and several liquid desiccants have been developed. The common liquid desiccants are mainly

categorized into two types, i.e., organic desiccant and inorganic desiccant. The inorganic liquid desiccants include Triethylene Glycol (TEG), Diethylene Glycol (DEG), Tetraethylene Glycol (T4EG), Dipropylene Glycol (DPG), Propylene Glycol (PG), Dipropylene Glycol (DPG), etc. [29]. The Triethylene Glycol (TEG) is one of the earliest liquid desiccants, but it has its limitations, such as easy adhesion to equipment or pipes due to high viscosity, which might affect the stability of the dehumidification system. In addition, the Triethylene Glycol is volatile because of the low surface vapor pressure and it may evaporate with air and enter the air-conditioned rooms [30]. As the operating concentration of Triethylene Glycol can be as high as 90%-98% by weight, the annular loss of Triethylene Glycol is very high.

The inorganic liquid desiccants such as Lithium Chloride (LiCl), Lithium Bromide (LiBr) and Calcium Chloride (CaCl₂) are very popular due to their high absorption capacity, good stability, low viscosity and volatility. The LiCl and LiBr can dry air to 15% and 6% relative humidity, respectively, but these salts are naturally corrosive [31]. In addition, the high price of LiCl and LiBr may limit their wide application [32]. Some researchers selected CaCl₂ as liquid desiccant due to the lower price. However, the vapor pressure of CaCl₂ is relatively high and CaCl₂ solution is unstable, which limits its widespread use.

The properties of liquid desiccants have been investigated for several years [33,34, 35, 36, 37]. Conde [34] developed formulations for the thermal properties, including solubility boundary, vapour pressure, density, surface tension, dynamic viscosity, thermal conductivity, specific thermal capacity and differential enthalpy of dilution, of lithium and calcium chlorides.

As the liquid desiccant shows direct effect on the heat and mass transfer between the processed air and desiccant solution, it is very important to choose suitable liquid desiccant. Several figures of merit have been proposed by researchers. Table 2.2 lists the weighting factors and figures of merit for the selection of desiccant solution [38].

Table 2.2 Weighing factors and figures of merit for desiccant selection [38]

Characteristics	Weighting factor	Figure of merit
Safety	1.0	Lethal dose (LD50)
Corrosion	0.8	Corrosion rate
Mass transfer potential	0.8	Equilibrium vapor pressure
Heat of mixing	0.6	Energy/kg of absorbed water
Cost of desiccant	0.5	Cost/100 kg of solution
Heat transfer potential	0.5	Thermal conductivity
Parasitic power loss	0.3	Viscosity

2.2 Structures of falling film liquid desiccant dehumidifiers

The liquid desiccant dehumidifier is one of the core components in liquid desiccant dehumidification system. Various types of dehumidifiers have been developed, which are mainly classified into two types, i.e., adiabatic dehumidifier and internally-cooled dehumidifier, according to whether cooling unit is equipped or not [39], as shown in Fig. 2.3.

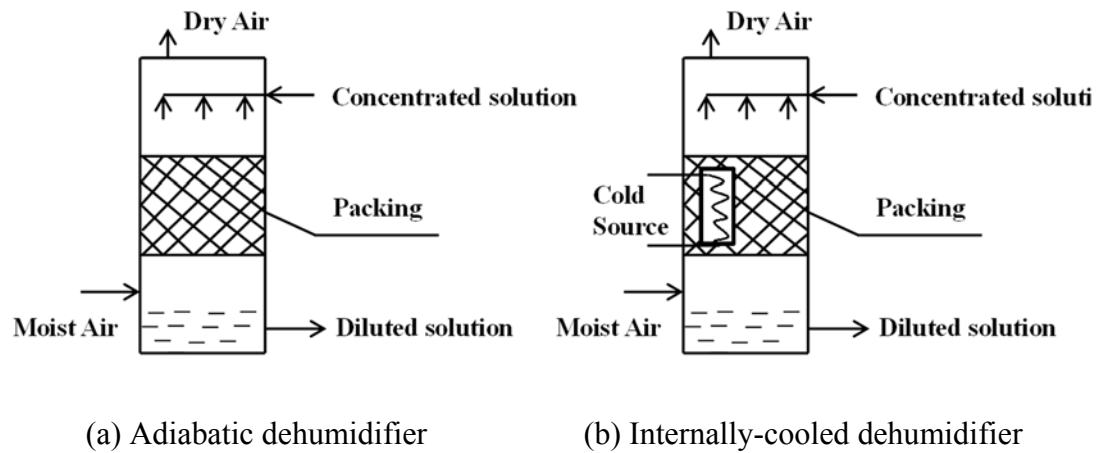


Fig. 2.3 The structure diagram of two dehumidifiers

In internally-cold liquid desiccant dehumidifiers, the latent heat released during dehumidification process is removed by cooling fluid, which helps to maintain the temperature of desiccant solution and improve the dehumidification efficiency. Many researches have investigated the internally-cold liquid desiccant dehumidifiers for decades [40-47]. The summary of the internally-cold liquid desiccant dehumidifiers is present in Table 2.3.

Table 2.3 Summary of internally-cold falling film liquid desiccant dehumidifiers

Sources	Structures	Desiccant types	Materials	Flow patterns	Cooling type	Specific surface area (m^2/m^3)	Operating conditions
Pesaran et al. [40]	Heat pipe	LiCl (37 wt. %) and TEG (95 wt. %)	[-]	Co-current		[-]	$T_a = 35^\circ\text{C}$, $m_a = 0.283 \text{ kg/s}$ $m_s = 228 - 408 \text{ L/s}$
Jain et al. [41]	Tubular absorber	LiCl	[-]	Co-current		[-]	
Saman and Alizadeh [42]	Plate heat exchanger	CaCl_2 (40 wt. %)	Plastic tubes	Cross-flow	Indirect evaporation	[-]	$T_a = 28.5 - 38^\circ\text{C}$, $\omega_a = 12 - 20 \text{ g/kg}$ $m_a = 0.15 - 0.50 \text{ kg/s}$, $m_s = 0.06 \text{ kg/s}$
Yin et al. [12]	Plate-fin heat exchanger	LiCl (39 wt. %)	Stainless steel plates	Counter-current	Cooling water	267	$T_a = 26 - 32^\circ\text{C}$, $\omega_a = 9.5 - 14.5 \text{ g/kg}$ $m_a = 0.04 - 0.08 \text{ m}^3/\text{s}$, $m_s = 0.10 \text{ kg/s}$ $T_s = 23 - 32^\circ\text{C}$, $m_f = 0.151 \text{ kg/s}$ $T_f = 19 - 25^\circ\text{C}$
Kessling et al. [43]	Parallel plate exchanger	LiCl (40.2 wt. %)	Polypropylene plates	Counter-current	Cooling water	121	$T_a = 23.9 - 26.9^\circ\text{C}$, $\omega_a = 14.5 \text{ g/kg}$ $m_a = 6.36 - 24.83 \text{ g/s}$ $m_s = 0.116 - 1.242 \text{ kg/s}$, $T_f = 24.1^\circ\text{C}$

Sources	Structures	Desiccant types	Materials	Flow patterns	Cooling type	Specific surface area (m^2/m^3)	Operating conditions
Liu et al. [44]	Tubes with fins	LiBr (38.8-42.4 wt. %)	Thermally conductive plastic	Cross-flow	Cooling water	342	$T_a = 33.5 - 36.3^\circ\text{C}$ $\omega_a = 14.2 - 24.6 \text{ g/kg}$ $m_a = 0.118 - 0.180 \text{ kg/s}$ $m_s = 0.017 - 0.059 \text{ kg/s}$ $T_s = 28.6 - 31.5^\circ\text{C}$, $T_f = 11.1 - 17.0^\circ\text{C}$ $m_f = 0.126 - 0.292 \text{ kg/s}$
Bansal et al. [45]	Packed tower	CaCl ₂ (37 wt. %)	Cellulose paper pads	Cross-flow	Cooling water	608	$T_a = 20.9 - 30.3^\circ\text{C}$, $T_s = 30.4^\circ\text{C}$ $m_s = 2 - 10 \text{ L/min}$, $T_f = 4.8 - 8.7^\circ\text{C}$
Zhang et al. [46]	Fin heat exchanger	LiBr (45 wt. %)	Stainless steel	Cross-flow	Cooling water	790	$T_a = 29.6 - 33.4^\circ\text{C}$, $\omega_a = 15.4 - 17 \text{ g/kg}$ $m_a = 0.358 - 0.370 \text{ kg/s}$ $m_s = 0.041 - 0.178 \text{ kg/s}$ $T_s = 24.2 - 28.5^\circ\text{C}$, $T_f = 16.4 - 25.5^\circ\text{C}$ $m_f = 0.101 - 0.358 \text{ kg/s}$
Chung et al. [47]	Fin coils	TEG (88-95.2 wt. %)	Stainless steel	Co-current	Cooling refrigerant	160	$T_a = 21 - 26.9^\circ\text{C}$, $\omega_a = 13.6 - 17.8 \text{ g/kg}$ $m_a = 1.94 - 3.77 \text{ kg/min}$ $T_s = 22.3 - 30.0^\circ\text{C}$, $T_f = 18.4 - 21.9^\circ\text{C}$

2.3 Simulation models of falling film dehumidifier

Apart from the experimental study of liquid desiccant dehumidifier, several simulation models of liquid desiccant dehumidifier have been developed to investigate the heat and mass transfer mechanism in liquid desiccant dehumidifier. The well validated simulation models could provide researchers and engineers valuable guidance to better understand the heat and mass characteristics. The development of the simulation models for heat and mass transfer in liquid desiccant dehumidifier can be summarized and categorized into four stages, as below:

(1) In 1980s, the parameters of the liquid desiccant in the thickness direction were considered constant and the thickness of the falling film was ignored [48].

(2) In Hellmann and Grossman's model [49], the thickness of the falling film was considered in the model, which meant that the heat and mass transfer resistance inside the liquid desiccant was taken into consideration. However, the plate or tube surface in the dehumidifier was assumed to be fully wetted by the liquid desiccant, which did not accord with the actual situation.

(3) To improve the prediction accuracy of the simulation models, the incomplete wetting conditions was taken into consideration. Jain et al. [41] proposed a wetting factor in the simulation model to investigate the effect of incomplete wetting condition

on the dehumidification performance. Ren et al. [50] developed a 2-D model of liquid desiccant dehumidifier considering the heat and mass transfer resistance inside the liquid falling film and the incomplete wetting conditions.

(4) Ali et al. [9] developed a theoretical model to investigate the heat and mass transfer of liquid desiccant dehumidifier concerning the un-uniform distribution of thermal properties in the thickness direction. However, the falling film thickness was assumed constant. Mesquita et al. [51] developed an improved model based on Ali et al. model [9] considering the variable falling film thickness along the flow direction caused by moisture exchange.

According to the simulation methods, the simulation models can also be categorized into three main types, i.e., the finite difference model, the effectiveness NTU ($\varepsilon - NTU$) model and simplified simulation models.

2.3.1 Finite difference model

In finite difference models, the heat and mass transfer is calculated within the control volumes. Many researchers investigated the heat and mass transfer characteristics using finite difference model due to high predictive accuracy. Amongst these existing finite different models, Jain et al [41] model is famous for considering the incomplete

wetting conditions, which is present in detail as follows.

Jain et al. [41] developed a simple steady state model of heat and mass transfer between processed air and liquid desiccant solution for both dehumidifier and regenerator. Two wetness factors, F_w and F_h , were introduced in Jain et al. [41] model to account for the effect of improper wetting on dehumidification/regeneration performance. On taking suitable values of F_w and F_h , the theoretical model showed good agreement with the experimental results. To simplify the model, several assumptions were made:

- (1) The air and desiccant flows were assumed as slug flows.
- (2) The contractor was assumed to be well insulated and adiabatic.
- (3) The properties of desiccant solution, air and cooling water were considered constant within the control volume.
- (4) The packing was assumed fully wetted and the heat and mass transfer area was assumed equal to the specific value of the packings.
- (5) The heat and mass transfer only occurred in thickness direction and no heat and mass transfer occurred in the flow direction.
- (6) The heat and mass transfer resistance inside the liquid desiccant was neglected.

For liquid desiccant dehumidifier, the mass and energy conservation equations

between processed air, liquid desiccant and cooling water in the typical control volume, as shown in Fig. 2.4, are shown as follows.

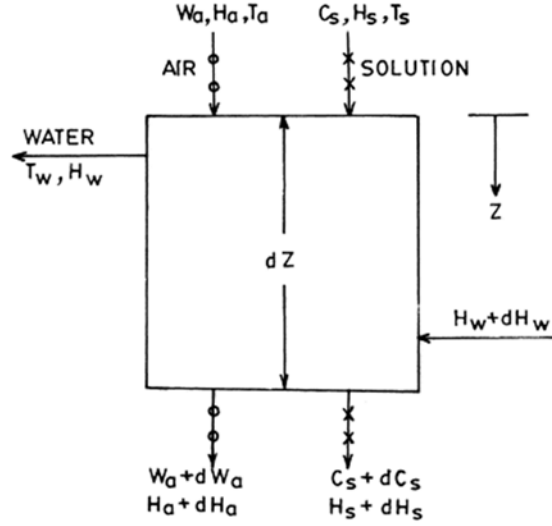


Fig. 2.4 Control volume for liquid desiccant dehumidifier [41]

Mass conservation:

For processed air,

$$m_a \frac{dW_a}{dZ} = -h_m P_w (W_a - W_e) \quad (2.1)$$

For desiccant solution,

$$m_s \frac{dC_s}{dZ} = h_m P_w (W_a - W_e) \quad (2.2)$$

Energy conservation:

For processed air,

$$m_a C_{pm} \frac{dT_a}{dZ} = U_a P_a (T_s - T_a) \quad (2.3)$$

For desiccant solution,

$$m_s \frac{dH_s}{dZ} = -m_s C_{pm} \frac{dT_a}{dZ} - m_w C_{pw} \frac{dT_w}{dZ} - m_a H_{fg} \frac{dW_a}{dZ} \quad (2.4)$$

For cooling water,

$$m_w C_{pw} \frac{dT_w}{dZ} = -U_w P_a (T_s - T_w) \quad (2.5)$$

where W_e is the equilibrium humidity of desiccant solution, which is given as follows:

$$W_e = 0.62197 \frac{P_e}{P_{atm} - P_e} \quad (2.6)$$

The mass transfer coefficient h_m is calculated as follows:

$$h_m = \frac{J_D \rho_a V_a}{(Sc)^{2/3}} \quad (2.7)$$

where J_D is the dimensionless Colburn factor [52].

$$J_D = 0.023 Re_a^{-0.17} \quad (2.8)$$

Sc is Schmidt number.

$$Sc = \frac{\mu_a}{\rho_a D_{AB}} \quad (2.9)$$

Besides, the heat transfer coefficient on air side can be calculated using mass transfer coefficient as follows [53]:

$$h_{ca} = C_{pm} h_m (Le)^{2/3} \quad (2.10)$$

where Le is Lewis number, $Le = Sc / Pr_a$.

The heat transfer coefficient on the desiccant solution side is given as follows [54]:

$$Nu_s = 0.67 Re_s^{0.11} \left(\frac{Pr_s S_r}{L_a} \right)^{0.33}, \quad Re < 2300 \quad (2.11)$$

where Re_s is the desiccant solution flow rate and Γ is the linear wetting density.

$$Re_s = \frac{4\Gamma}{\mu_a} \quad (2.12)$$

$$\Gamma = \frac{m_s}{N_T \pi D} \quad (2.13)$$

S_r is the reduced film thickness, which is obtained as follows:

$$S_o = \left(\frac{3\Gamma\mu_s}{\rho_s^2 \times 9.8} \right)^{1/3}, \quad Re_s < 1600 \quad (2.14)$$

$$S_r = \frac{(1 - 0.022(V_a - 4))S_o}{0.9085 Re_s^{1/3}} \quad (2.15)$$

Therefore, the heat transfer coefficient on desiccant solution side h_s is obtained as follows:

$$h_s = \frac{Nu_s K_s}{S_r} \quad (2.16)$$

where K_s is the thermal conductivity of desiccant solution.

The heat transfer coefficient of cooling water h_w is obtained as follows [55]:

$$h_w = \frac{Nu_w K_w}{D_{eq}} \quad (2.17)$$

$$Nu_w = 0.36 Re_w^{0.55} Pr_w^{1/3}, \quad 2000 < Re_w < 1 \times 10^6 \quad (2.18)$$

where D_{eq} is the equivalent diameter and can be calculated as follows for triangular pitch.

$$D_{eq} = \frac{8(P_t^2 \times 0.423 - \pi D_o^2 / 8)}{\pi D_o} \quad (2.19)$$

In addition, the flow area is given as follows:

$$a_s = \frac{D_s (P_t - D_o) B_s}{P_t} \quad (2.20)$$

Finally, the overall heat transfer coefficient from the cooling water to the desiccant solution is obtained as follows:

$$\frac{1}{U_w} = \frac{1}{h_w} + \ln \left(\frac{D_o}{D_i} \right) \frac{D_o}{2K_w} + \frac{D_o}{D_i} \frac{1}{h_s} + 0.0002 \quad (2.21)$$

(2) For liquid desiccant regenerator

The mass and energy conservation equations between processed air and liquid desiccant in the typical control volume, as shown in Fig. 2.5, of liquid desiccant regenerator are shown as follows.

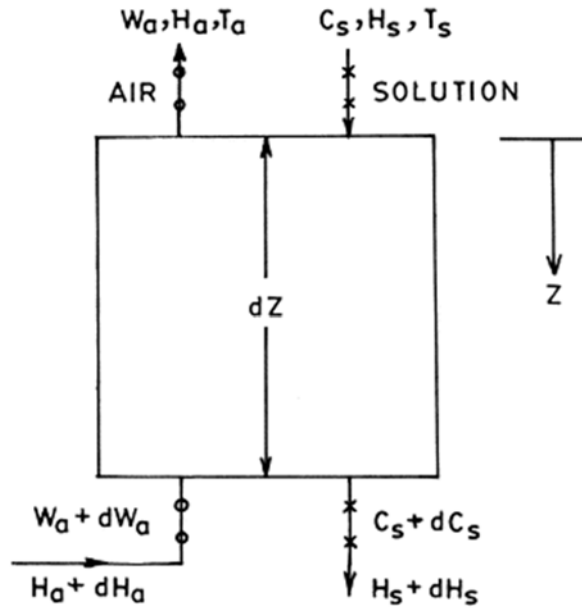


Fig. 2.5 Control volume for liquid desiccant regenerator [41]

Mass conservation:

For processed air,

$$m_a \frac{dW_a}{dZ} = -h_m P_w (W_e - W_a) \quad (2.22)$$

For desiccant solution,

$$m_s \frac{dC_s}{dZ} = -h_m P_w (W_a - W_e) \quad (2.23)$$

Energy conservation:

For processed air,

$$m_a C_{pm} \frac{dT_a}{dZ} = -U_a P_a (T_s - T) \quad (2.24)$$

For desiccant solution,

$$m_s \frac{dH_s}{dZ} = -U_a P_a (T_s - T_a) + m_a H_{fg} \frac{dW_a}{dZ} \quad (2.25)$$

The heat transfer coefficient between liquid desiccant and processed air is calculated as follows:

$$h_a = \frac{Nu_a K_a}{D} \quad (2.26)$$

where Nu_a is Nusselt number of the processed air, which is obtained using Gnielinski correlation.

$$Nu_a = \frac{f \times Pr ((Re_a - 1000) / 2)}{1 + 12.7 \sqrt{\frac{f}{2}} (Pr^{2/3} - 1)} \quad (2.27)$$

f is the friction factor.

$$\frac{1}{\sqrt{f}} = (1.58 \ln Re_a - 3.28) \quad (2.28)$$

The mass transfer coefficient h_m between liquid desiccant and processed air is

calculated using heat transfer coefficient.

$$h_m = \frac{h_c}{C_{pm} (Le)^{2/3}} \quad (2.29)$$

A numerical solution was proposed in Jain et al. [41] model to estimate the dehumidification and regeneration performance of liquid desiccant dehumidifiers and regenerators. As the inlet parameters of the processed air, liquid desiccant solution and cooling fluid are measured, the outlet parameters can be calculated using the model.

2.3.2 Effectiveness NTU model

Stevens et al. [56] developed a heat and mass transfer model for cooling towers based on a simple effectiveness model. Finite difference element was used to solve the mode. In addition, two more assumptions were made including the assumption of the linear relationship of the saturation enthalpy and temperature and the ignorance of moisture removal in the calculation of solution energy conservation. In the $\varepsilon - NTU$ model, the effective heat and mass transfer process was assumed. The equations and calculation process of $\varepsilon - NTU$ model were shown as follows:

(1) The calculation of NTU ,

$$NTU = \frac{h_D A_v V_T}{G_a} \quad (2.30)$$

(2) The calculation of effectiveness for the dehumidifier,

$$\varepsilon = \frac{1 - e^{-NTU(1-m^*)}}{1 - m^* e^{-NTU(1-m^*)}} \quad (2.31)$$

(3) The calculation of outlet air enthalpy,

$$h_{a,o} = h_{a,i} + \varepsilon(h_{Ts,sat} - h_{a,i}) \quad (2.32)$$

(4) The calculation of effective saturation enthalpy,

$$h_{Ts,sat,eff} = h_{a,i} + \frac{h_{a,o} - h_{a,i}}{1 - e^{-NTU}} \quad (2.33)$$

(5) The calculation of outlet air humidity ratio,

$$\omega_{a,o} = \omega_{Ts,sat,eff} + (\omega_{a,i} - \omega_{Ts,sat,eff})e^{-NTU} \quad (2.34)$$

2.3.3 Simplified simulation models

As both finite difference models and effective NTU models consume lots of numerical power and iterative calculations. It is hard to get the final results directly. Therefore, simplified simulation models are necessary to simplify the calculation process.

Khan et al. [57] developed a simplified model to predict the annual energy consumption of packed liquid dehumidifiers and regenerators based on their experimental results. In the simplified model, the outlet air temperature and humidity ratio can be quickly calculated as below:

$$W_o = s_0 + s_1 W_i + s_2 T_{si} + s_3 T_{si}^2 \quad (2.35)$$

$$W_o = a_0 + a_1 W_i + a_2 T_{ao} + s_3 T_{ao}^2 \quad (2.36)$$

where T_{si} is the solution spray temperature, °F . W_o and W_i are the process air

humidity ratios of the exit and outlet air, $\text{lb} \cdot \text{lb}^{-1}$. T_{ao} is the air exit temperature, $^{\circ}\text{F}$. $a_0 \sim a_3$ and $s_0 \sim s_3$ are constant factors determined by a least-squares analysis. However, as the constant factors depend heavily on the experimental database, it is hard to extend the application of the model to other operating conditions beyond the database.

Qi et al. [58] developed a semi-empirical model to quickly predict the performance of plate dehumidifiers and regenerators. Three types of effectiveness were introduced to represent the heat and mass transfer during the dehumidification and regeneration process. Enthalpy effectiveness, ε_{ha} , is the ratio of the actual energy change of air to the maximum possible one. Moisture effectiveness, ε_{ma} , is the ratio of the actual mass change of air to the maximum possible one. Temperature effectiveness, ε_{tf} , is the ratio of the actual heat change of desiccant to the maximum possible one.

$$\varepsilon_{ha} = \frac{h_{a,in} - h_{a,out}}{h_{a,in} - h_{I,in}}; \varepsilon_{ma} = \frac{\omega_{a,in} - \omega_{a,out}}{\omega_{a,in} - \omega_{I,in}}; \varepsilon_{tf} = \frac{t_{f,in} - t_{f,out}}{t_{f,in} - t_{s,in}} \quad (2.37)$$

where h means the enthalpy, ω is the moisture content and t is the temperature. The subscripts a, s, f, I stand for the air, desiccant solution, cooling/heating fluid, and the interface between air and solution, respectively. The subscripts *in* and *out* mean the inlet and outlet characteristics.

Based on the experimental results, the correlations for the three types of effectiveness

were developed by linear regressions. For dehumidifiers:

$$\varepsilon_{de,ha} = \frac{10 \cdot (|t_{f,in} - t_{s,in}|)^{0.0486} (\omega_{a,in} - \omega_{l,in})^{0.525} (m_s / m_a)^{0.349} m_f^{0.0773} a_w^{0.0764}}{(h_{a,in} - h_{l,in})^{0.547} \delta_a^{0.378}} \times (-0.0022 \cdot W_d + 0.0102 \cdot H)^{0.0407} \quad (2.38)$$

$$\varepsilon_{de,ma} = \frac{0.0829 \cdot (|h_{a,in} - h_{l,in}|)^{0.195} (m_s / m_a)^{0.350} m_f^{0.0619} a_w^{0.07}}{(|t_{f,in} - t_{s,in}|)^{0.009} (\omega_{a,in} - \omega_{l,in})^{0.0441} \delta_a^{0.375}} \times (-0.0032 \cdot W_d + 0.0248 \cdot H)^{0.0854} \quad (2.39)$$

$$\varepsilon_{de,tf} = \frac{0.115 \cdot (h_{a,in} - h_{l,in})^{0.304} (\omega_{a,in} - \omega_{l,in})^{0.394} a_w^{0.757} (W_d \cdot H)^{0.754}}{m_f^{0.857} (m_s / m_a)^{0.261} (|t_{f,in} - t_{s,in}|)^{0.759} \delta_a^{0.602}} \times \frac{t_{f,in} - t_{s,in}}{|t_{f,in} - t_{s,in}|} \quad (2.40)$$

For regenerators:

$$\varepsilon_{re,ha} = \frac{27.061 \cdot (1000 \cdot (\omega_{l,in} - \omega_{a,in}))^{0.987} (m_s / m_a)^{0.770} a_w^{0.0838}}{(|h_{a,in} - h_{l,in}|)^{1.532} (|t_{f,in} - t_{s,in}|)^{0.0038} m_f^{-0.012} \delta_a^{0.368}} \times (0.196 \cdot W_d + 0.287 \cdot H)^{0.125} \quad (2.41)$$

$$\varepsilon_{re,ma} = \frac{46.219 \cdot (1000 \cdot (\omega_{l,in} - \omega_{a,in}))^{0.728} (m_s / m_a)^{0.844}}{(|h_{a,in} - h_{l,in}|)^{1.332} (|t_{f,in} - t_{s,in}|)^{0.0168}} \times m_f^{0.001} a_w^{0.0691} \delta_a^{0.0324} (W_d \cdot H)^{0.0242} \quad (2.42)$$

$$\varepsilon_{re,tf} = \frac{0.0554 \cdot (|h_{a,in} - h_{l,in}|)^{0.794} a_w^{0.622} ((1.552 \cdot W_d + 0.118 \cdot H))^{0.896}}{(1000 \cdot (\omega_{l,in} - \omega_{a,in}))^{0.636} m_f^{0.908} (|t_{f,in} - t_{s,in}|)^{1.07} \delta_a^{0.480}} \times (m_s / m_a)^{0.0032} \frac{t_{f,in} - t_{s,in}}{|t_{f,in} - t_{s,in}|} \quad (2.43)$$

As discussed above, several models have been developed to estimate the

dehumidification performance of falling film liquid desiccant dehumidifiers. The summary of existing models of falling film dehumidifiers are present as follows.

Table 2.3 Summary of simulation models for falling film liquid desiccant dehumidifiers

Classification	Film thickness	Source	Flow pattern	Dimensionality	Wetting area
Finite difference models	Not considered	Jain et al. [41]	Co-current	1-D	Constant wetness factors
		Liu et al. [59]	Six different configurations	2-D	Complete wetting
		Ren et al. [50]	Four different configurations	2-D	Complete wetting
		Yin et al. [60]	Co-current	2-D	Constant wetness factor
	Constant film thickness	Ali et al. [9]	Co-current/ Counter-current/ Cross	2-D	Complete wetting
		Mesquita et al. [51]	Counter-current	2-D	Complete wetting
		Dai et al. [61]	Cross	2-D	Complete wetting
		Mesquita et al. [51]	Counter-current	2-D	Complete wetting
		Peng et al. [62]	Counter-current	2-D	Complete wetting
		Hueffed et al. [63]	Cross	2-D	Complete wetting
$\varepsilon - NTU$ models	[-]	Stevens et al. [56]	Counter-current	1-D	Complete wetting

Classification	Film thickness	Source	Flow pattern	Dimensionality	Wetting area
Simplified models	[-]	Liu et al. [64]	Counter-current/ Cross	[-]	[-]
	[-]	Khan et al. [57]	Counter-current	[-]	[-]
	[-]	Chen et al. [65]	Counter-current/ Co-current	[-]	[-]
	[-]	Qi et al. [58]	Counter-current	[-]	[-]

2.4 Investigation on wetting characteristics in falling film applications

The wetting area of liquid desiccant is an important parameter in the dehumidifier. In early stage of the simulation model for liquid desiccant dehumidifier, the working plate was usually assumed to be fully wetted by liquid desiccant, which did not comply with the experimental observation. In actual situations, the working surfaces were usually observed to be incompletely wetted by the liquid desiccant, as shown in Fig. 2.6 [66]. Therefore, it is very important to exactly predict the wetting area of liquid desiccant in dehumidifiers.

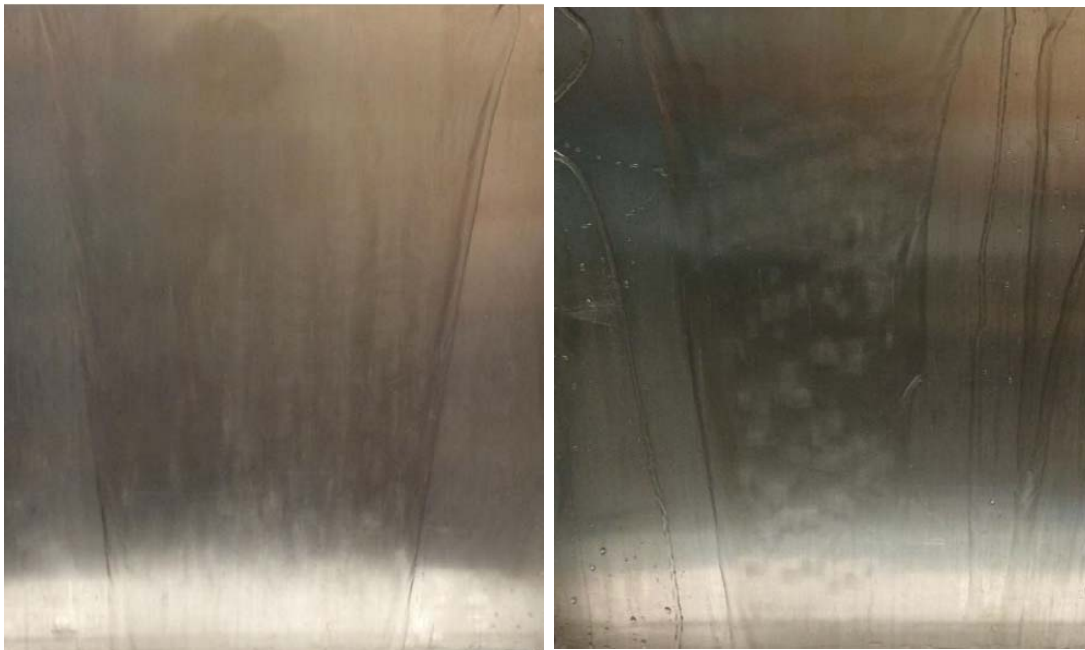


Fig. 2.6 Pictures of working surfaces incompletely wetted by the liquid desiccant [66]

Howell et al. [67] investigated a counter-flow absorber built of a falling film fin-tube exchanger. The experimental data were correlated with predictions of a simulation

model only if a very small fraction of the exchanger surface was supposed to be wetted by the desiccant solution.

Park et al. [8] studied the coupled heat and mass transfer between liquid desiccant and cross-flowing air numerically and experimentally and found that the a large part of the fin surface was not wetted by liquid desiccant.

Kessling et al. [39] investigated the dehumidification performance of an internally cooled dehumidifier with a parallel plate exchanger. It was found that it was difficult to achieve adequate wetted surfaces by small solution flow. According to the experimental results, the dehumidification performance was almost proportionate to the solution flow rate under the constant air flow rate.

Jain et al. [41] experimentally investigate a falling film tubular absorber and a falling film plate regenerator. Jain et al. [41] proposed two wetness factors, i.e., heat transfer factor (F_h) and mass transfer factor (F_w), to account for the incomplete wetting conditions of the exchanger surfaces. As the heat transfer might occur in the unwetted surface, F_h is larger than F_w .

Yin et al. [68] developed and investigated an internally cooled/heated dehumidifier/regenerator using plate-fin heat exchangers, and the wetting factor was

set as 0.7 according to the experimental results.

Pietruschka et al. [69] developed a theoretical model to investigate the liquid desiccant cooling system and found that the wetting area was heavily affected by the heat and mass transfer conditions.

Liu et al. [70] investigated the heat and mass transfer between the liquid desiccant and the processed air in a cross-flow regenerator experimentally and theoretically. During the simulation, the wetting factor was assumed to be 0.8 regardless of the operating conditions.

Some investigators claimed that the incomplete wetting phenomenon attributed to the uneven distribution of the surface tension on the liquid-vapor surface. The uneven distribution of surface tension induced a solution flow in the transverse direction and therefore causing the contraction or expansion of the desiccant solution falling film [71].

Yoshimura et al. [72] experimentally investigated the falling film deformation waves caused by the inherently instability and studied their effect on mass transfer coefficient. The experimental results indicated that the mass transfer coefficient was determined by the diffusivity in the film and the wave frequency.

Geng et al. [73] experimentally investigated the wetting length of falling film using water as the working fluid and found that the wetting length was affected by surface temperature.

Zhang et al. [74] developed a theoretical model to investigate the shrinkage distance of the falling film along the flow direction and indicated that the uneven distribution of the surface tension was much stronger than that in the flow direction. Zhang et al. [74] also investigated the effect of opening width of the liquid distributor on wetting area.

Broome et al. [75] investigated the liquid distribution on the surface of an evaporator tube and developed a semi-empirical correlation to predict the minimum wetting rate.

Morison et al. [76] investigated the minimum wetting and distribution rates in falling film evaporators and then developed an improved model to estimate the minimum wetting rate by taking into account of the effect of liquid distributor. Morison et al. [76] found that the minimum wetting rate is heavily determined by surface tension and contact angle.

In addition, as the wettability can be partly reflected by the contact angles of the liquid desiccant on the working surface, some researchers also investigated the effect of

contact angles on the wetting area. Al-Farayedhi et al. [77] developed an equation to predict the contact angles of desiccant solution.

Qi et al. [78] theoretically investigated the effect of contact angles on the wetting area as well as the dehumidification performance. They reported that the decrease of contact angles could significantly improve the dehumidification efficiency by increasing the wetting area and reducing the falling film thickness of the liquid desiccant.

In conclusion, the wetting area or wetting factor of the liquid desiccant in the previous research was usually assumed to be constant and the values differed significantly. The exact shape of the falling film was neglected. Therefore, it is necessary to develop a model to accurately predict the exact shape of the falling film on the working plate.

2.5 Investigation on performance enhancing methods for falling film applications

The dehumidification efficiency is the most important index for a dehumidifier. Increasing the dehumidification efficiency can reduce the size of the dehumidifier and therefore reduce the initial cost. Investigators have investigated the performance enhancing methods for several years [79]. The methods can be mainly summarized and categorized into four types, i.e., modification of working surface, addition of

surfactant, optimization of the absorber structure and addition of nanofluid.

2.5.1 Surface modification

The microstructure of plate surface can significantly affect the flow patterns of liquid desiccant and the dehumidification efficiency accordingly. Many researchers adopted enhanced tubes or plates with complex microstructures instead of the conventional smooth tubes or plates to increase the heat and mass transfer performance between the liquid desiccant and process air. On one hand, the micro-structures of the working surface can increase the mixture of the liquid desiccant and process air at low flow rates and enlarge the contact area and time. In addition, the capillary effect can accelerate the replenishment of the interfacial liquid desiccant and reduce the heat and mass transfer resistance between the liquid desiccant and the process air. On the other hand, the complex micro-structure of the working surface can reduce the heat transfer boundary layers and enhance the heat transfer between the liquid desiccant and the internally-cooled unit. Thus, the latent heat released during absorption process can be effectively removed by the cooling water flowing at the back of the working surface, which strengthens the driving force of the heat and mass transfer.

Yang and Jou [80] investigated the heat and mass transfer of absorption process for the falling film flow inside a porous medium and the porous media could effectively

increase the wetting ratio of the working surface and therefore enhance the absorption process. Nakao et al. [81] also investigated the heat and mass transfer process between LiBr aqueous solution and vapour using different types of tubes, including smooth tubes, corrugated tubes and finned tubes, as shown in Fig. 2.7. The fin was equipped on the outside surface of the tubes with 45° upward. Through experiment, they found that the best heat and mass transfer performance was achieved with finned tubes. The performance enhancement is attributed to the mixing effect of finned tubes on liquid falling film.

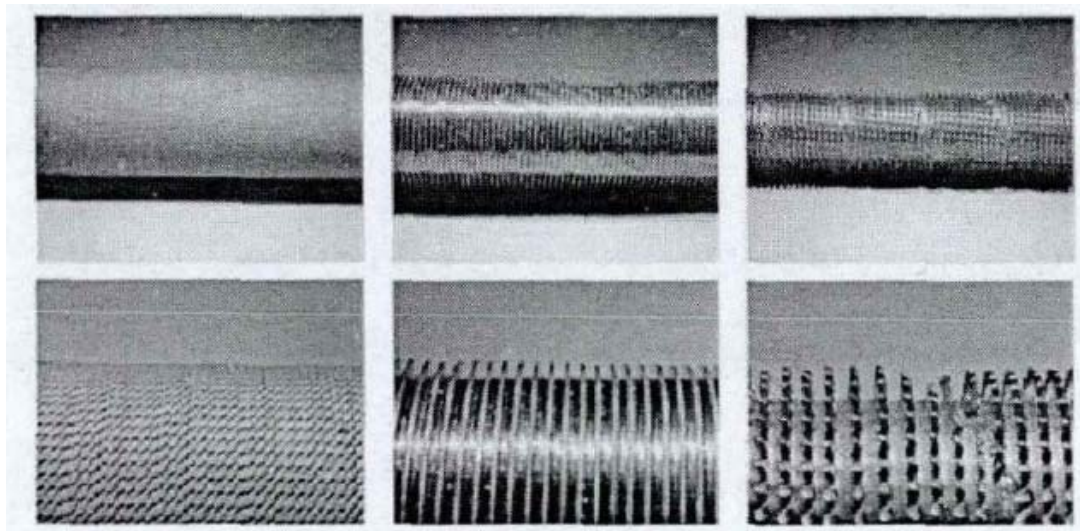


Fig. 2.7 Schematic diagram of different types of tubes

Fujita and Ueda [17] experimentally investigated the heat and mass transfer process on the outside of the smooth tubes. To increase the absorption process, metal wires were twined isometrically around the smooth tubes.

Kim et al. [82] and Cho et al. [83] investigated the effect of micro-scale surface treatment on heat and mass transfer performance for a falling film $\text{H}_2\text{O}/\text{LiBr}$ absorber. The micro-hatched tubes is shown in Fig. 2.8. Through experimental analysis, they found that increasing the surface roughness could significantly improve the surface wettability and then increase the absorption rates. The heat and mass transfer performance of tubes with rough surface could be significantly improved by 100% compared with that of the smooth tubes.



Fig. 2.8 Schematic of micro-hatched tube [83]

Chen [84] investigated the heat and mass performance of falling film with four low ribs enhanced tubes, as shown in Fig. 2.9. Chen indicated that the heat transfer coefficient and mass transfer coefficient of the DAC enhanced tubes were improved by 100% and 50%, respectively, compared with those of the smooth tubes.

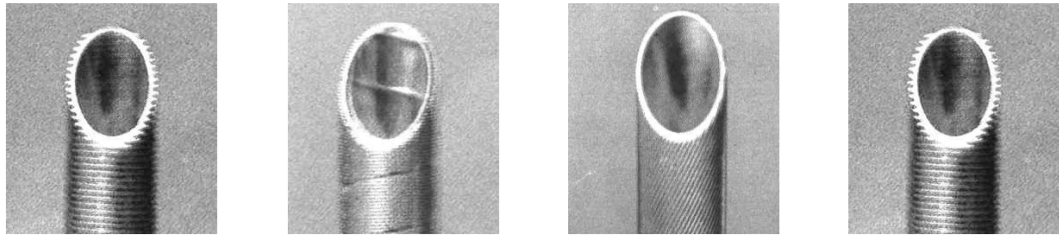


Fig. 2.9 Schematic of four low ribs enhanced tubes [84]

Yin et al. [85] studied the absorption process between LiBr aqueous solution and air on the outside surface of the vertical tubes. Yin et al. [85] found that the complex surface structure could improve the surface wettability and reduce the falling film thickness, which could enhance the heat and mass transfer process. In addition, the complex structure can also accelerate the replenishment of the liquid desiccant on the interface with capillary effect and therefore reduce the heat and mass transfer resistance.

2.5.2 Addition of surfactant

The addition of surfactant can change the surface tension at the interface between the liquid desiccant and air. The eddy caused by the Marangoni effect can enhance the heat and mass transfer between the liquid desiccant and processed air. The Marangoni effect takes place when there is a gradient of surface tension at the interface between two phases, in most situations, a liquid-gas interface. The surface tension typically changes due to variations in solute concentration, surfactant concentration, and

temperature variations along the interface.

In some eutectics or multicomponent liquids, the direction of the gradient of surface tension tangential to the interface can be changed by altering the concentration of the solutes at the surface or by adding surfactants. Depending on the fluid, a rather strong convective motion may be produced, which results in a shear stress at the surface, similar to what the wind can create.

In cases where the concentration drives the variation of the surface tension, the Marangoni effect is referred as the solute-capillary effect. In cases where the surface tension varies with the temperature, the Marangoni effect is referred as the thermocapillary effect. Both effects can take place simultaneously.

Kang and Kashiwagi [86] investigated the heat transfer enhancement by Marangoni convection process. NH_3 aqueous solution was used in the experiment and the images of eddies were captured by holographic interferometer caused by the surfactant, as shown in Fig. 2.10. Similar images were also captured by Nishimura et al. [87] in LiBr aqueous solution.

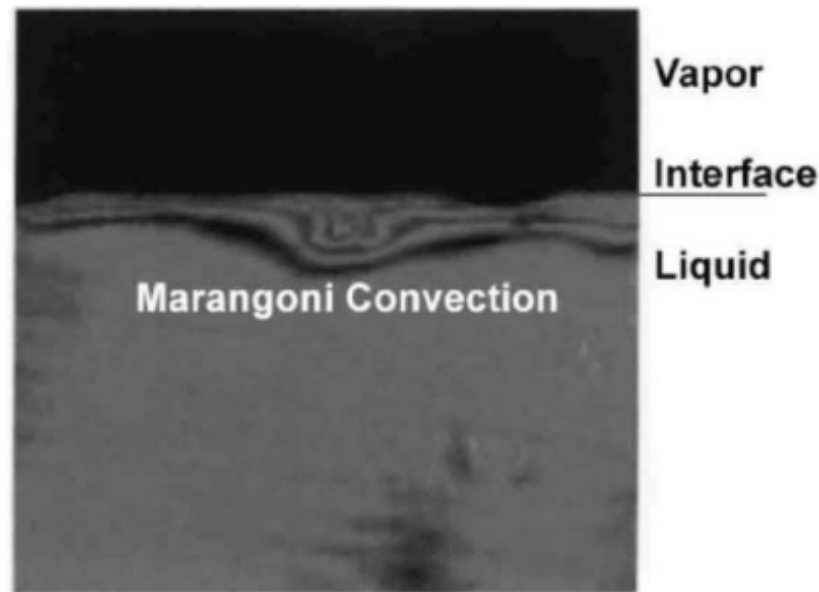


Fig. 2.10 Images of Marangoni convection using holographic interferometer

Hihara and Saito [88] investigated the effect of surfactant on falling film absorption. Ethyl alcohol and octanol were selected as the surfactant in the experiment. The results indicated that the addition of ethyl alcohol could significantly increase the absorption rates of the LiBr aqueous solution while the octanol could reduce the absorption rates.

Cheng et al. [89] experimentally investigated the effect of octyl alcohol and isooctyl alcohol on the absorption capability of NH_3 aqueous solution. Cheng et al. [89] found that for a single absorption cycling, the additives with a suitable concentration range might enhance the heat and mass transfer performance. In addition, Cheng et al. [90] also investigated the effect of octyl alcohol and isooctyl alcohol on the absorption capability of the LiBr aqueous solution. The experimental results indicated that the surfactant could significantly improve the heat and mass transfer process.

2.5.3 Optimization of the absorber structure

In traditional absorbers, heat and mass transfer only occurs in the thin layer between the liquid solution and air. The majority of the liquid solution cannot contact with the air, which reduces the heat and mass transfer rates. To increase the contact area and reduce the heat and mass transfer resistance inside the liquid solution, investigators tried to develop optimized absorber structures.

Islam et al. [91, 92] developed two falling film absorbers with film-inverting configuration, as shown in Fig. 2.11. Baffles were used in the absorber to invert the falling film. The inverting of the falling film successfully achieves the contact between the processed air and the inner liquid desiccant. The simulation and experimental results indicated that the absorption rates were significantly increased by 100% compared with those of the smooth plates.

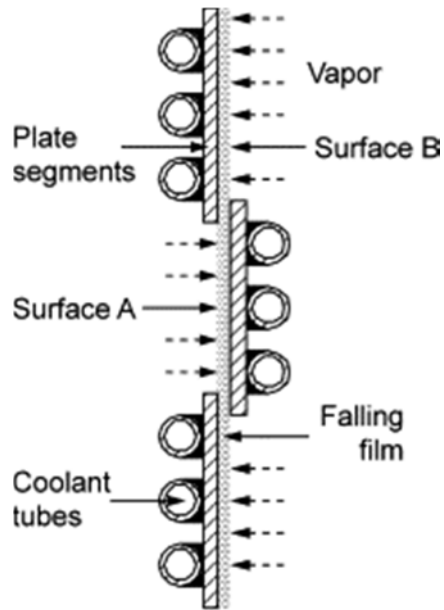


Fig. 2.11 Schematic diagram of the film-inverting absorbers [91]

Another film-inverting absorber was developed by Cui et al. [93], as shown in Fig. 2.12. Cui et al. [93] also investigated the plate falling film absorber with film inverting configuration theoretically and experimentally. Through analysis, the inverting structures could significantly increase the heat and mass transfer coefficients.

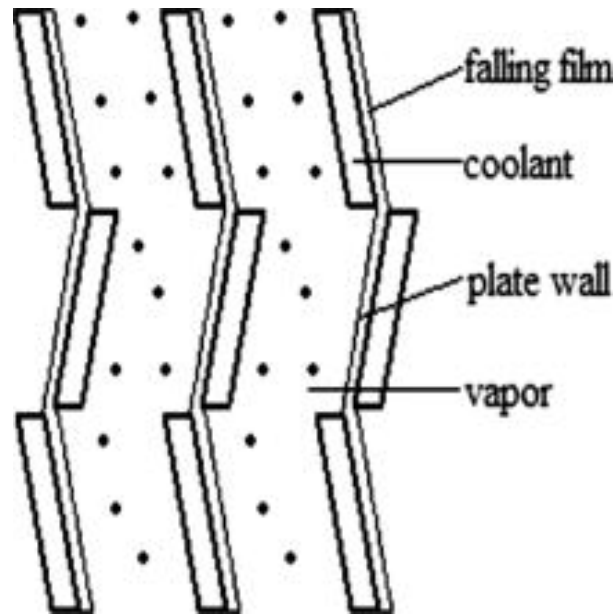


Fig.2.12 Schematic diagram of plate falling film absorber with the film-inverting configuration [93]

2.5.4 Addition of nanofluid

Kim et al. [94] developed binary nanofluid using Cu/CuO nanoparticles and applied it into NH_3 aqueous solution for absorption application. The heat and mass transfer enhancement caused by the binary nanofluid was investigated experimentally and the results indicated that the binary nanofluid could significantly improve the performance. In addition, Kim et al. [95] developed nanofluid to increase the heat and mass transfer of the bubble absorption using Fe/CNT nanoparticles. Kim et al. [95] found that the enhancing performance of CNT nanoparticles was better than that of the Fe nanoparticles.

Ma et al. [23,96] investigated the effect of CNTs-NH₃ binary nanofluid on bubble absorption process with NH₃ aqueous solution. Through experimental analysis, an optimized amount of CNTs was proposed, at which they could achieve the best enhancing performance. In addition, the experimental results indicated that the enhancing ratio of the bubble absorption increased as the initial concentration of the NH₃ aqueous solution increased.

Pang et al. [97] adopted Mono silver (Ag) nanoparticles to enhance the mass transfer during the ammonia-water bubble absorption. The results indicated that the absorption rate with 0.02wt% Ag nanoparticles was significantly enhanced by 55% compared with that of base fluid. Besides, it was found that the mass transfer performance in the binary nanofluids with the coolant is enhanced more than that without the coolant.

2.6 Investigation on surface wettability and super-hydrophilic surfaces

Surface wettability represents the ability of the liquid wetting on the solid surface. The wettability of the solid surface is mainly determined by surface forces, including the adhesive and cohesive forces. The adhesive forces between the solid force and liquid cause the liquid to spread over the solid surface, while the cohesive forces within the liquid droplet cause the liquid to avoid contact with the solid surface.

The wettability can be categorized according to the contact angles of the liquid droplets on the surface. The contact angle is the angle at which the liquid-vapor interface meets the solid-liquid interface. Fig. 2.13 shows the water droplets on different wetting surfaces. Surface A is hydrophobic surface and Surface B is hydrophilic surface. Surface A has a large contact angle, and the surface B has a small contact angle. The contact angle is determined by the resultant between adhesive and cohesive forces. As the tendency of a drop to spread out over a flat, solid surface increases, the contact angle decreases. As shown in Table 2.5, the wettability can be divided into four stages, i.e., super-hydrophilic, hydrophilic, hydrophobic and super-hydrophobic, according to the contact angles.

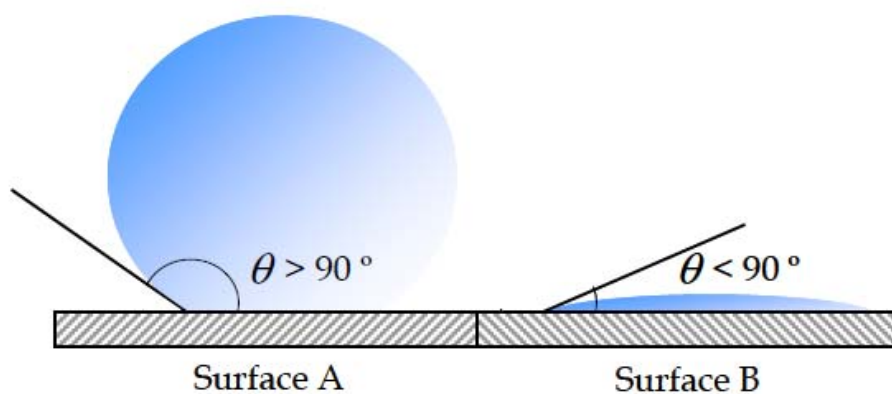


Fig. 2.13 Water droplets on different wetting surfaces

Table 2.5 Wettability and contact angels

Surface types	Contact angles (°)
Super-hydrophilic surface	$\theta < 10^\circ$
Hydrophilic surface	$10^\circ < \theta < 1^\circ$
Hydrophobic surface	$90^\circ < \theta < 150^\circ$
Super-hydrophobic surface	$150^\circ < \theta < 180^\circ$

2.6.1 Wetting models

There are several model for interface force equilibrium. Young [98] developed a simple equation to describe the relationship between the interface force among the three phases, as shown in Fig. 2.14.

$$\gamma_{SG} = \gamma_{SL} + \gamma_{LG} \cos \theta \quad (2.44)$$

where $\gamma_{SG}, \gamma_{SL}, \gamma_{LG}$ represent solid-gas surface tension, solid-liquid surface tension and liquid-gas surface tension, respectively. Subsequently, this predicts the contact angle of a liquid droplet on a solid surface from knowledge of the three surface energies involved.

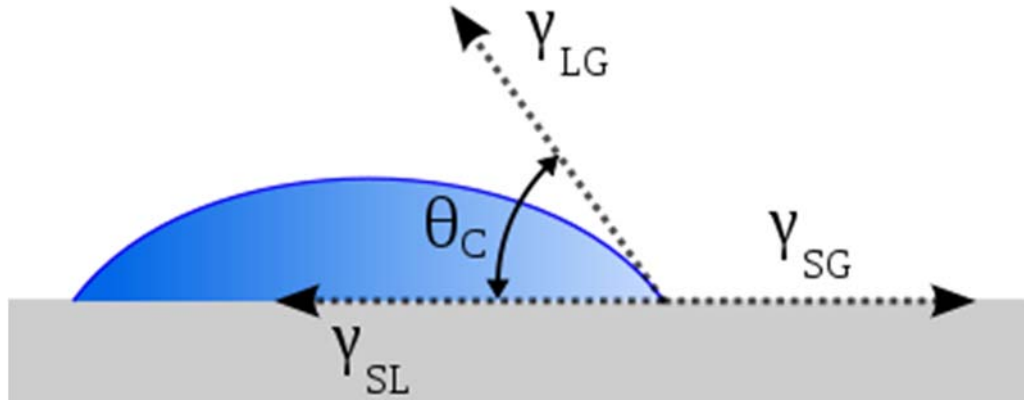


Fig. 2.14 Contact angle of the liquid droplet on the solid surface

As Young Equation can only be applied in ideal smooth solid surface, many investigators developed improved models based on Young Equation to describe the force equilibrium on rough solid surface. Amongst the existing models, Wenzel model [99] and Cassie-Baxter model [100] are the two main models that attempt to describe the wettability on rough solid surface.

Wenzel [99] developed an equation to describe the relationship between the apparent contact angle on rough solid surface and the ideal contact angle on smooth surface calculated by Young Equation. Fig. 2.15(a) shows the schematic of Wenzel model.

$$\cos \theta_r = r \cos \theta \quad (2.45)$$

where θ_r is the apparent contact angle on rough solid surface and θ is the ideal contact angle on ideal smooth solid surface. r is the roughness ratio, which is defined as the ratio of the actual area of the solid surface to the apparent area. In Wenzel model,

the roughness grooves of the solid surface was assumed to be fully filled with liquid, as shown in Fig. 2.15(a), therefore, the roughness ratio r was usually bigger than one.

As the small grooves of the solid surface cannot be filled by the liquid due to the surface tension effect in some cases, Cassie and Baxter [100] developed a compound model based on Wenzel model. In Cassie-Baxter model, the roughness grooves was filled by gas instead of liquid, as shown in Fig. 2.15(b). Two wetting area factors, f_1 and f_2 , were introduced in the model. f_1 represents the ratio of the contact area between the liquid and the solid surface to the total area, while f_2 represents the ratio of the contact area between the liquid and gas in the roughness grooves to the total area.

$$\cos \theta_c = f_1 \cos \theta + f_2 \cos \theta_g \quad (2.46)$$

where θ_g is the contact angle of the liquid in the air, which is usually assumed to be 180° . Therefore, Equation (2.125) can be simplified as follows:

$$\cos \theta_c = f_1 (\cos \theta + 1) - 1 \quad (2.47)$$

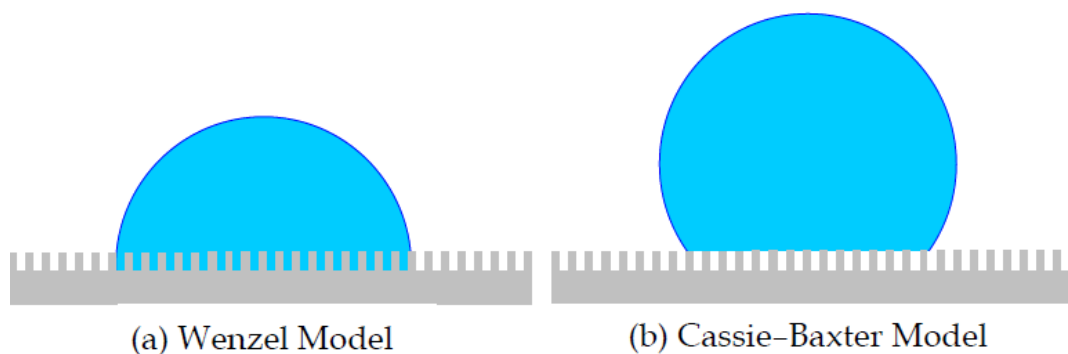


Fig. 2.15 Models for rough surface

2.6.2 Preparation of super-hydrophilic surfaces

The enhancement of hydrophilicity of surfaces can be achieved through either deposition of a molecular or microscopic film of a more hydrophilic chemical, or by modification of the chemistry of the substrate surface. Molecular modification or deposition of coatings is more common for inorganic substrates. Modification of surface chemistry is broadly used in the case of polymeric materials. In this section, these two methods are briefly reviewed.

(1) Deposited molecular structures

Many organic molecules can be used to deposit on the solid surface and change the wetting characteristics [101]. The most commonly studied densely packed molecular structures include alkanethiols on gold, silver, copper, platinum, and palladium, as

well as chlorosilanes on silicon oxide, aluminium, titanium and other oxides. Both mono- and multi-layers can be deposited on the solid surface mechanically with Langmuir–Blodgett film technique. Deposited organic layers can make the surface hydrophilic as the end group is polar.

In addition to arranging self-assembled monolayers of chemically bonded short functional molecules on solid surfaces, a great deal of research has focused on macromolecules and biomacromolecules coating and this technology is especially popular in modification of polymers [102]. Albumin and heparin have been widely used as the biomacromolecules.

(2) Modification of surface chemistry

Many approaches, such as plasma, corona, flame, photons, electrons, ions, X-rays, g-rays, and ozone, have been developed to change the chemistry of polymer surfaces without affecting their bulk properties [103, 104]. In both plasma and corona treatments, the accelerated electrons bombard the polymer with energies 2-3 times that necessary to break the molecular bonds, producing free radicals which generate cross-linking and react with surrounding oxygen to produce oxygen-based functionalities [105]. In flame treatment, surface combustion of the polymer takes place with formation of hydroperoxide and hydroxyl radicals [106].

UV is another treating methods of polymer surface. The exposure of the polymer to UV radiation causes chain scission, crosslinking, and increases the density of oxygen-based polar groups at the substrate surface, making the surface more hydrophilic. As UV light has a wavelength from 10 nm to 400 nm, the incident photons have enough energy for breaking intermolecular bonds of most of the polymers, promoting structural and chemical changes of the macromolecules [107].

2.6.3 Application of super-hydrophilic surfaces

Super-hydrophilic surfaces can be used in many engineering fields for its special properties of liquid on solid surface.

(a) Anti-fogging surfaces

In recent years, the demand for anti-fogging surface arises rapidly in response to the challenge of visualization in humid environment. As the humidity ratio is related with the temperature, the variation of the temperature can lead to the condensation of the moisture. Therefore, the initial transparent surface will fog and lose the optical clarity due to the water droplets on the surface. It is necessary to develop technologies to prevent the condensation of the moisture or quickly remove the water droplets on surface.

The super-hydrophilic surface can be used to solve the problem. On super-hydrophilic surface, thin film instead of water droplets will be formed when the moisture condenses. Fig. 2.16 shows the comparison of the condensation and optical clarity of polyester films under high relative humidity [108]. The right side is the plasma-treated super-hydrophilic polyester film while the left side is the untreated polyester film. As shown in Fig. 2.16, the plasma-treated super-hydrophilic polyester film remained clear due to the formation of a continuous water film while the untreated polyester film was covered by the water droplets, losing the optical clarity.

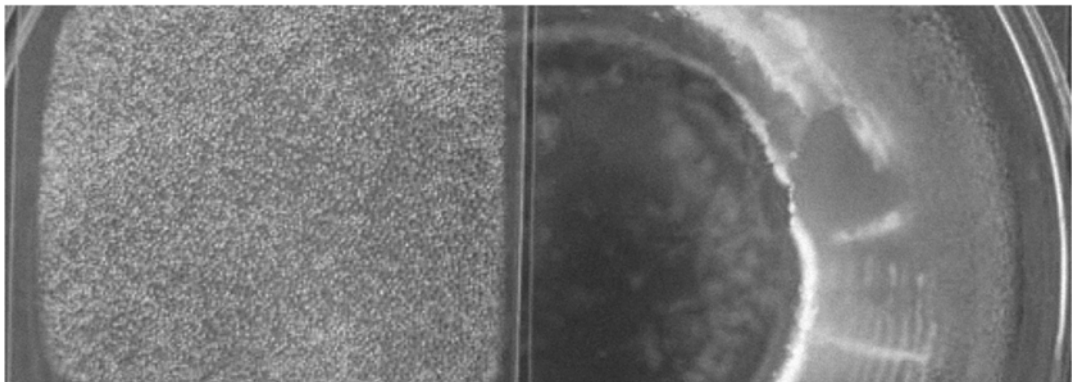


Fig. 2.16 Comparison of the condensation and optical clarity of polyester films under high relative humidity [108]

(b) Enhanced boiling heat transfer

Boiling, as one of the most efficient cooling approach, is widely used in many engineering fields, such as nuclear power plants, refrigeration, cooling of electronics and chemical reactors [109]. The heat transfer performance of boiling is significantly

affected by the wettability of the surface. Fig. 2.17 shows a boiling curve correlating the heat flux with wall superheat [110]. Nucleate boiling starts from point A, with vapor bubbles forming on the overheated surface. The nucleate boiling continues to fully develop from B to C. At point C, the heat flux eventually reaches its maximum value, known as critical heat flux (CHF). Beyond CHF, a continuous vapor film is formed as an effective thermal insulation layer between the coolant and the device surface. Further heating beyond CHF will lead to a dramatic increase of wall temperature and thus device failure. Therefore, CHF marks the maximum heat flux that can be provided by a boiling-based cooler.

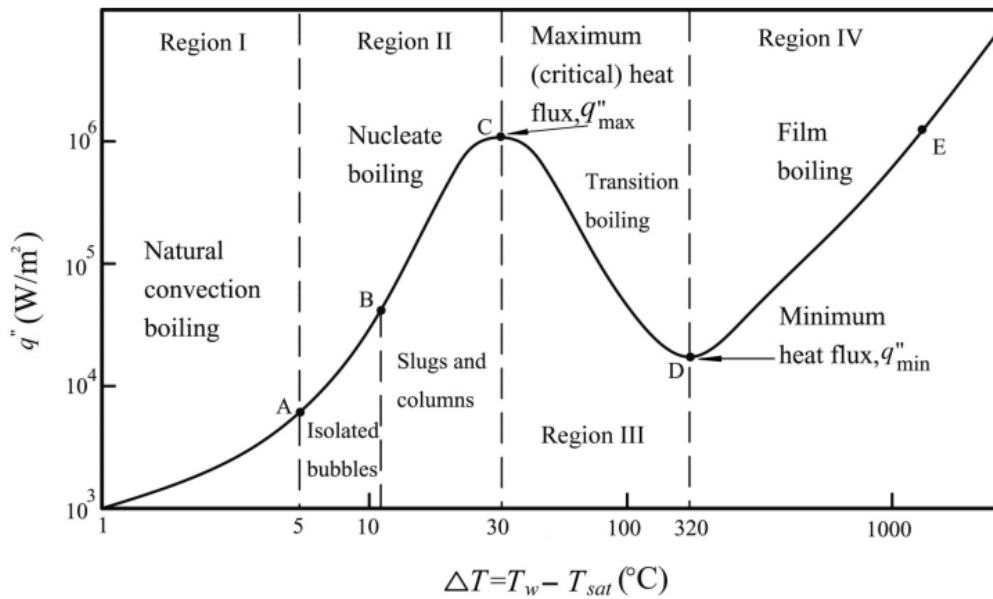


Fig. 2.17 A boiling curve correlating the heat flux with wall superheat

It was investigated that the continuous water film formed on the super-hydrophilic coating can effectively decay the formation of vapor film in boiling process and thus

improve the CHF [111,112]. Chen et al. [113] experimentally investigated the effect of super-hydrophilic surface on the heat transfer performance and indicated that heat transfer coefficient (HTC) have been improved by more than 100%. Such improvements have been attributed to the dramatically increased density of nucleation sites, high surface tension forces of super-hydrophilic nano-structures for pumping in fresh liquid and the cavity stability provided by the nano-pores.

(3) Prevention of bio-fouling

In marine engineering, bio-fouling is a serious problem caused by the growth of microorganisms, algae, plant, etc., on the surface immersed in the seawater. The fouling usually changes the original property of the surface negatively and significantly impacts the performance of the device or equipment. As the surface chemistry can significantly affect the fouling, researchers tried to change the chemistry of the surface and then reduce the bio-fouling. It was found that for high surface energy materials, the degree of fouling decreases as the surface energy increased. For surface with high surface energy, the strong affinity between the water and surface can establish a barrier to prevent the interaction between the fouling agent and the surface. Meng [114] found that the fouling was effectively reduced by fluorescein and fluorescent proteins after the surface was treated to be super-hydrophilic.

2.7 Research gaps and methodology

An extensive literature review of falling film liquid desiccant air dehumidification system and heat/mass transfer enhancement methods is conducted in this chapter. Although many efforts have been conducted in this research area, there still exist several limitations. The research gaps are summarized as follows.

- (1) The dehumidification efficiency of the plate liquid desiccant dehumidifier is relatively low due to the incomplete wetting conditions. The effective and industrially feasible performance enhancing methods of liquid desiccant dehumidifiers are limited.
- (2) The effect of solid-liquid interaction on dehumidification performance is rarely investigated. The mechanism for the influencing effect of surface properties on dehumidification performance is unclear. Solid-liquid interaction is not considered in existing mass transfer correlations for liquid desiccant dehumidifiers.
- (3) The shrinkage phenomenon in falling film dehumidifier is rarely investigated. The prediction models of the accurate wetting area in falling film dehumidifier are limited.
- (4) The wetting area is usually assumed to be constant in existing heat and mass transfer models of falling film liquid desiccant dehumidifiers without considering solid-liquid interaction effect, which does not accord with the facts. In addition, the effect of surface wettability on heat and mass transfer performance during dehumidification process is rarely investigated.

To solve existing problems, both experimental and theoretical approaches are adopted.

The research flowchart of this thesis is presented in Fig. 2.18.

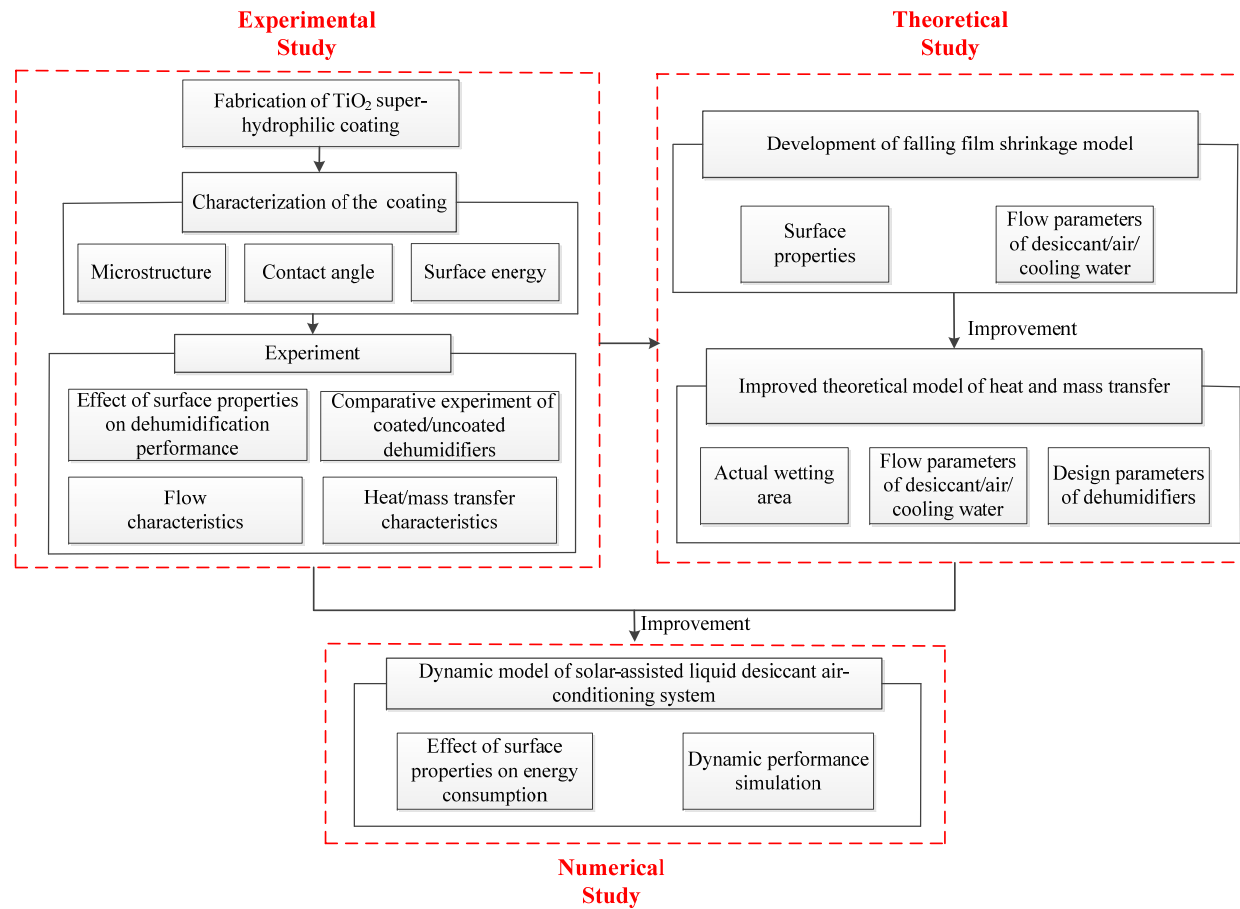


Fig. 2.18 Research flow chart of the thesis

Firstly, an experimental setup of a single-channel falling film liquid desiccant dehumidifier with substitutable working plates is fabricated to investigate the effect of surface wettability on dehumidification performance. Several commonly-used plate dehumidifiers, i.e., Stainless plate dehumidifier, Titanium plate dehumidifier and Polytetrafluoroethylene (PTFE) plate dehumidifier, with distinctive surface properties are adopted in this thesis. The microscopic surface structures of different working plates are investigated with Scanning Electron Microscope (SEM) test. The contact angle of desiccant solution and surface free energy are also investigated to characterize the plate dehumidifiers. The effect of surface wettability on flow and heat/mass characteristics are investigated experimentally.

Based on the analysis of surface wettability on dehumidification performance, surface modification technology is adopted in this project to significantly improve the surface wettability of falling film plate dehumidifiers. A novel super-hydrophilic coating is developed using nanoscale TiO_2 particles to significantly improve the surface wettability. The characterization of the novel coating is conducted in terms of microscopic structures, contact angles and surface free energy.

Then, an experimental setup with two single-channel internally-cold liquid desiccant dehumidifier is fabricated. One plate dehumidifier is treated with TiO_2 super-

hydrophilic coating, while the other is just cleaned with ethanol. A comprehensive investigation on dehumidification performance of coated and uncoated liquid desiccant plate dehumidifiers are conducted. The mechanism of performance enhancement by TiO_2 super-hydrophilic coating is investigated in detail. Besides, the effect of operating parameters, including the flow rates, temperature and concentration of liquid desiccant solution, flow rates, temperature and humidity of processed air as well as the flow rates and temperature of the cooling fluid, on dehumidification performance are comprehensively analysed. Finally, a novel mass transfer correlation of liquid desiccant plate dehumidifiers considering solid-liquid interaction effect is developed.

Based on the experimental results, an improved heat and mass transfer model considering solid-liquid interaction effect of the internally-cold liquid desiccant plate dehumidifier is developed. The contact angles of desiccant solution are considered in newly-developed model to account for the effect of solid-liquid interaction effect on flow and heat/mass transfer performance. The shrinkage of falling film in liquid desiccant plate dehumidifier is theoretically investigated and a shrinkage model is developed to accurately estimate the actual wetting area of desiccant solution on working plate. The model is well validated by the experimental results. Then, the effect of surface wettability on dehumidification performance is investigated theoretically

using the new model. Besides, the distribution of air parameters along the flow direction in plate dehumidifier is estimated.

Finally, a dynamic energy consumption model of solar-assisted liquid desiccant air-conditioning system considering solid-liquid interaction effect is developed. A typical commercial building in Hong Kong is selected as a case building to analyse the solid-liquid interaction effect on energy consumption of the whole liquid desiccant air-conditioning system. Besides, the effect of solar collectors on system energy consumption is also investigated.

CHAPTER 3

ANALYSIS OF SURFACE PROPERTIES ON FLOW AND HEAT/MASS TRANSFER PERFORMANCE FOR FALLING FILM LIQUID DESICCANT DEHUMIDIFIERS

3.1 Introduction

Surface property, which affects both flow and heat/mass transfer characteristics during dehumidification process, is one of the key influencing factors on dehumidification performance. This chapter aims to investigate the effect of surface properties on dehumidification performance. Both flow and heat/mass transfer characteristics in plate dehumidifiers with different surface properties are comprehensively investigated, and the main academic contributions are summarized as follows:

(1) An experimental setup with single-channel falling film liquid desiccant dehumidifiers is fabricated to investigate the surface properties on flow and heat/mass transfer characteristics. The single-channel structure is used to measure the wetting area and variable falling film thickness, which is very useful in analyzing the influencing mechanism of surface properties.

(2) Three commonly-used plate dehumidifiers, i.e., Stainless plate dehumidifier,

Titanium plate dehumidifier and Polytetrafluoroethylene (PTFE) plate dehumidifier, with distinctive surface properties are adopted to analyze the influence solid-liquid interaction effect on dehumidification efficiency. The surface properties of plate dehumidifiers are well characterized in terms of microscopic surface structure, heat conductivity, contact angle and surface free energy.

(3) The flow characteristics of liquid desiccant falling film in plate dehumidifiers with different surface properties are experimentally investigated in terms of wetting area and falling film fluctuation. The effect of flow parameters on wetting area and film thickness are experimentally investigated.

(4) More than 150 experimental conditions are conducted for plate dehumidifiers with different surface properties. The influence of surface properties on dehumidification performance is comprehensively analyzed.

(5) The effect of operating parameters i.e., solution flow rates and temperature, air flow rates and temperature, air humidity and cooling water temperature, on dehumidification performance for plate dehumidifiers with different surface properties are discussed in detail.

3.2 Description of experimental test rig

3.2.1 Experimental setup

An experimental setup of single-channel liquid desiccant dehumidifier with substitutable working plates was fabricated to investigate the effect of surface properties on dehumidification performance, as shown in Fig. 3.1. Three commonly-used plate dehumidifiers, i.e., Stainless plate dehumidifier, Titanium plate dehumidifier and Polytetrafluoroethylene (PTFE) plate dehumidifier, were adopted in this study. The experimental setup mainly consisted of three sub-systems, i.e., the air supply system (green line), the liquid desiccant supply system (red line) and the cooling water system (blue line).

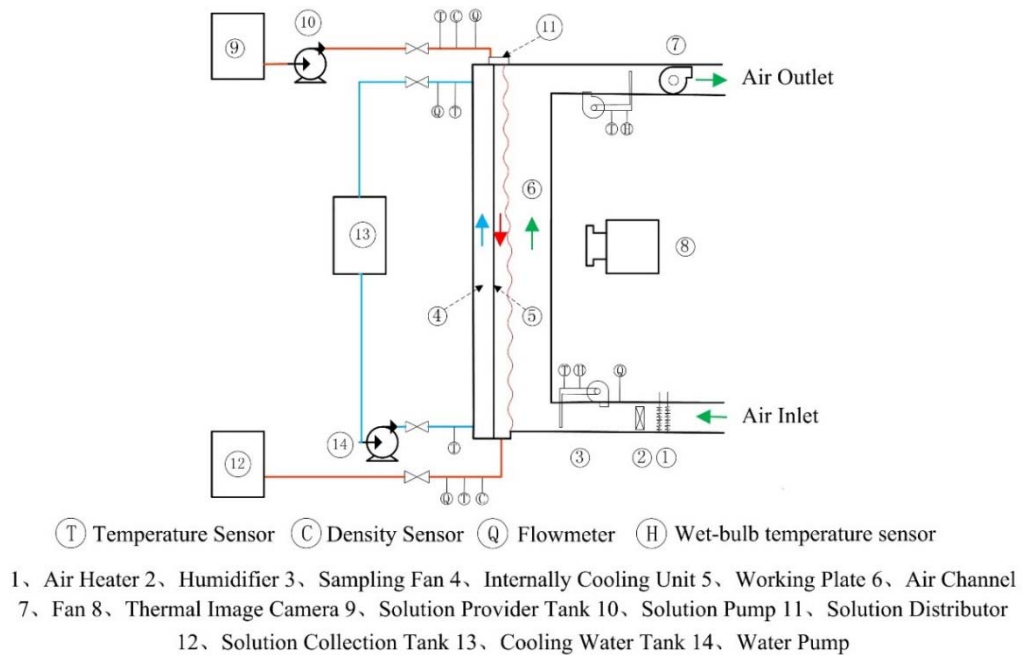


Fig. 3.1 Schematic diagram of the experimental setup

The air was supplied by fans, and then heated and humidified to the required conditions. The processed air interacted with the desiccant solution and the extra moisture exchanged from processed air to desiccant solution. Finally, the dry air flowed out at the top of the dehumidifier.

The liquid desiccant solution was supplied by a plastic magnetic pump and well distributed on working plates by the newly-designed liquid distributor. After absorbing the extra moisture of processed air, the weak solution was collected and regenerated in regeneration system which was driven by solar energy. The inlet and outlet liquid desiccant temperatures, density and flow rate were measured simultaneously in the experiment.

Besides, the latent heat released in absorption process could increase the solution temperature and deteriorate the dehumidification performance. Therefore, an internal cooling unit was designed to take away the released latent heat. In addition, ⑤ in Fig. 3.1 represents the working plate which is substitutable during the experiment. Different plate dehumidifiers, i.e., Stainless plate dehumidifier, Titanium plate dehumidifier and PTFE plate dehumidifier, were used to analyse the influence of plate properties on dehumidification performance.

As contact area between processed air and desiccant solution was critical to

dehumidification capacity, a thermal image camera was utilized to record the shapes of the solution film and then to calculate the wetting area on different working plates. A picture processing software package was used to detect the actual wetting area of falling film in the thermal images. Besides, the film thickness was measured by a capacitance micrometer.

To achieve the even distribution of the liquid desiccant falling film, a new solution distributor was designed, as shown in Fig. 3.2. Three entrance holes were set up at the top of the distributor to ensure the even inlet of the desiccant solution. It was observed that some eddies occurred as the desiccant solution flowed from the inlet pipe to the chamber of the distributor. These eddies could lead to unstable solution levels, which seriously affected the distribution of the desiccant solution. To reduce the effect of the solution eddies on the solution distribution, a baffle was fixed inside the distributor which separated the chamber into two parts. The desiccant solution firstly flowed into Chamber I and stored. When the solution level was above the baffle, the solution began to flow over the baffle smoothly. The effect of the solution eddies was effectively eliminated by the baffle. In addition, an outlet slot was opened in Chamber II and the even distribution of the falling film could be achieved once the solution level was above the outlet slot.

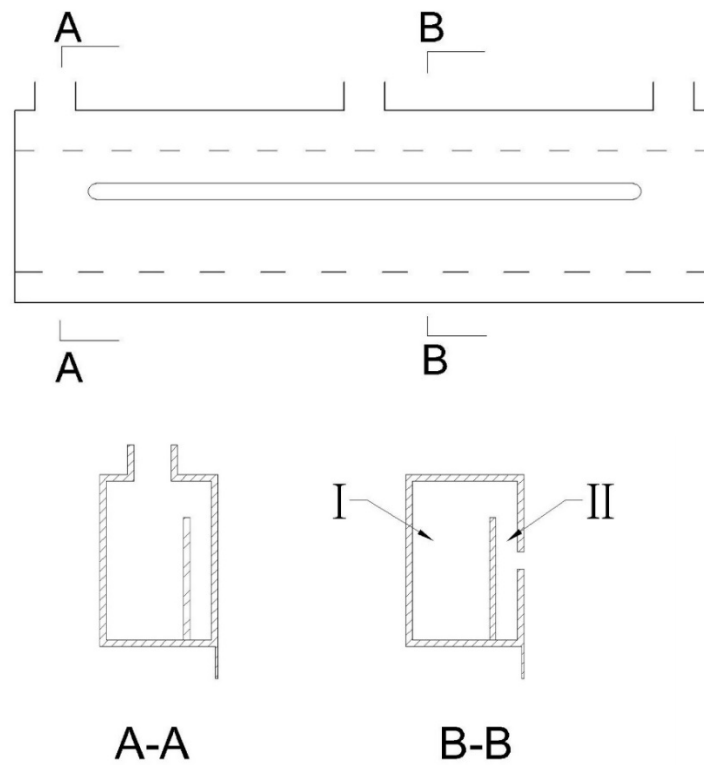


Fig. 3.2 Schematic diagram of the solution distributor

3.2.2 Measuring and controlling devices

In the experiment, the inlet parameters of processed air, liquid desiccant solution and cooling water were controlled and adjusted. The air flow rate was controlled by the voltage regulator of the fan. The air temperature was regulated by the air heater with PID controller and the air humidity by the electromagnetic humidifier which was controlled by adjusting the input voltage. In addition, the solution flow rate was regulated by the valve installed at the outlet of the pump and the temperature was controlled by the heat exchanger fixed inside the solution tank. These main devices in the experiment are presented in Fig. 3.3.



(a) Air humidifier



(b) Air heater



(c) Water chiller



(d) Air fan



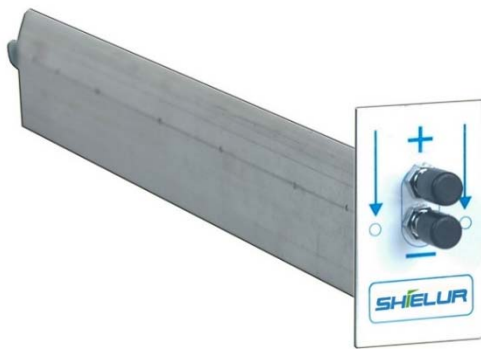
(e) Magnetic pump



(f) Control board

Fig. 3.3 Main devices in the experimental setup

The inlet and outlet parameters of processed air, liquid desiccant solution and cooling water were measured for each test. The temperature was measured by platinum resistance temperature detectors (Pt RTDs). The air flow rate was measured by air velocity sensors with the accuracy of 0.3%. The desiccant solution and cooling water flow rates were measured by turbine flow rate sensors. Besides, the concentration of the liquid desiccant solution was calculated based on temperature and density which was measured by a specific gravity hydrometer. As the wetting area was one of the key parameters in dehumidification process, a thermal image camera was used to record the wetting area in the experiment. Each test lasted for more than ten minutes under steady conditions and the data were acquired by a data logger. The main measuring devices are shown in Fig. 3.4 and the specifications are listed in Table 3.1.



(a) Air velocity sensor



(b) Turbine flow rate sensor



(c) Specific gravity hydrometer



(d) Thermal image camera



(e) Data logger

Fig. 3.4 Measuring devices in the experimental setup

Table 3.1 Specifications of different measuring devices

Parameter	Device	Brand	Model	Accuracy	Operational range
Air dry-/wet-bulb temperature	Pt RTD	Heraeus	LN222-A	0.1 K	223-573 K
Air flow rate	Air velocity sensor	Shielur	ASF-100	0.3%	9-10000 Pa
Solution temperature	Pt RTD	Heraeus	LN222-A	0.1 K	223-573 K
Solution flow rate	Turbine flow rate sensor	Gems Sensors	173936-C	3%	0.5-5 L/min
Solution density	Specific gravity hydrometer	Daho	DH-300x	1 kg/m ³	1-99,999 kg/m ³
Cooling water temperature	Pt RTD	Heraeus	LN222-A	0.1 K	223-573 K
Cooling water flow rate	Turbine flow rate sensor	Sea	YF-S201	2%	1-30 L/min

3.2.3 Measurement of falling film thickness

As the liquid desiccant spreads as falling film on the working plates and absorbs the extra moisture of the processed air, the flow characteristics of the falling film are very important to dehumidification performance. Thus, the falling film thickness and its

fluctuation are measured. To investigate the flow characteristics of falling film along the flow direction, two test points are selected to measure the local falling film thickness, as shown in Fig. 3.5. The instantaneous falling film thickness is measured by a Capacitance micrometer (JDC-2008). The fluctuation of the falling film can result in various capacitance between the capacitance probe and the falling film as well as the output voltage of the Capacitance micrometer. As the output voltage is proportional to the falling film thickness, the time-varied falling film thickness is measured accurately.

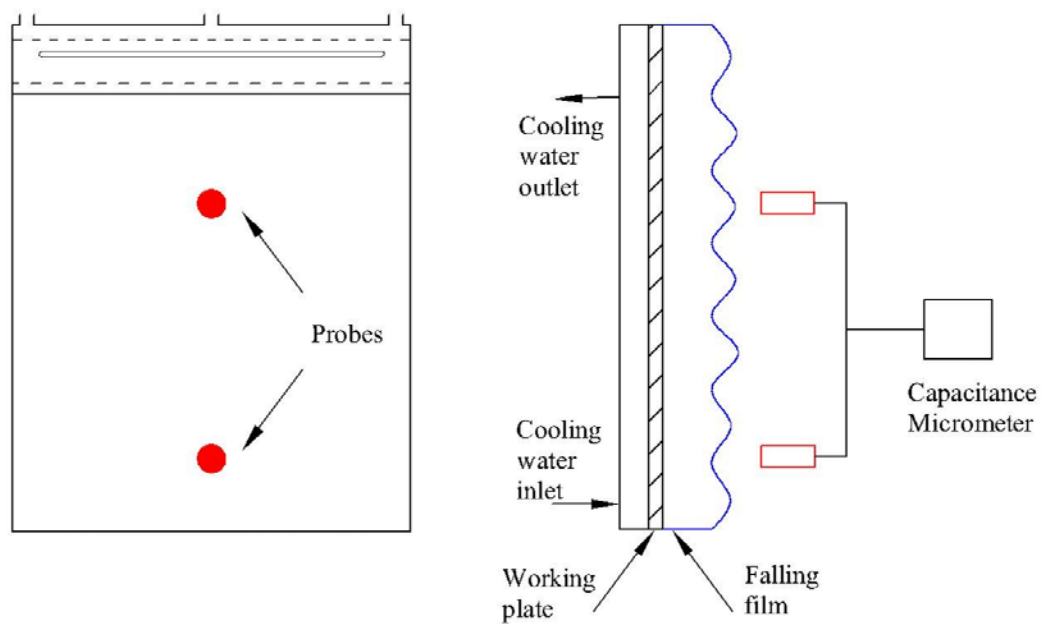


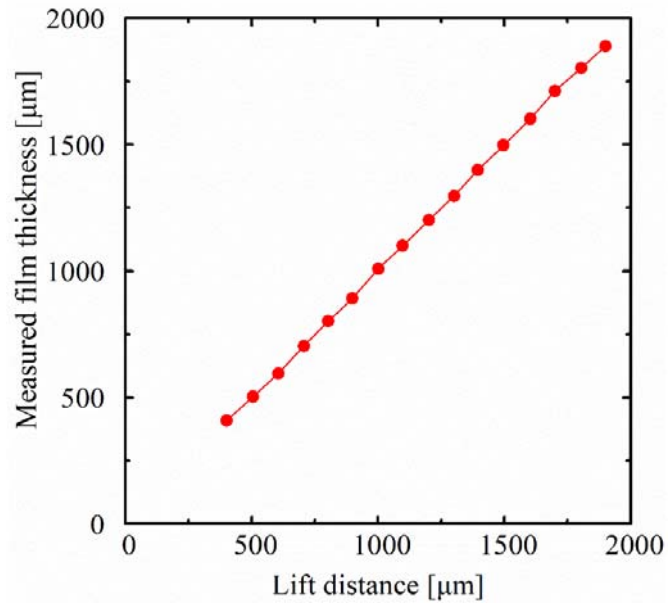
Fig. 3.5 Schematic diagram of falling film measuring system

As the Capacitance micrometer is sensible to the surroundings, calibration is necessary before the experiment. Static calibration is adopted in this experiment. The calibration

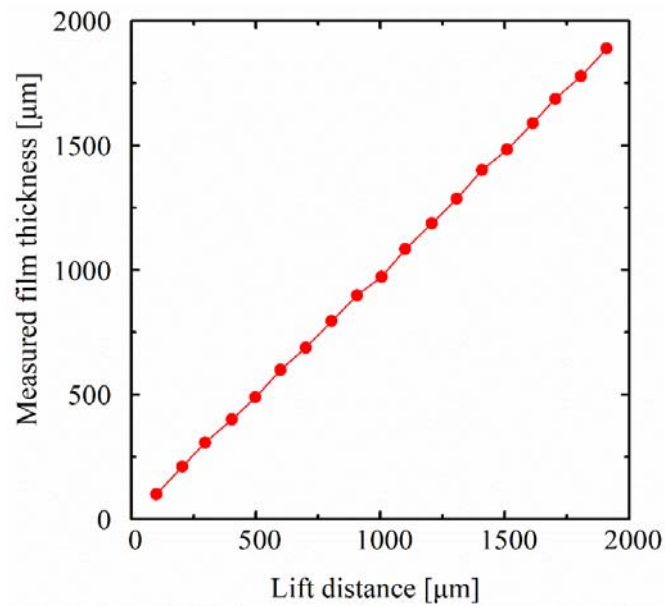
of Capacitance micrometer is conducted using both deionized water and LiCl aqueous solution (39 wt.%). The detailed procedure is presented as follows.

- (1) Fill the metal container with deionized water or LiCl aqueous solution (39 wt.%) and make sure that the bottom of the metal container is fully covered by liquid.
- (2) Put the container on the calibration platform.
- (3) Adjust the lifting platform to linear region of the Capacitance micrometer and make sure that the output voltage of is around 4000 mV.
- (4) Adjust the output voltage of the Capacitance micrometer to zero and lift the metal container with certain distance (around 100 μm). Then record the measured film thickness by the Capacitance micrometer and the accurate lifting distance as well.
- (5) Repeat Sept (4) to obtain the calibration curve.

The calibration curves of the Capacitance micrometer using deionized water or LiCl aqueous solution (39 wt.%) are shown in Fig. 3.6. The calibration results indicate that the measured thickness agrees well with the real thickness for both deionized water or LiCl aqueous solution (39 wt.%).



(a) LiCl aqueous solution (39 wt.%)



(b) Deionized water

Fig. 3.6 Calibration curves of the Capacitance micrometre

3.3 Performance indices and uncertainty analysis

In the experiment, the extra moisture was removed from the process air to the liquid

desiccant due to the superficial vapor pressure difference. To evaluate the dehumidification performance of the plate dehumidifiers, three performance indices, the moisture removal rate, m_ω , the dehumidification efficiency, η_ω , and the mass transfer coefficient, h_D , were introduced. In addition, the performance enhancing ratio ε was proposed to compare the dehumidification performance of the coated and uncoated plate dehumidifiers.

The moisture removal rate, m_ω , represents the moisture handling capacity of the plate dehumidifier and is defined as follows:

$$m_\omega = m_a (\omega_{a,in} - \omega_{a,out}) \quad (3.1)$$

where m_a is the mass flow rate of air, kg/s. $\omega_{a,in}$ and $\omega_{a,out}$ represent the inlet and outlet air humidity, g/kg dry air, respectively.

The dehumidification efficiency, η_ω , is defined as the ratio of the actual moisture change between process air and liquid desiccant to the maximum possible change. η_ω can be calculated as follows.

$$\eta_\omega = \frac{\omega_{a,in} - \omega_{a,out}}{\omega_{a,in} - \omega_{equ,in}} \quad (3.2)$$

where $\omega_{equ,in}$ represents the air absolute humidity in equilibrium with the inlet solution at its temperature and concentration, g/kg dry air.

The mass transfer coefficient h_D represents the mass transfer rate between process air and liquid desiccant solution, $\text{g}/(\text{m}^2 \cdot \text{s})$.

$$h_D = \frac{m_a (\omega_{a,in} - \omega_{a,out})}{A \Delta \omega} \quad (3.3)$$

where A is the wetting area of the falling film, m^2 , and $\Delta \omega$ is the mean humidity difference between process air and desiccant solution, g/kg dry air.

As the measuring errors exist in the experimental setup, the uncertainty analysis of the experimental results is necessary. The uncertainty analysis was conducted by using the uncertainty propagation method [115], as shown in Eq. (3.4).

$$\delta U = \sqrt{\left(\frac{\partial U}{\partial x_1} \delta x_1\right)^2 + \left(\frac{\partial U}{\partial x_2} \delta x_2\right)^2 + \left(\frac{\partial U}{\partial x_3} \delta x_3\right)^2 + \dots + \left(\frac{\partial U}{\partial x_n} \delta x_n\right)^2} \quad (3.4)$$

where δU is the uncertainty of the calculated parameter U . δx_1 , δx_2 and δx_3 represent the absolute uncertainty of the measured values, x_1 , x_2 , x_3 . According to Eq. (3.4) and Table 3.1, the uncertainty of the moisture removal rate, dehumidification efficiency and mass transfer coefficient are 3.2%, 3.4% and 5.4%, respectively.

3.4 Results and discussion

3.4.1 Energy conservation and results validation analysis

In this chapter, more than 150 experimental conditions were selected based on Hong Kong climate to investigate the effect of surface properties on dehumidification

performance. The detailed ranges of the experimental conditions are listed in Table 3.2 and part of the experimental conditions are listed in Table 3.3.

Table 3.2 Ranges of the inlet experimental parameters

Parameter	Symbol	Unit	Range
Air temperature	$T_{a,in}$	°C	28.3-40.2
Air humidity	$\omega_{a,in}$	g/kg dry air	13.9-24.6
Air flow rate	$m_{a,in}$	kg/s	0.028-0.079
Solution flow rate	$m_{s,in}$	kg/s	0.015-0.046
Solution temperature	$T_{s,in}$	°C	18.1-30.2
Solution concentration	X_s	%	38%
Cooling water flow rate	m_f	kg/s	0.03-0.10
Cooling water temperature	$T_{f,in}$	°C	16.6-25.9

Table 3.3 Part of the experimental conditions

No.	$T_{a,in}$ (°C)	$\omega_{a,in}$ (g/kg)	$T_{s,in}$ (°C)	$T_{f,in}$ (°C)	m_a (kg/s)	$T_{a,out}$ (°C)	$\omega_{a,out}$ (g/kg)	$T_{s,out}$ (°C)	$T_{f,out}$ (°C)	m_s (kg/s)
1	30.7	21.4	24.5	16.2	0.061	27.0	17.5	25.3	17.7	0.046
2	35.8	21.6	24.4	16.3	0.060	30.2	18.1	25.3	17.8	0.047
3	29.8	17.5	24.9	16.3	0.062	26.8	15.1	25.3	17.4	0.048
4	30.3	21.6	25.2	16.8	0.061	27.9	17.4	25.8	18.8	0.048
5	30.6	21.1	27.3	16.7	0.069	28.8	17.5	28.3	18.1	0.046
6	30.5	21.3	26.0	16.9	0.050	28.3	17.4	26.6	18.1	0.046
7	30.7	21.8	24.4	17.4	0.062	28.0	18.3	26.4	18.6	0.028
8	30.8	21.8	25.1	16.5	0.062	28.7	18.6	28.6	17.8	0.016
9	30.9	22.2	27.0	24.2	0.061	29.3	19.1	27.6	25.2	0.047
10	29.5	21.3	30.1	16.7	0.061	27.8	18.3	30.4	17.8	0.046

The energy conservation analysis is necessary to validate the experimental results. During the experiment, the energy released by processed air should be equal to that absorbed by desiccant solution and cooling water, which is given as follows.

$$m_a(h_{a,in} - h_{a,out}) = (m_{s,out}h_{s,out} - m_{s,in}h_{s,in}) + m_f C_{p,f}(T_{f,out} - T_{f,in}) \quad (3.4)$$

where m_a , m_s and m_f represent mass flow rates of processed air, solution and cooling fluid, respectively. h_a and h_s are enthalpies of processed air and liquid desiccant respectively.

The energy conservation amongst processed air, solution and cooling fluid is shown in Fig. 3.7. Most of the experimental data fell within $\pm 30\%$ with the average relative deviation (ARD) of 4.3%, validating the reliability of the experimental results.

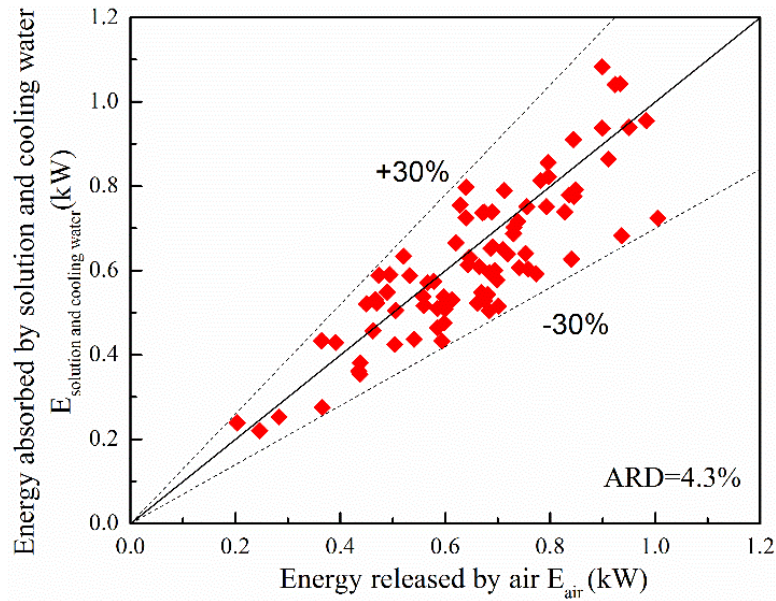
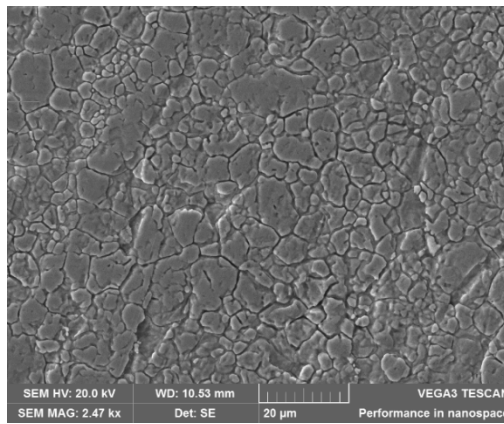


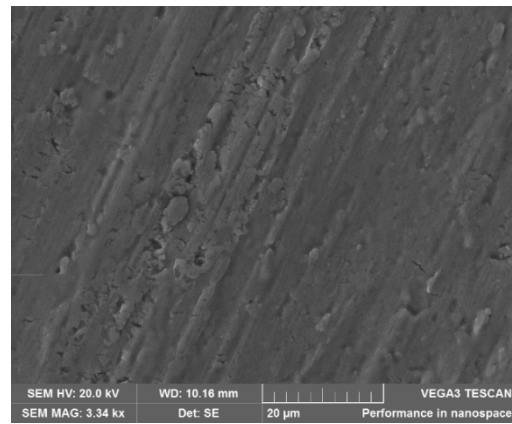
Fig. 3.7 Energy conservation of air, liquid desiccant and cooling water

3.4.2 Characterization of plate dehumidifiers with different surface properties

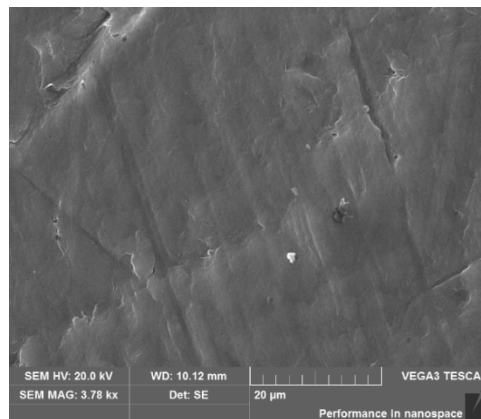
In this chapter, three commonly-used plate dehumidifiers, i.e., stainless steel plate dehumidifier, titanium plate dehumidifier and PTFE plate dehumidifier, with distinctive surface properties were chosen to study the influence of surface properties on dehumidification efficiency. FESEM test was conducted to investigate the plate microstructures. Fig. 3.8 shows the FESEM images of different plate dehumidifiers.



(a) Stainless steel plate



(b) Titanium plate



(c) PTFE plate

Fig. 3.8 FESEM images of different plate dehumidifiers

Apart from the analysis of microscopic structures for different plate dehumidifiers, surface free energy is another key influencing parameter of surface wettability. Therefore, the surface free energy of different plate dehumidifiers are analyzed in this section. Several methods for calculating surface free energy have been proposed based on the partition of the quantity into independent components [116]. In this chapter, Owens-Wendt method [117] is adopted to estimate the surface free energy of different working plates. In Owens-Wendt approach, surface free energy is assumed to be composed of polar and dispersive components.

$$\gamma = \gamma^P + \gamma^D \quad (3.5)$$

where γ^P and γ^D represent polar and dispersive component of surface free energy, respectively.

According to Young Equation [98] and the analysis in this chapter, Owens-Wendt's geometric average equation is shown as follows.

$$\gamma_L (1 + \cos \theta) = 2(\gamma_S^D \gamma_L^D)^{1/2} + 2(\gamma_S^P \gamma_L^P)^{1/2} \quad (3.6)$$

where γ_L and γ_S represent liquid and solid surface free energy, respectively. As both polar component, γ_S^P , and dispersive component, γ_S^D , are unknown in Eq. (3.6), two liquid reagents with known surface free energy and its component, γ_L^P and γ_L^D , are necessary to estimate the surface free energy of solid. Therefore, Eq. (3.6) is rewritten as follows:

$$\gamma_{L1}(1 + \cos \theta) = 2(\gamma_S^D \gamma_{L1}^D)^{1/2} + 2(\gamma_S^P \gamma_{L1}^P)^{1/2} \gamma_L^D \quad (3.7)$$

$$\gamma_{L2}(1 + \cos \theta) = 2(\gamma_S^D \gamma_{L2}^D)^{1/2} + 2(\gamma_S^P \gamma_{L2}^P)^{1/2} \quad (3.8)$$

where the subscripts $L1$ and $L2$ represent two different liquid reagents with unknown surface free energy. The solid surface free energy can be estimated by solving the Eqs. (3.7) and (3.8). In this thesis, deionized water and diiodomethane are used and the contact angles of these liquid reagents on the coated substrates are measured using the contact angle meter (JCY20-13). The detailed surface free energy and its components of deionized water and diiodomethane are presented in Table 3.4.

Table 3.4 Surface free energy and its components of different liquid reagents

Reagents	γ_L	γ_L^P	γ_L^D	γ_L^P / γ_L^D	Polarity
	[mJ/m ²]	[mJ/m ²]	[mJ/m ²]	[mJ/m ²]	
Deionized water	72.80	51.00	21.80	2.36	Polar
Diiodomethane	50.80	2.30	48.50	0.05	Non-polar

The contact angles of liquid reagents on different plate dehumidifiers are presented in Fig. 3.9.

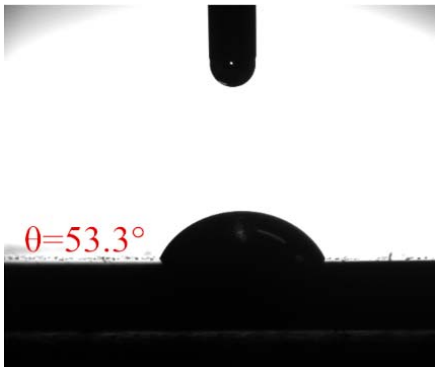
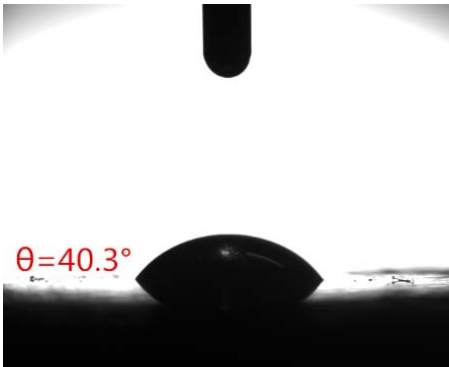

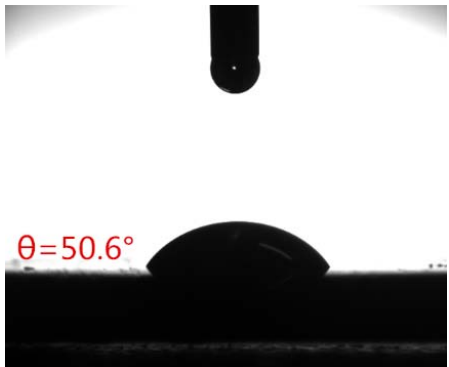
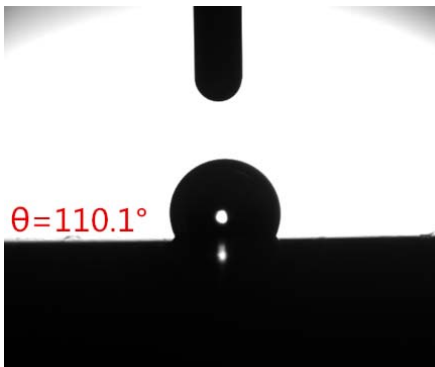
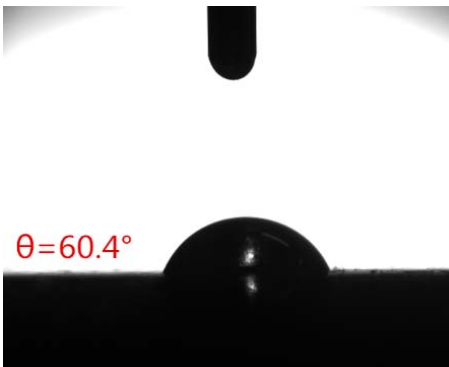
	Deionized water	Diiodomethane
Titanium plate		
Stainless plate		
PTFE plate		

Fig. 3.9 Contact angles of diiodomethane and deionized water in different plate dehumidifiers

Surface free energy is the main index to evaluate the surface wettability due to its independence from the liquid reagents used in the test. As surface free energy represents adhesion between liquid and solid surface, higher surface free energy

represents higher wetting degree. Table 3.5 shows the surface free energy of different working plates calculated based on the contact angels of deionized water and diiodomethane using Owens-Wendt method. The Titanium plate showed the highest surface free energy, indicating that the Titanium plate was most hydrophilic amongst these three different working plates. As the dispersive component of PTFE plate was almost equal to zero, its low surface free energy represented strong repellence between liquid and PTFE surface. Besides, the wettability difference between working plates will be shown below in terms of wetting area.

Table 3.5 Surface free energy of different plate dehumidifiers

	Dispersive component	Polar component	Surface free energy
	γ_s^D [mJ/m ²]	γ_s^P [mJ/m ²]	γ_s [mJ/m ²]
Titanium plate	29.45	21.16	50.61
Stainless plate	33.83	3.15	36.98
PTFE plate	30.28	0.06	30.34

The thermal properties of the plate dehumidifiers are also important to dehumidification performance, especially in internally-cooled liquid desiccant dehumidifier. Table 3.6 presents the physical properties, i.e., thermal conductivity, melting point and extension strength, of different plate dehumidifiers.

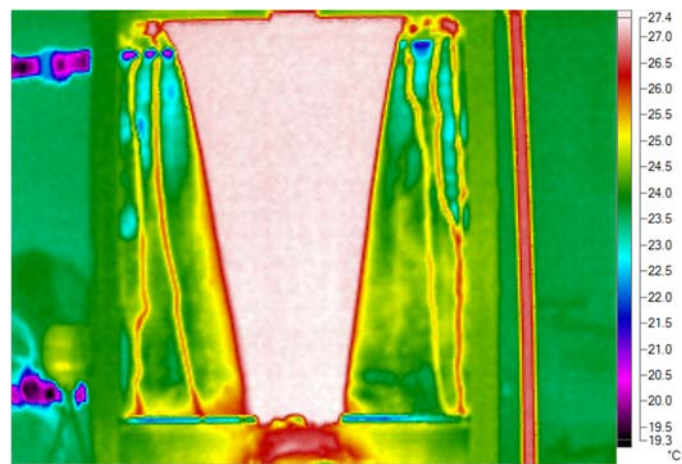
Table 3.6 Physical properties of different plate dehumidifiers

	Thermal conductivity [W/(m · K)]	Temperature interval [°C]	Extension strength [MPa]
Titanium plate	15.24	1725 (melting point)	370-530
Stainless plate	16.3	1500 (melting point)	>520
PTFE plate	0.25	<250	22.0-35.0

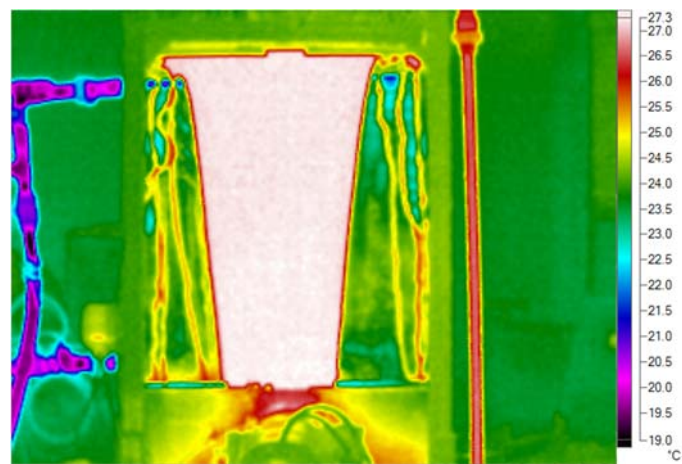
3.4.3 Flow characteristics of falling film in plate dehumidifiers with different surface properties

3.4.3.1 Wetting ratio

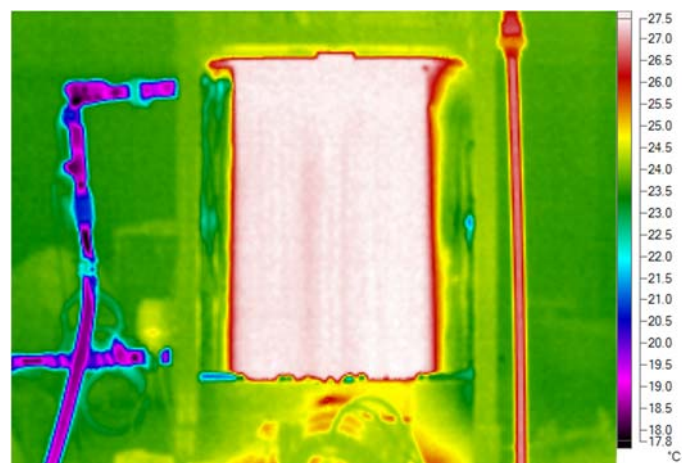
Wetting area of desiccant solution in plate dehumidifiers is an important influencing parameter for dehumidification performance. In this study, the wetting area was captured by a thermal image camera. Fig. 3.10 presents the thermal images of desiccant solution film in different plate dehumidifiers. In PTFE plate dehumidifier, the falling film of desiccant solution shrank sharply along the flow direction with the initial wetting length of 45 cm and the outlet wetting length of only 16 cm, reducing the contact area between solution and humid air rapidly. However, the falling film of desiccant solution shrank slightly in Titanium plate dehumidifier due to higher surface free energy, which improved the dehumidification performance.



(a) PTFE plate dehumidifier



(b) Stainless steel plate dehumidifier



(b) Titanium plate dehumidifier

Fig. 3.10 Thermal images of falling film in different plate dehumidifiers

The wetting ratio, ϕ_A , was adopted to analyze the wetting area in different plate dehumidifiers. Fig. 3.11 shows the variation of wetting ratio with solution flow rates in different plate dehumidifiers. The desiccant flow rates demonstrate positive effect on wetting ratios for all plate dehumidifiers. It was found that the wetting ratio in Titanium plate dehumidifier was much higher than that of PTFE plate dehumidifiers. The highest wetting ratio was attributed to the little shrinkage of falling film in Titanium plate dehumidifiers, as shown in Fig. 3.10. The maximum wetting ratios were around 89%, 75% and 61% for Titanium plate dehumidifier, Stainless steel plate dehumidifier and PTFE plate dehumidifier, respectively. Besides, the minimum wetting flow rate in Titanium plate dehumidifier was around 0.018 kg/s, which was the smallest among these three different plate dehumidifiers. The minimum wetting flow rate represents the minimum required solution flow rate to avoid the falling film breakdown. This lowest minimum wetting flow rates for Titanium plate dehumidifier resulted from the highest surface free energy.

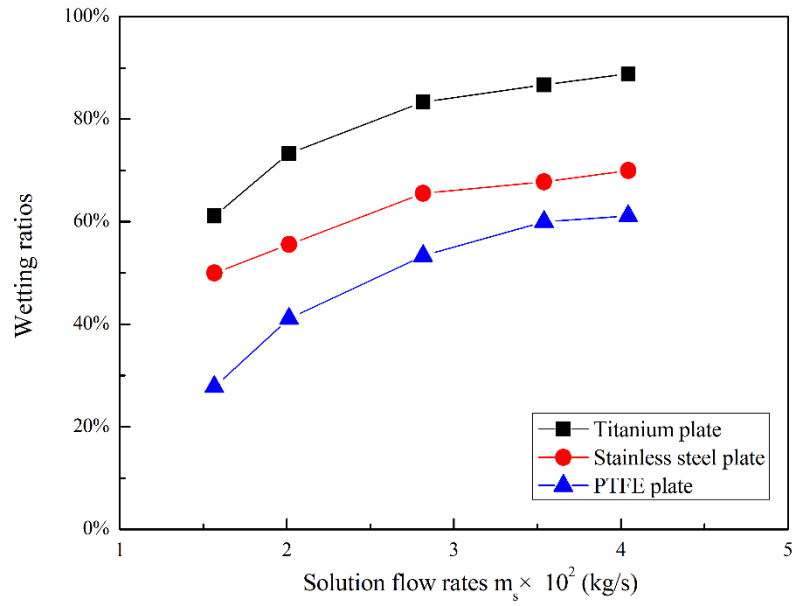


Fig. 3.11 Effect of solution flow rates on wetting ratios in different plate dehumidifiers

3.4.3.2 Falling film thickness

As the extra moisture of processed air is absorbed by the liquid desiccant spreading as thin film in plate dehumidifier, the fluctuation of falling film is very important to dehumidification performance. To investigate the flow characteristics of the falling film in surface-modified plate dehumidifier, a Capacitance micrometer is used to measure the time-varying falling film thickness. Two test points are selected and the detailed arrangement of the test probes is shown in Fig. 3.11. The mean falling film thickness, i.e. time- and location-averaged thickness, is proposed to characterize the flow characteristics.

$$\bar{\delta} = \frac{1}{2n} \left(\sum_{i=0}^n \delta_L + \sum_{i=0}^n \delta_U \right) \quad (3.9)$$

where n is the number of data acquired in each test. L and U represent the lower test point and the upper test points, respectively.

The present research of flow characteristics for falling film mainly focuses on tube falling film. The research of plate falling film is limited. To better investigate the flow characteristics of falling film, several existing correlations of the mean falling film thickness are summarized, as given in Table 3.7.

Table 3.7 Correlations of mean film thickness for tubes

Resources	Correlations	Ranges
Nusselt [118]	$\delta = 0.909 \left(\frac{\nu^2}{g} \right)^{1/3} Re^{1/3}$	$0 < Re < 1000 \sim 2000$
Ganchev et al. [119]	$\delta = 0.137 \left(\frac{\nu^2}{g} \right)^{1/3} Re^{0.58}$	[-]
Gimbutis [120]	$\delta = 0.136 \left(\frac{\nu^2}{g} \right)^{1/3} Re^{0.583}$	[-]
Takahama and Kato [121]	$\delta = 0.228 \left(\frac{\nu^2}{g} \right)^{1/3} Re^{0.526}$	[-]
Karapantsios et al. [122]	$\delta = 0.214 \left(\frac{\nu^2}{g} \right)^{1/3} Re^{0.538}$	$509 < Re < 13090$
Jiang and Yan [123]	$\delta = 0.295 \left(\frac{\nu^2}{g} \right)^{1/3} Re^{0.498}$	$400 < Re < 5000$

Fig. 3.12 presents the variation of mean falling film thickness in different plate dehumidifiers. The mean falling film thickness increases slightly with the liquid desiccant Reynolds number. The falling film in PTFE plate dehumidifier is the thickest amongst these three different plate dehumidifiers. This phenomenon can be explained by the fact that the wetting area of desiccant solution in PTFE plate dehumidifier is the lowest due to the severe shrinkage along the flow direction. As the falling film thickness depends on wetting area under certain flow rate, the lowest wetting area results in the thickest falling film thickness. Besides, the measured falling film thickness in Titanium plate dehumidifier agrees well with Nusselt equation [118] which was developed from the experimental results of falling film in pipes. However, the measured falling film thicknesses in Stainless steel plate dehumidifier and PTFE plate dehumidifier are higher than the calculated values by Nusselt equation [118]. The reason is that no shrinkage is considered in Nusselt equation [118], which does not accord with the actual situations in Stainless steel and PTFE plate dehumidifiers.

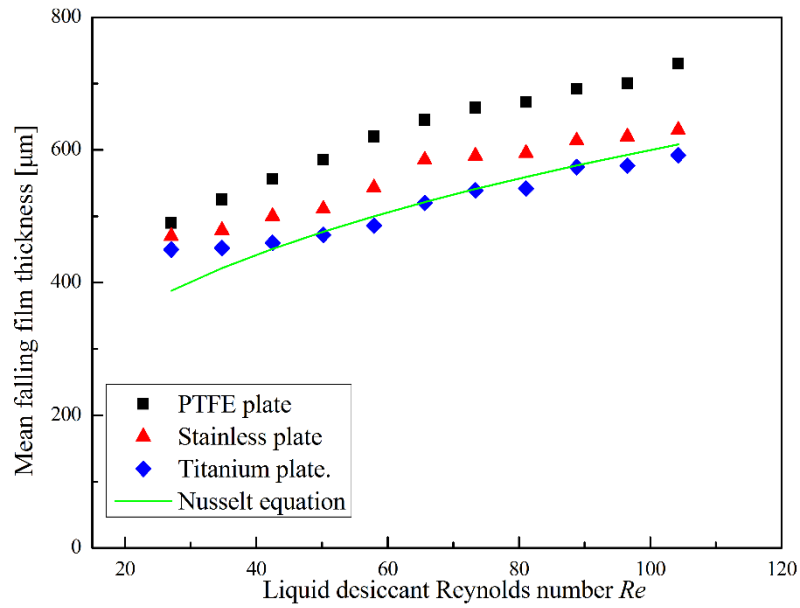
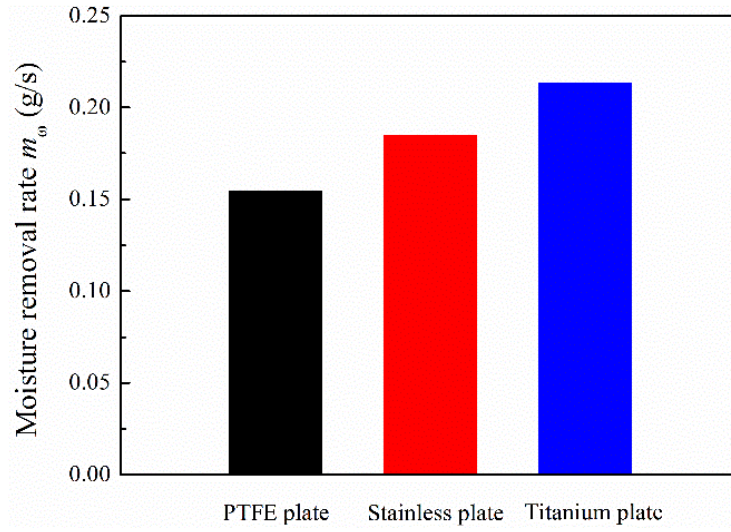


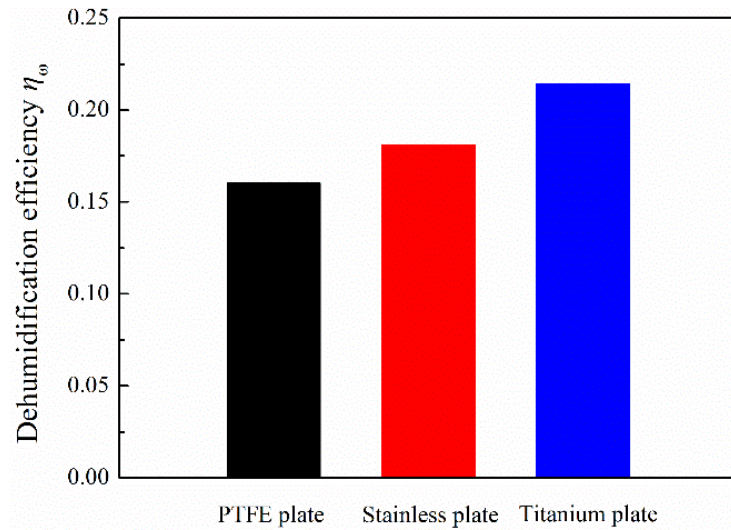
Fig. 3.12 Mean falling film thickness in different plate dehumidifiers

3.4.4 Dehumidification performance analysis

Fig. 3.13 presents the dehumidification performance of three different liquid desiccant dehumidifiers. Titanium plate dehumidifier achieved superior dehumidification capacity compared with the other plate dehumidifiers. This difference is attributed to several reasons. Firstly, the wetting area on Titanium plate dehumidifier is the largest, as shown in Fig. 3.10, due to the highest surface free energy and lowest contact angle, which contributes significantly to the dehumidification performance. Secondly, the falling film on Titanium plate dehumidifier is the thinnest, as shown in Fig. 3.12, which reduces the mass transfer resistance. Besides, the heat conductivity of Titanium plate is much larger than that of PTFE plate and the latent heat is quickly removed by cooling water in Titanium plate dehumidifier.



(a) Moisture removal rate m_ω



(b) Dehumidification efficiency η_ω

$T_{a,in}$	$\omega_{a,in}$	$m_{a,in}$	$T_{s,in}$	$m_{s,in}$	$T_{f,in}$
(°C)	(g/kg)	(kg/s)	(°C)	(kg/s)	(°C)
36	21.0	0.061	24.6	0.047	16.5

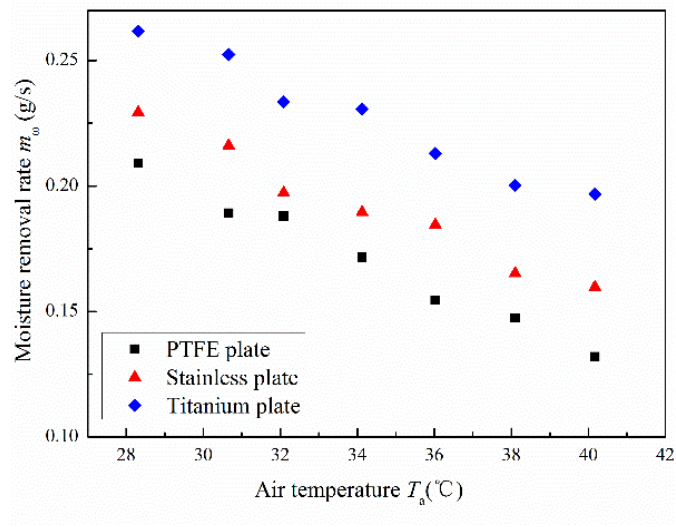
Fig. 3.13 Comparison of dehumidification performance in different plate dehumidifiers

3.4.5 Analysis of influencing factors on dehumidification performance

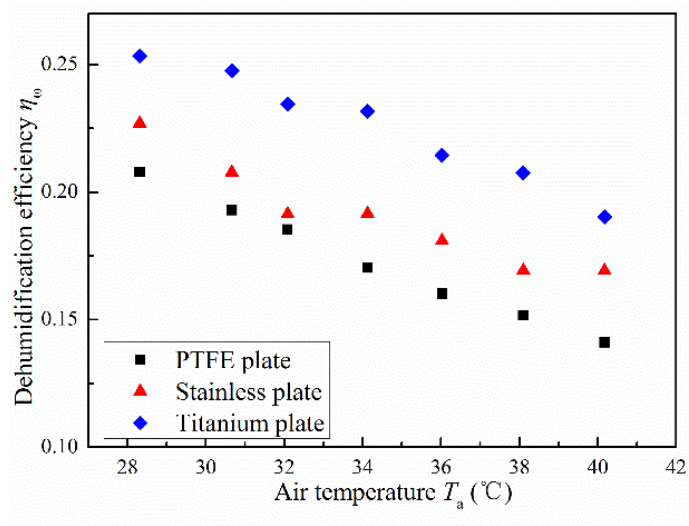
To analyze the dehumidification characteristics of different plate dehumidifiers, controlling variable method (CVM) was adopted in the experiment. The influence of flow parameters on dehumidification capacity in different plate dehumidifiers was investigated comprehensively.

3.4.5.1 Air temperature

The dehumidification capacity decreased rapidly with air temperature, as shown in Fig. 3.14. The negative influence of air temperature on dehumidification capacity resulted from the fact that the solution was heated by hot air during dehumidification process. As the equilibrium pressure above desiccant solution increased with solution temperature, the driving force of dehumidification process between processed air and liquid desiccant reduced and thus the dehumidification performance decreased with air temperature. In addition, the difference of dehumidification performance between each plate dehumidifiers varied little with air temperature, indicating that the air temperature demonstrated the same effect on different plate dehumidifiers.



(a) Moisture removal rate m_ω



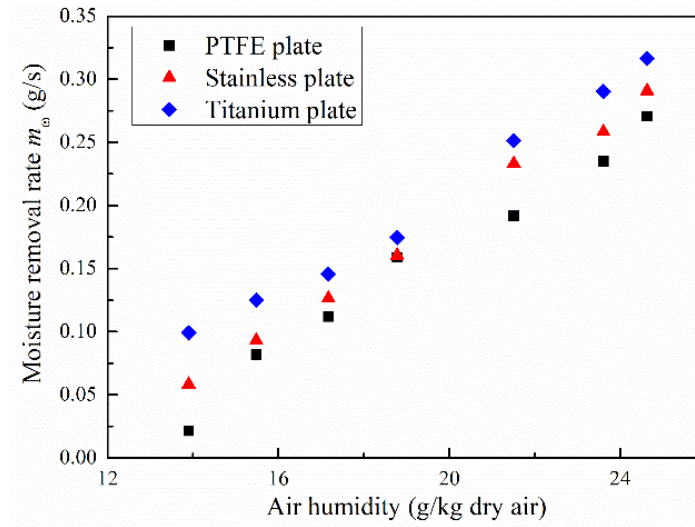
(b) Dehumidification efficiency η_ω

$T_{a,in}$	$\omega_{a,in}$	$m_{a,in}$	$T_{s,in}$	$m_{s,in}$	$T_{f,in}$
(°C)	(g/kg)	(kg/s)	(°C)	(kg/s)	(°C)
28.3-40.2	21.0	0.061	24.6	0.047	16.5

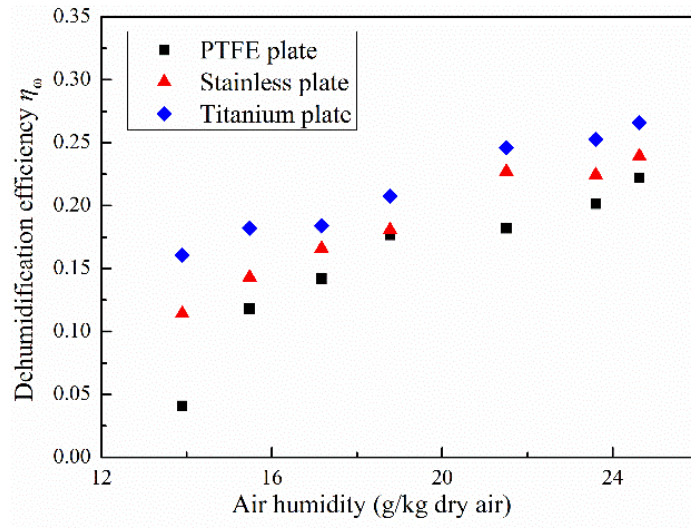
Fig. 3.14 Influence of air temperature on dehumidification capacity in different plate dehumidifiers

3.4.5.2 Air humidity

Fig. 3.15 presents the variation of dehumidification capacity with air humidity. It is clearly observed that m_ω increases linearly with air humidity due to the humidity difference of air and the saturated water vapour above desiccant solution. Besides, the dehumidification performance difference between plate dehumidifiers becomes less obvious with higher air humidity. The condensation of water vapor might occur on the unwetted plate surface under high humidity condition, which might increase the dehumidification performance of PTFE plate dehumidifier and reduce the difference of dehumidification performance between these plate dehumidifiers.



(a) Moisture removal rate m_ω



(b) Dehumidification efficiency η_{ω}

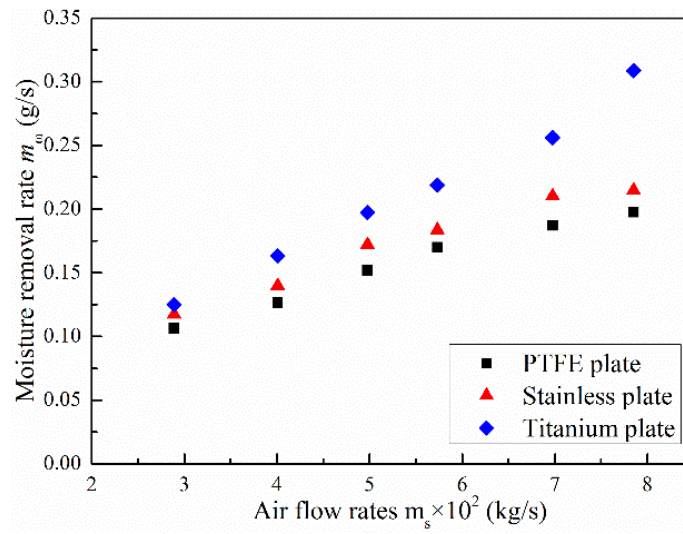
$T_{a,in}$	$\omega_{a,in}$	$m_{a,in}$	$T_{s,in}$	$m_{s,in}$	$T_{f,in}$
(°C)	(g/kg)	(kg/s)	(°C)	(kg/s)	(°C)
30.2	13.9-24.6	0.062	25.2	0.047	16.4

Fig. 3.15 Influence of air humidity on dehumidification performance in different plate dehumidifiers

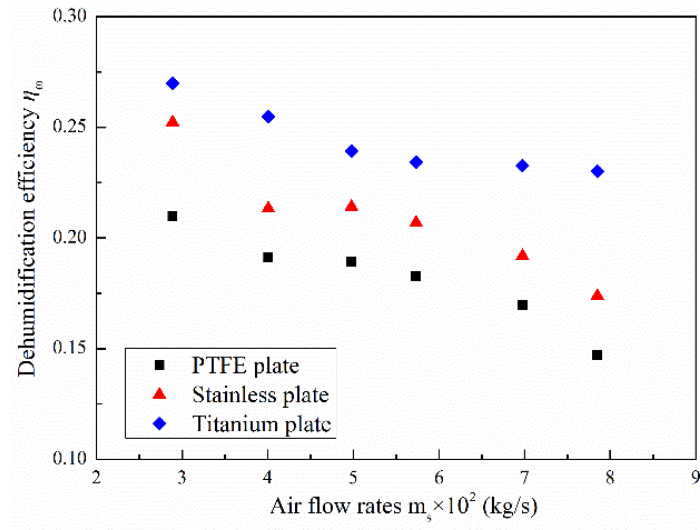
3.4.5.3 Air flow rate

Fig. 3.16 presents the variation of dehumidification performance with air flow rates in different plate dehumidifiers. The moisture removal rate increased linearly along air flow rates but the dehumidification efficiency dropped. The improvement of the moisture removal rate is explained by concentration polarization theory. The vapor moisture within boundary layer of processed air was depleted during dehumidification process and the driving force between processed air and liquid desiccant reduced due

to concentration polarization. Increasing air velocity can attenuate the boundary layer and lower the concentration polarization. The dehumidification performance of Titanium plate dehumidifier is much higher than that of the other plate dehumidifiers by about 50%, at higher air flow rate. In addition, the dehumidification performance difference between Titanium plate dehumidifier and the other two plate (Stainless plate and PTFE plate) dehumidifiers became larger with higher air flow rate, indicating that the Titanium plate dehumidifier possessed higher moisture handling capacity at higher air velocity.



(a) Moisture removal rate m_e



(b) Dehumidification efficiency η_ω

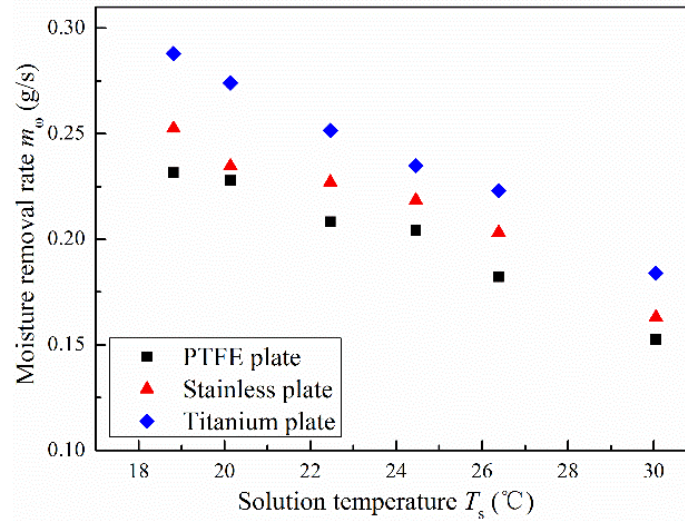
$T_{a,in}$	$\omega_{a,in}$	$m_{a,in}$	$T_{s,in}$	$m_{s,in}$	$T_{f,in}$
(°C)	(g/kg)	(kg/s)	(°C)	(kg/s)	(°C)
30.3	21.1	0.028-0.078	25.5	0.047	16.8

Fig. 3.16 Influence of air flow rates on dehumidification performance in different plate dehumidifiers

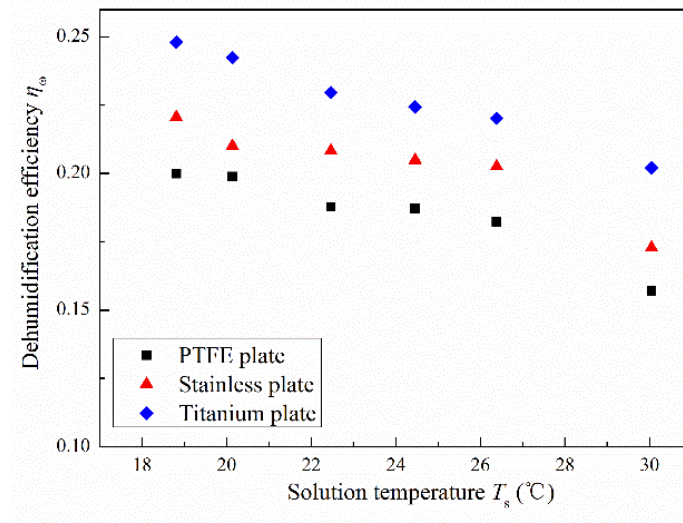
3.4.5.4 Desiccant solution temperature

The water vapor exchange is driven by the pressure difference between solution and humid air. Therefore, the equilibrium pressure of desiccant solution, which mainly depends on solution temperature and concentration, is critical to dehumidification capacity. Fig. 3.17 presents the influence of desiccant solution temperature on dehumidification capacity. The dehumidification capacity dropped with the increase of desiccant solution temperature due to the increase of equilibrium pressure. In Fig.

3.17(a), the dehumidification performance difference between different plate dehumidifiers decreased with solution temperature. According to Qi et al. [124], the film shrinkage was deteriorated at higher solution temperature. Therefore, the wetting area difference (difference of falling film shrinkage) between different plate dehumidifiers was reduced with temperature increase and the dehumidification performance difference was narrowed accordingly.



(a) Moisture removal rate m_w



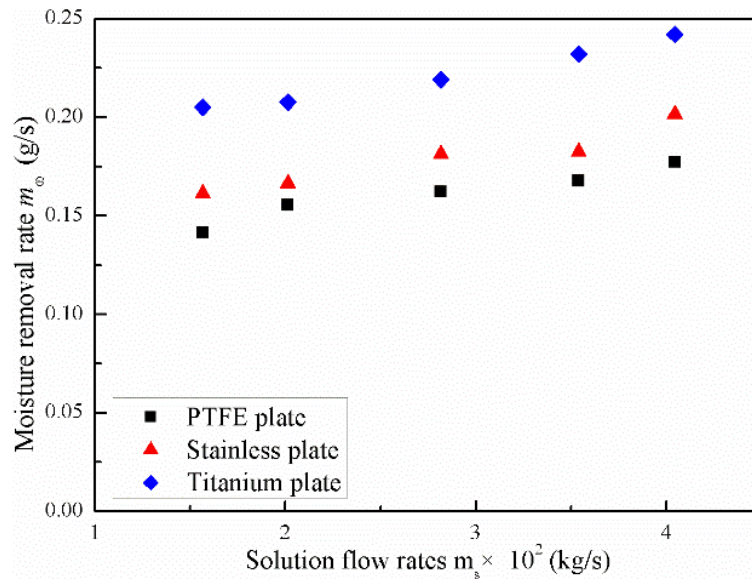
(b) Dehumidification efficiency η_ω

$T_{a,in}$	$\omega_{a,in}$	$m_{a,in}$	$T_{s,in}$	$m_{s,in}$	$T_{f,in}$
(°C)	(g/kg)	(kg/s)	(°C)	(kg/s)	(°C)
29.5	21.6	0.061	18.8-30	0.046	16.9

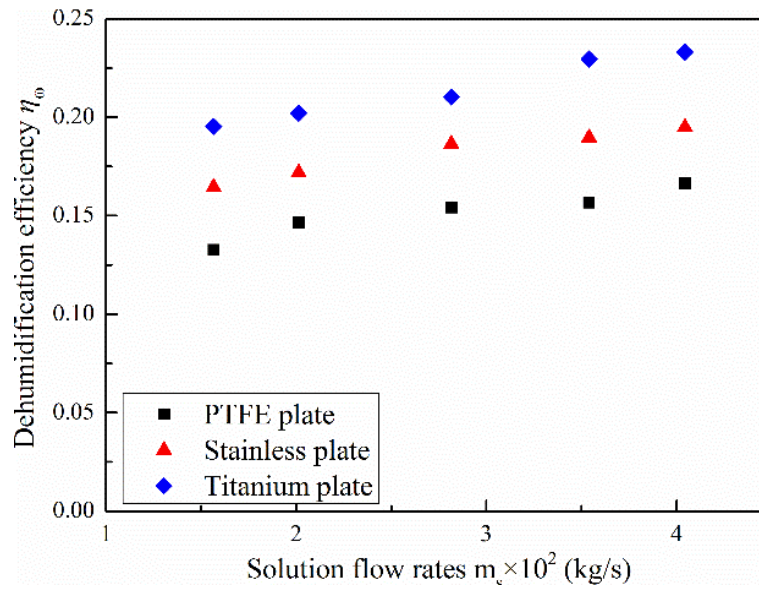
Fig. 3.17 Influence of liquid desiccant temperature on dehumidification performance in different plate dehumidifiers

3.4.5.5 Desiccant solution flow rate

Fig. 3.18 shows that the dehumidification performance increases with desiccant solution flow rate. The enhancement of dehumidification performance by desiccant solution is ascribed to several aspects. On one hand, the contact area increased with solution flow rates. On the other hand, the fluctuation of falling film was also enhanced, which reduced the concentration polarization effect at the interface between desiccant solution and processed air.



(a) Moisture removal rate m_ω



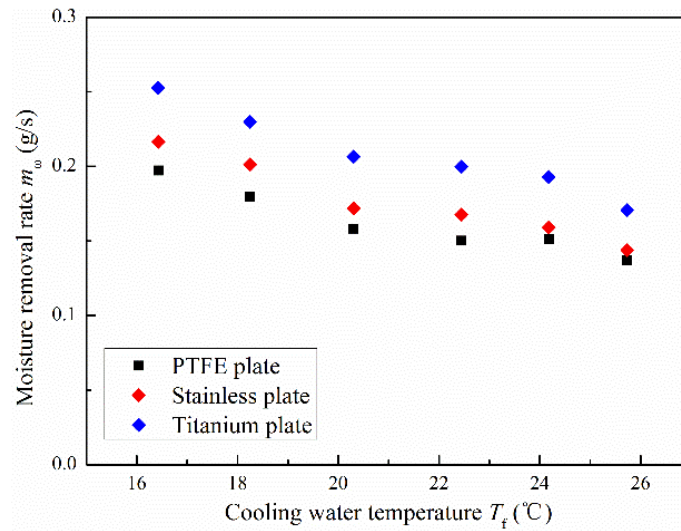
(b) Dehumidification efficiency η_ω

$T_{a,in}$	$\omega_{a,in}$	$m_{a,in}$	$T_{s,in}$	$m_{s,in}$	$T_{f,in}$
(°C)	(g/kg)	(kg/s)	(°C)	(kg/s)	(°C)
30.4	21.8	0.062	25.8	0.015-0.041	16.6

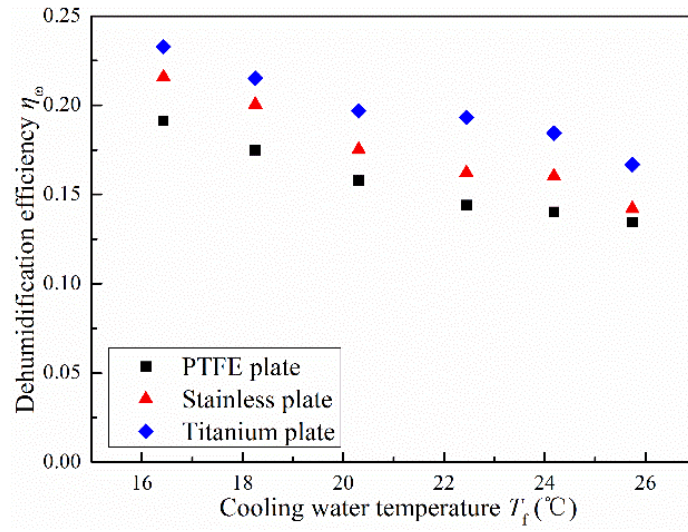
Fig. 3.18 Influence of liquid desiccant flow rates on dehumidification performance in different plate dehumidifiers

3.4.5.6 Cooling water temperature

As presented in Fig. 3.19, the cooling fluid temperature acted as a negative contributor to dehumidification performance. The heat transfer between desiccant and cooling fluid was reduced at higher cooling water temperature, which resulted in temperature increase of desiccant solution and deteriorated dehumidification performance. As the thermal conductivity of PTFE plate was much lower than that of Titanium plate, the effect of cooling water was weakened at lower temperature.



(a) Moisture removal rate m_ω



(b) Dehumidification efficiency η_ω

$T_{a,in}$	$\omega_{a,in}$	$m_{a,in}$	$T_{s,in}$	$m_{s,in}$	$T_{f,in}$
(°C)	(g/kg)	(kg/s)	(°C)	(kg/s)	(°C)
30.9	21.6	0.062	26	0.046	16.6-25.9

Fig. 3.19 Influence of cooling water temperature on dehumidification performance in different plate dehumidifiers

3.5 Summary

In this chapter, the effects of surface properties on flow and heat/mass transfer characteristics of falling film liquid desiccant dehumidifiers are investigated using three commonly-used plate dehumidifiers, i.e. Titanium plate, Stainless plate and PTFE plate, with distinctive surface properties. The main conclusions are summarized as follows:

- (1) Three types of falling film dehumidifiers with distinctive surface properties was used to investigate the effect of surface properties on dehumidification performance.

The surface free energy of Titanium plate surface, Stainless plate surface and PTFE plate surface were 50.61 mJ/m², 36.98 mJ/m² and 30.34 mJ/m², respectively, indicating that Titanium plate demonstrated the superior wettability compared with the other plates.

(2) The effect of surface properties on flow characteristics of falling film was investigated. Surface wettability demonstrated positive effect on wetting area of falling film. The falling film shrank seriously along the flow direction in falling film dehumidifier with poor surface wettability (PTFE plate dehumidifier) due to the strong repulsion between liquid desiccant and solid surface, while it shrank little in falling film dehumidifier with better surface wettability (Titanium plate dehumidifier). Besides, the PTFE plate dehumidifier presented the thickest falling film which increased the transfer resistance inside the solution and deteriorated dehumidification capacity.

(3) The effect of surface wettability on dehumidification performance was comprehensively investigated. The surface wettability contributed positively to dehumidification performance. As the surface free energy increased from 30.34 mJ/m² (PTFE plate dehumidifier) to 50.61 mJ/m² (Titanium plate dehumidifier), the moisture removal rate increased from 0.155 to 0.213 with the enhancing ratio of 37.4%

and dehumidification efficiency increased from 0.160 to 0.214 with the enhancing ratio of 33.8%, respectively.

This research is very useful to other falling film applications and the findings in this research could provide guidance to improve the operating performance to other falling applications, such as evaporators, condensers and chemical columns.

CHAPTER 4

FABRICATION AND CHARACTERIZATION OF TiO₂ SUPER-HYDROPHILIC COATING

4.1 Introduction

As investigated in Chapter 3, higher surface wettability could lead to larger wetting area and higher dehumidification performance. Therefore, it is critical to improve the surface wettability of falling film liquid desiccant dehumidifiers and enhance the adhesion between solid surface and desiccant solution. This chapter aims to develop a novel super-hydrophilic coating using nanoscale anatase TiO₂ particles to increase the surface wettability of falling film plate dehumidifiers and to improve the dehumidification performance as well. The main academic contributions in this chapter are summarized as follows.

(1) A novel super-hydrophilic coating is fabricated on dehumidifier plate using nanoscale anatase TiO₂ particles. The super-hydrophilicity is effectively achieved by UV activation.

(2) The microstructures of TiO₂ super-hydrophilic coating is captured using XRD, FESEM and HRTEM test. The surface characteristics of the new coating are investigated intensively.

(3) The basic principles of the super-hydrophilicity for TiO_2 coating are comprehensively investigated. The surface free energy of TiO_2 coating before and after UV activation are analysed to characterize the super-hydrophilicity of TiO_2 coating.

4.2 Fabrication of TiO_2 super-hydrophilic paste

Mechanical ball-milling (MM) method is adopted to produce the nanoscale TiO_2 super-hydrophilic coating in this thesis. To make the development approach more suitable for mass production, the commercial Titanium ethoxide, as shown in Fig. 4.1, and ethyl alcohol are used in the synthesis process.

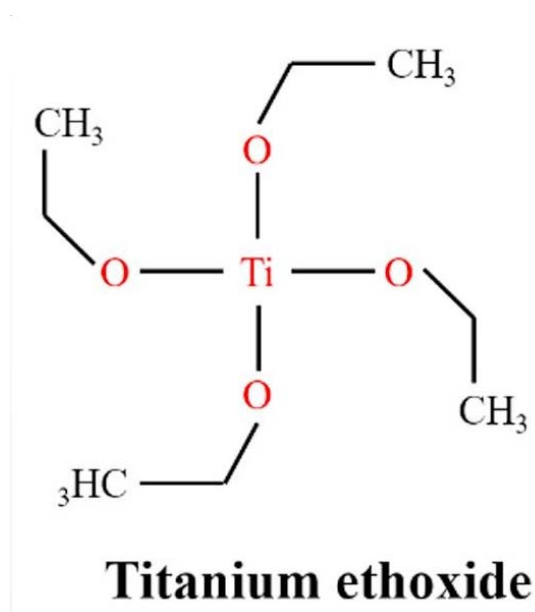


Fig. 4.1 Structure of Titanium ethoxide

Firstly, the Titanium ethoxide (30 ml, Ti 7.3 wt.%) is diluted with the ethyl alcohol

under vigorous stirring. Then, the colloidal solution is concentrated using a rotary evaporator. After the rotary evaporation process, the hydrochloric acid (36 wt.%) and nitric acid (60 wt.%), acting as the corporative acid catalyst, are put into the solution. Then, the synthesized solution is heated to 70°C for 3 hours and autoclaved in an autoclave at 160°C for 8 hours. Finally, the nanoscale TiO₂ is successfully fabricated. Then, the nano-sized TiO₂ particle is dispersed in water and terpinol using high-speed stirring and the highly-dispersed TiO₂ paste is fabricated, as shown in Fig. 4.2. Finally, the highly-dispersed TiO₂ paste is coated on the substrates by the automatic spraying equipment with high durability. The detailed fabircation process is shown in Fig. 4.3.



Fig. 4.2 Picture of nanoscale TiO₂ super-hydrophilic paste

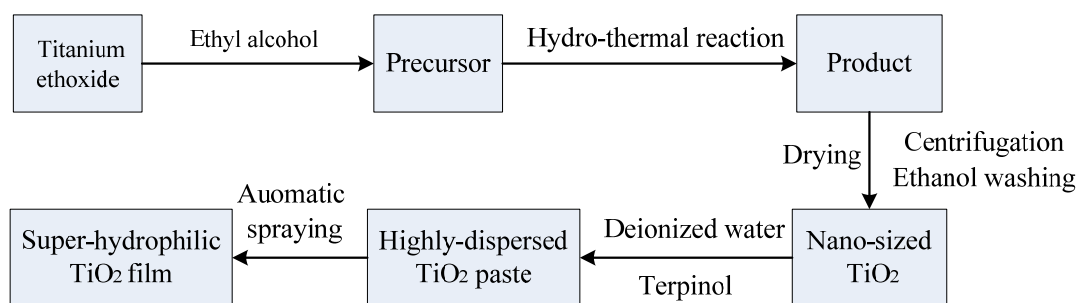


Fig. 4.3 Fabrication process of TiO₂ super-hydrophilic film

4.3 The microstructures of TiO₂ super-hydrophilic nanocrystals?

To characterize the TiO₂ nanocrystals, X-ray diffraction (XRD) tests are conducted using Bruker D8 Advance at 50 kV and 150 mA by scanning at $5^\circ 2\theta$. Fig. 4.4 shows the XRD patterns of TiO₂ nanocrystals. It is clearly observed that there is not any other crystal characteristics, indicating that the TiO₂ particles are well synthesized.

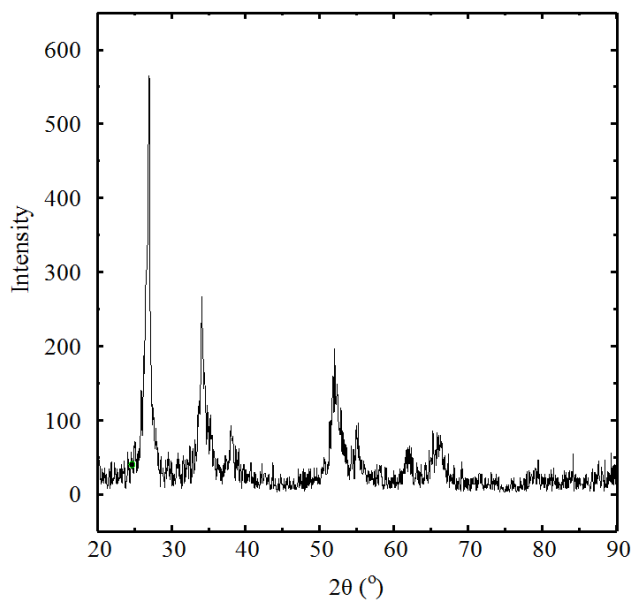


Fig. 4.4 XRD test of TiO₂ nanocrystals

The microscopic characteristics of TiO₂ paste are also investigated through high resolution transmission electron microscopy (HRTEM) test. Fig. 4.5 presents the HRTEM image of TiO₂ colloid solvent. Further quantitative analysis shows that the particle size is around 10 nm, indicating the high dispersion of the newly-developed TiO₂ super-hydrophilic particles.

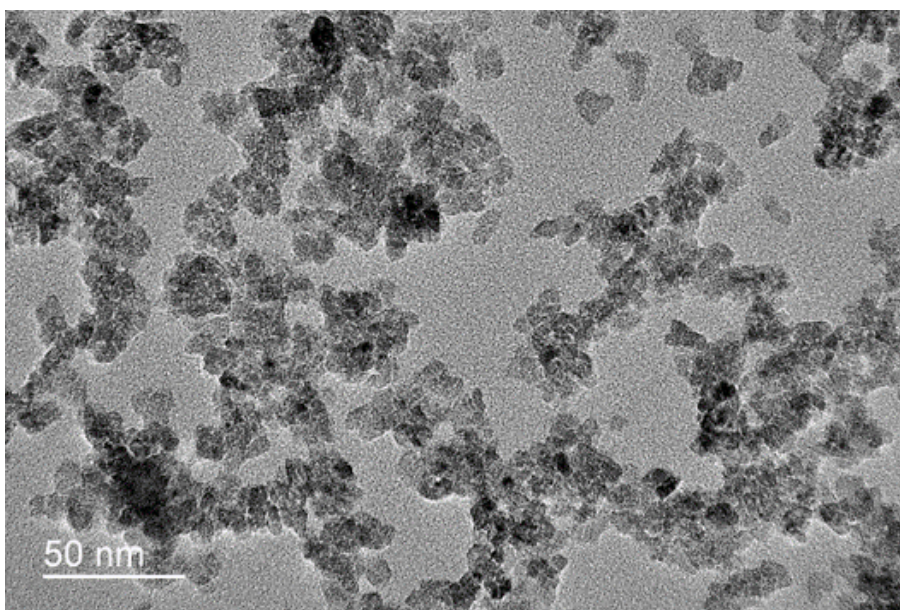


Fig. 4.5 HRTEM test of nanoscale TiO₂ colloid solvent

Besides, to prevent the corrosion of the substrate plate caused by the LiCl aqueous solution, a double-layer structure of the coating with an inorganic compact protective layer beneath the TiO₂ coating is developed. The double-layer structure is detected using field emission scanning electron microscopy (FESEM) test, as shown in Fig. 4.6.

Part I, II and III represent the substrate plate, the inorganic compact protective layer and the TiO₂ superhydrophilic layer, respectively. As the TiO₂ superhydrophilic layer and the protective layer are much thinner than the stainless steel plate, the thermal conductivity of the coating is ignored during the calculation of heat transfer resistance between the liquid desiccant and the cooling water.

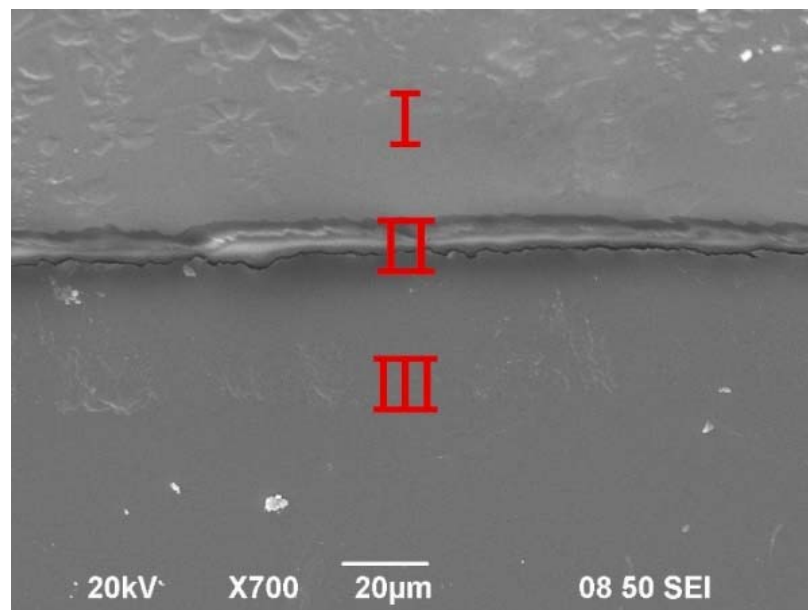


Fig. 4.6 HRTEM test of nanoscale TiO₂ super-hydrophilic particles

4.4 Surface free energy of TiO₂ super-hydrophilic coating

The adhesion between liquid and solid surface is determined by the free energy of solid surface. Higher surface free energy means strong adhesion between liquid and solid surface. Therefore, it is very important to investigate the free energy of the newly-developed TiO₂ super-hydrophilic coating.

The solid free energy is calculated using Young-Good-Girifalco-Fowke equation [125].

According to Van Oss et al. [126] theory, the surface free energy consists of two components, the Lifshitz-van der Waals component, γ^{LW} , and the acid-base component, γ^{AB} .

$$\gamma = \gamma^{LW} + \gamma^{AB} \quad (4.1)$$

where the Lifshitz-van der Waals component, γ^{LW} , represents long-term interaction, including dispersion interaction, dipole-dipole interaction and dipole-induced-dipole interaction. The acid-base component, γ^{AB} , which is also called acidic and basic interaction, is composed of acidic component, γ^A , and basic component, γ^B .

$$\gamma^{AB} = 2(\gamma^A \gamma^B)^{1/2} \quad (4.2)$$

Substituting Eq. (4.2) into Eq. (4.1) yields:

$$\gamma = \gamma^{LW} + 2(\gamma^A \gamma^B)^{1/2} \quad (4.3)$$

Therefore, the interface free energy between liquid phase and solid phase, γ_{SL} , is expressed as the geometric function of Lifshitz-van der Waals component, γ^{LW} , and the acid-base component, γ^{AB} .

$$\gamma_{SL} = \gamma_S + 2\gamma_L (\gamma_S^{LW} \gamma_L^{LW})^{1/2} - 2(\gamma_S^A \gamma_L^B)^{1/2} - 2(\gamma_S^B \gamma_L^A)^{1/2} \quad (4.4)$$

According to Young's equation [98] on the thermodynamic balance between solid, liquid and vapour, it gets:

$$\gamma_L \cos \theta = \gamma_{SV} - \gamma_{SL} \quad (4.5)$$

where γ_{SV} represents the surface tension of a solid in equilibrium with the liquid

vapor, while γ_s represents the surface tension of a solid in equilibrium with its own vapor. The difference between γ_{sv} and γ_s is defined as the equilibrium film pressure, π_e .

$$\pi_e = \gamma_s - \gamma_{sv} \quad (4.6)$$

Actually, the equilibrium film pressure, π_e , is much smaller than γ_s . Therefore, π_e is generally assumed to be 0 [127]. Thus, Eq. (4.5) is rewritten as follows:

$$\gamma_L \cos \theta = \gamma_s - \gamma_{SL} \quad (4.7)$$

Substituting Eq (4.7) into Eq. (4.4) yields:

$$\gamma_L (1 + \cos \theta) = 2(\gamma_s^{LW} \gamma_L^{LW})^{1/2} + 2(\gamma_s^A \gamma_L^B)^{1/2} + 2(\gamma_s^B \gamma_L^A)^{1/2} \quad (4.8)$$

To calculate the three unknown components of solid surface free energy, γ_s^{LW} , γ_s^A and γ_s^B , three liquid reagents with known surface free energy and its components γ_s^A , γ_s^B and γ_s^{LW} , are necessary. Therefore, Eq. (4.8) is rewritten as follows:

$$\gamma_{L1} (1 + \cos \theta_1) = 2(\gamma_s^{LW} \gamma_{L1}^{LW})^{1/2} + 2(\gamma_s^A \gamma_{L1}^B)^{1/2} + 2(\gamma_s^B \gamma_{L1}^A)^{1/2} \quad (4.9)$$

$$\gamma_{L2} (1 + \cos \theta_2) = 2(\gamma_s^{LW} \gamma_{L2}^{LW})^{1/2} + 2(\gamma_s^A \gamma_{L2}^B)^{1/2} + 2(\gamma_s^B \gamma_{L2}^A)^{1/2} \quad (4.10)$$

$$\gamma_{L3} (1 + \cos \theta_3) = 2(\gamma_s^{LW} \gamma_{L3}^{LW})^{1/2} + 2(\gamma_s^A \gamma_{L3}^B)^{1/2} + 2(\gamma_s^B \gamma_{L3}^A)^{1/2} \quad (4.11)$$

where 1, 2 and 3 represent three different liquid reagents with unknown surface free energy. By solving the Eqs. (4.9), (4.10) and (4.11), the solid surface free energy can be calculated. In this thesis, deionized water, formamide and ethylene glycol are

adopted and the contact angles of these liquid reagents on the coated substrates are measured using the contact angle meter (JCY20-13). The detailed surface free energy and its components are presented in Table 4.1.

Table 4.1 Surface free energy and its components of different liquid reagents

Reagents	γ_L	γ_L^{LW}	γ_L^{AB}	γ_L^A	γ_L^B
	[mJ/m ²]	[mJ/m ²]	[mJ/m ²]	[mJ/m ²]	[mJ/m ²]
Deionized water	72.80	21.80	51.00	25.50	25.50
Formamide	58.00	39.00	19.00	2.28	39.60
Ethylene glycol	48.00	29.00	19.00	1.92	47.00

The super-hydrophilicity of TiO₂ coating is activated by UV light. To investigate the mechanism on the super-hydrophilicity of TiO₂ coating, the contact angles of liquid reagents on coated substrates before and after UV activation are measured in the thesis, as shown in Fig. 4.7 and Table 4.2. The contact angles of liquid reagents on the coated substrates are significantly reduced by UV activation, indicating that the super-hydrophilicity of TiO₂ coating is effectively activated by UV light.

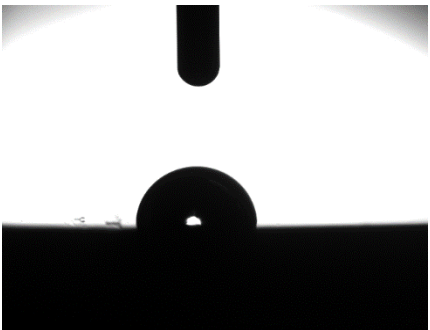

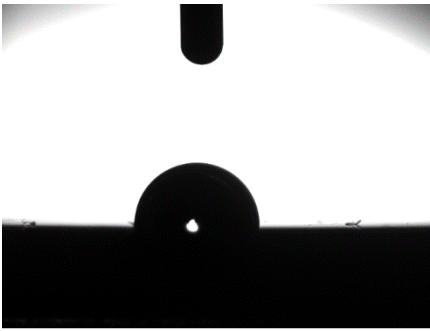
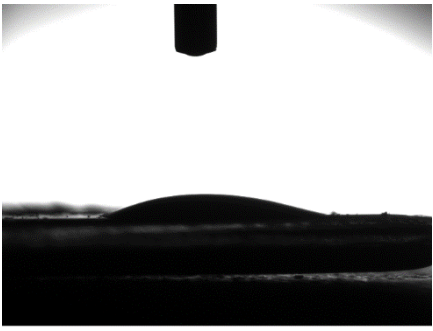
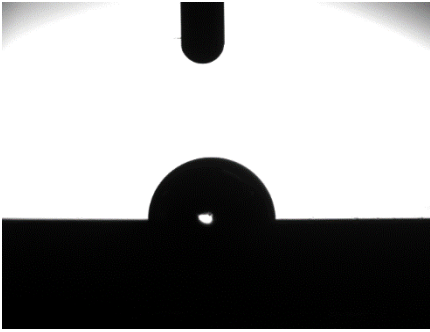
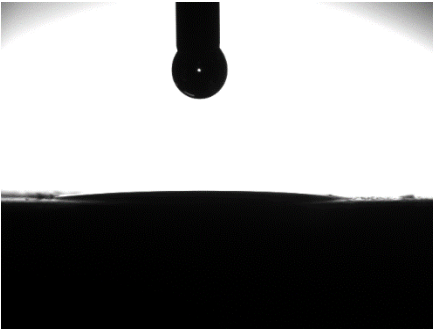
Reagents	Before	After
Deionized water		
Formamide		
Ethylene glycol		

Fig. 4.7 Contact angles of different liquid reagents on coated substrate before and after UV activation

Table 4.2 Contact angles of deionized water, glycerol and ethanol on TiO₂ film [°]

Samples		1	2	3	4	5	Average
Deionized water	Before	100.23	96.35	94.30	94.05	98.27	96.64
	After	10.00	11.25	10.80	9.65	9.95	10.33
Formamide	Before	90.20	92.36	91.80	89.10	92.54	91.20
	After	19.85	19.25	20.50	21.05	19.35	20.00
Ethylene glycol	Before	90.50	89.85	93.25	88.80	89.60	90.40
	After	3.50	4.60	5.65	3.80	4.75	4.46

The surface free energy of TiO₂ super-hydrophilic coating before and after UV activation is calculated using Eqs. (4.9), (4.10) and (4.11) based on the contact angles of three liquid reagents. The detailed specifications of the surface free energy and its components are shown in Table 4.3. The symbol of (+) means increment while (-) means decrement. The surface free energy of TiO₂ super-hydrophilic coating is effectively increased from 15.71 mJ/m² to 90.15 mJ/m² with the enhancement ratio of 573.8% by UV activation. Further analysis indicates that the increment of surface free energy of TiO₂ super-hydrophilic coating is mainly attributed to the increment of

the acid-base component. The acid-base component, γ^{AB} , increased from 14.94 mJ/m² to 89.44 mJ/m² with the enhancement ratio of 598.7%, while the Lifshitz-van der Waals component, γ^{LW} , is slightly reduced.

Table 4.3 Surface free energy and its components of TiO₂ coating

	γ_s	γ_s^{LW}	γ_s^{AB}	γ_s^A	γ_s^B
	[mJ/m ²]	[mJ/m ²]	[mJ/m ²]	[mJ/m ²]	[mJ/m ²]
Before	15.71	0.77	14.94	9.32	5.99
After	90.15	0.7	89.44	41.5	48.2
Enhancement ratio	(+) 573.8%	(-) 90.9%	(+) 598.7%	(+) 445.3%	(+) 804.7%

The mechanism of the super-hydrophilicity for TiO₂ coating by UV activation is complicated, which is usually explained by the modification of the microscopic crystal structure by UV irradiation. Fig. 4.8 and Fig. 4.9 present the mechanism of the UV-induced super-hydrophilicity of TiO₂ coating. The UV light can activate the crystal structure of the TiO₂ coating and an electron-hole pair can be created by UV light excitation. Then, the electrons interact with the Ti⁴⁺ cations and the Ti⁴⁺ cations are transformed into Ti³⁺ cations, which creates the tapped holes at the lattices. These tapped holes can weaken the bonds between oxygen and the titanium atoms and the oxygen atoms is easily released, creating oxygen vacancies at the lattice site of TiO₂,

as shown in Fig. 4.8 (a). Then the absorption of water molecules can make the Titania surface be hydroxylated (OH), which results in the hydrogen bridging interactions, as shown in Fig. 4.8 (b). Therefore, one hydroxyl group, which is coordinated to two neighbouring Titanium atoms, is converted into two hydroxyl groups, as shown in Fig. 4.8 (c). Finally, the super-hydrophilic area is created at the TiO_2 surface.

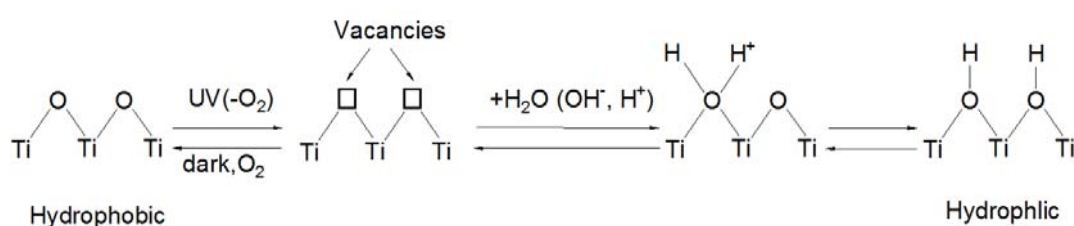


Fig. 4.8 Mechanism of the UV-induced super-hydrophilicity of TiO_2 coating

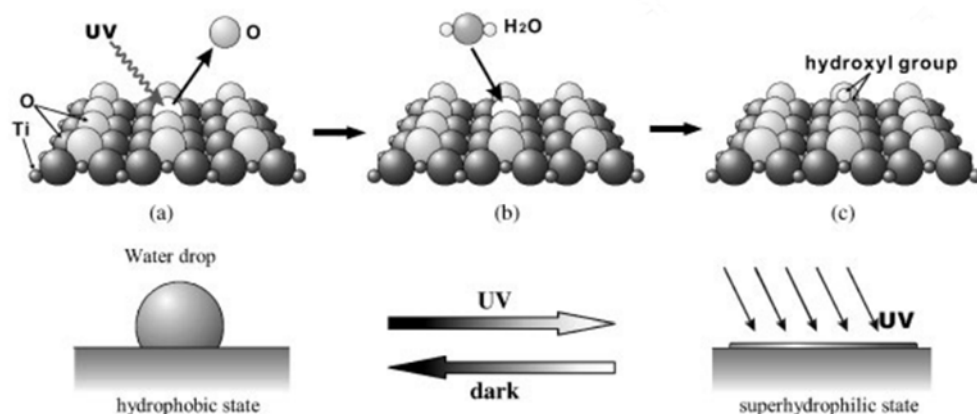
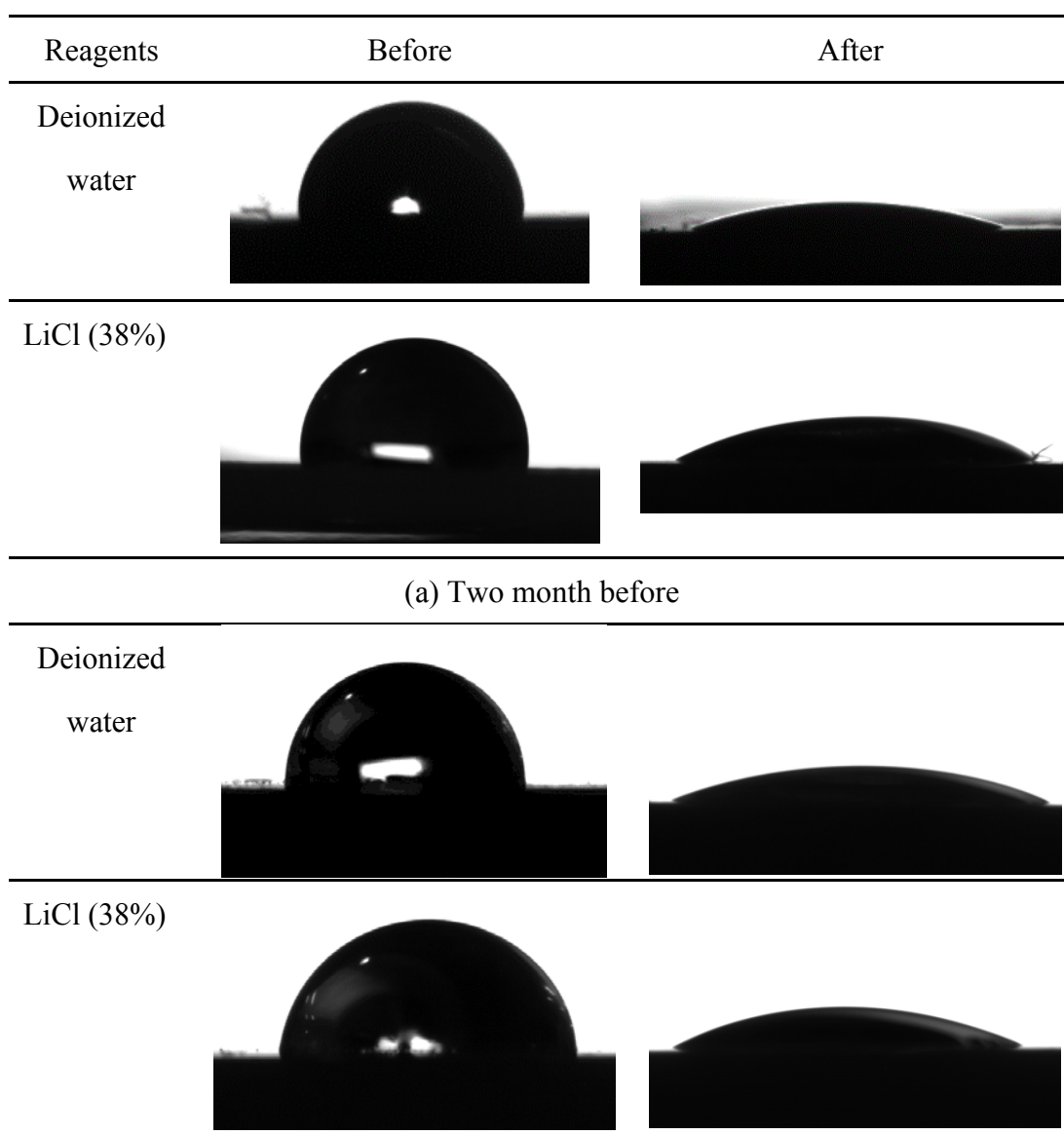


Fig. 4.9 Schematic of the UV-induced super-hydrophilicity of TiO_2 coating [128]

4.5 Durability test of TiO_2 super-hydrophilic coating

To investigate the durability of the TiO_2 super-hydrophilic coating, the durability test was conducted. The substrate plates were firstly coated by the TiO_2 super-hydrophilic

coating and stored in the LiCl aqueous solution (38% wt%). Two months later, the contact angles of deionized water and LiCl aqueous solution (38% wt%) before and after UV activation were tested, as shown in Fig. 4.10. The test results showed that the contact angles on coated plate after two-month immersion were still effectively reduced by UV activation, indicating that the durability of the TiO₂ super-hydrophilic coating is acceptable.



(b) Two month later

Fig. 4.10 Contact angles of different liquid reagents on coated substrate plates

4.6 Summary

In this chapter, a novel TiO₂ super-hydrophilic coating is successfully fabricated on dehumidifier plates using nanoscale anatase TiO₂ particles with high durability. The microscopic characteristics of TiO₂ super-hydrophilic nanocrystals and coating film are investigated in terms of XRD, HRTEM and FESEM test. The XRD test indicates that the nanoscale TiO₂ super-hydrophilic coating is successfully developed. The HRTEM test proves the high dispersion of the newly-developed TiO₂ super-hydrophilic particles and the FESEM indicates that the TiO₂ super-hydrophilic coating is well coated on the substrate surface.

Besides, the UV-induced super-hydrophilicity and the effect of UV irradiation on super-hydrophilicity of TiO₂ super-hydrophilic coating are investigated in detail. The surface free energy of TiO₂ super-hydrophilic coating before and after UV activation is calculated based on the measured contact angles of liquid reagents, i.e., deionized water, formamide and ethylene glycol, using Young-Good-Girifalco-Fowke method. The test results indicate that the surface free energy of TiO₂ super-hydrophilic coating is significantly improved by UV irradiation. In other words, the adhesion between

liquid and solid surface is effectively enhanced by TiO₂ super-hydrophilic coating. Finally, the mechanism of the UV-induced super-hydrophilicity is discussed and the super-hydrophilicity can be explained by the modification of the microscopic crystal structure by UV irradiation.

CHAPTER 5

EXPERIMENTAL STUDY ON DEHUMIDIFICATION PERFORMANCE ENHANCEMENT BY APPLYING TiO₂ SUPER-HYDROPHILIC COATING

5.1 Introduction

The dehumidification performance is one of the key parameters in liquid desiccant air-conditioning system. Efforts have been made in enhancing the dehumidification performance, as discussed in Chapter 2. Amongst these existing performance enhancing methods, the surface modification technology is simple but effective. Therefore, this thesis adopts surface modification approach, TiO₂ super-hydrophilic coating, to improve the dehumidification performance and to investigate the mechanism of performance enhancement of plate dehumidifiers.

This chapter aims to investigate the dehumidification performance of falling film plate dehumidifiers coated by nanoscale TiO_2 super-hydrophilic particles, which is well developed and characterized in Chapter 4. The flow and heat/mass transfer characteristics during dehumidification process in coated plate dehumidifiers are comprehensively investigated. Besides, the influencing factors of dehumidification performance are analyzed in detail. The main academic contributions in this chapter are summarized as follows:

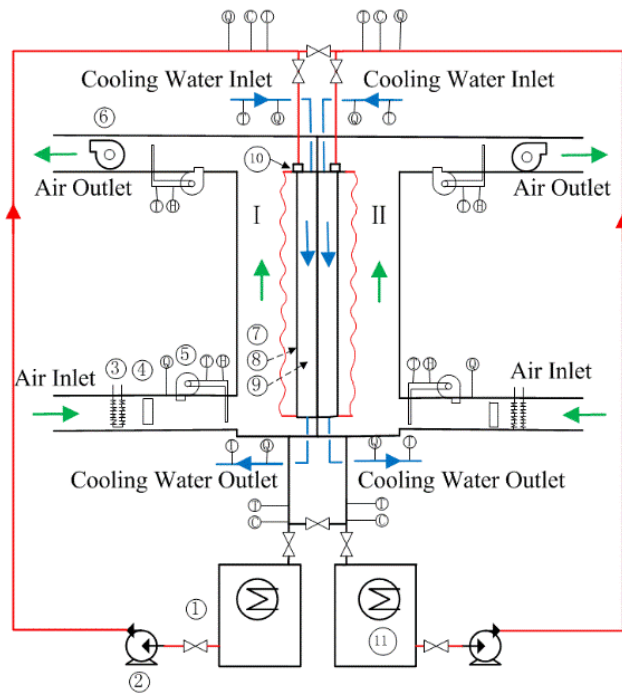
- (1) The contact angles and surface free energy of the coated and uncoated plate dehumidifiers are measured to characterize the solid-liquid interaction effect.
- (2) The experimental setup is reconstructed with two single-channel internally-cooled plate dehumidifiers to investigate the effect of super-hydrophilic coating on dehumidification performance. The flow characteristics of liquid desiccant falling film on surface-modified plate dehumidifier are experimentally investigated in terms of wetting area and falling film fluctuation. Besides, the effect of flow parameters on wetting area and film thickness are experimentally investigated.
- (3) The dehumidification performance of coated and uncoated internally-cold plate dehumidifiers are experimentally investigated and the mechanism of dehumidification performance enhancement is comprehensively analyzed.

(4) The influencing factors of dehumidification performance, i.e., solution flow rates and temperature, air flow rates and temperature, air humidity and cooling water temperature, are intensively discussed for surface-modified liquid desiccant plate dehumidifiers.

(5) A novel empirical mass transfer correlation is developed based on the experimental results, in which solid-liquid interaction effect is considered to account for its effect on dehumidification performance.

5.2 Description of experimental test rig

The experimental setup, as shown in Fig. 3.1, is reconstructed with two single-channel internally-cooled liquid desiccant dehumidifiers to investigate the hydrodynamics and heat/mass transfer characteristics of surface-modified falling film plate dehumidifiers, as shown in Fig. 5.1.



1、Solution tank 2、Solution pump 3、Air heater 4、Humidifier 5、Sampling fan 6、Fan
7、Air channel 8、Working surface 9、Internally cooling unit 10、Solution distributor 11、Heat exchanger
(T) Temperature Sensor (C) Density Sensor (Q) Flowmeter (H) Wet-bulb temperature sensor

Fig. 5.1 Schematic of the experimental setup

The real photographs of the experimental setup are shown in Fig. 5.2. The design of single-channel structure helps to measure the wetting area of falling film and the variable falling film thickness, which are important for the analysis of the performance enhancement mechanism.

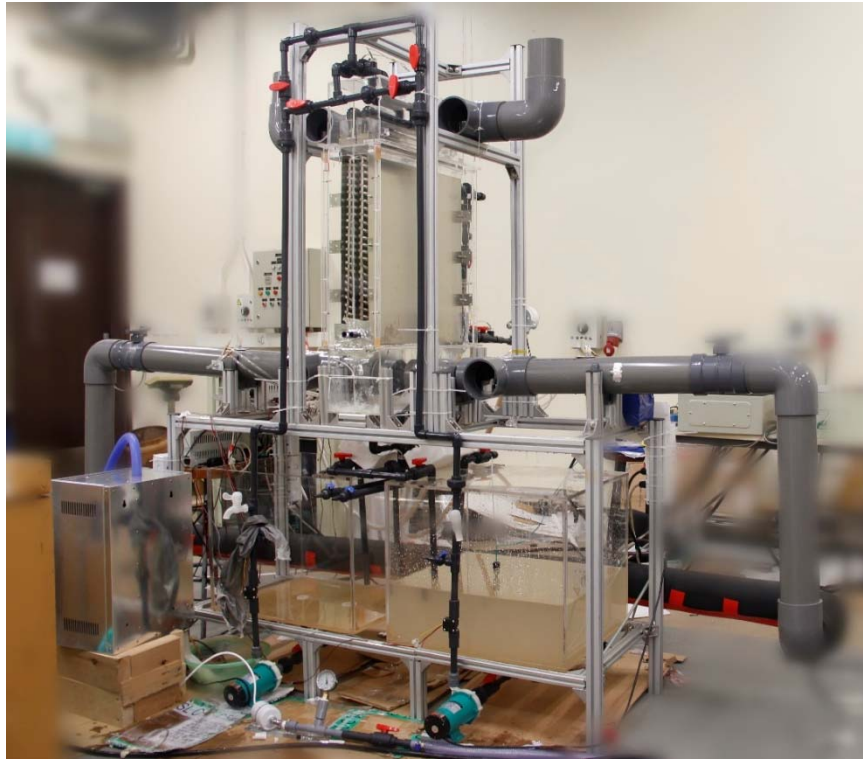
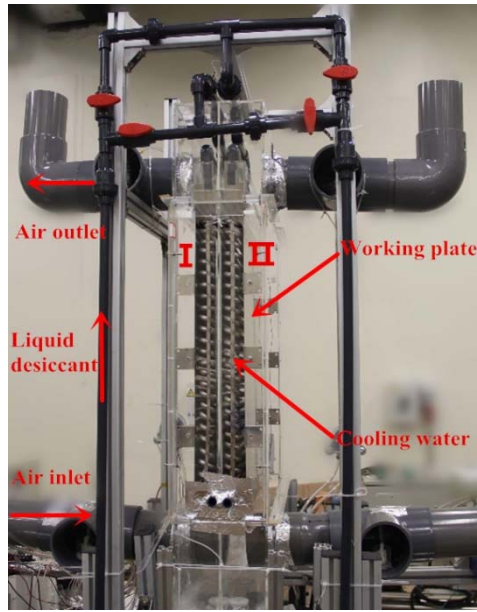
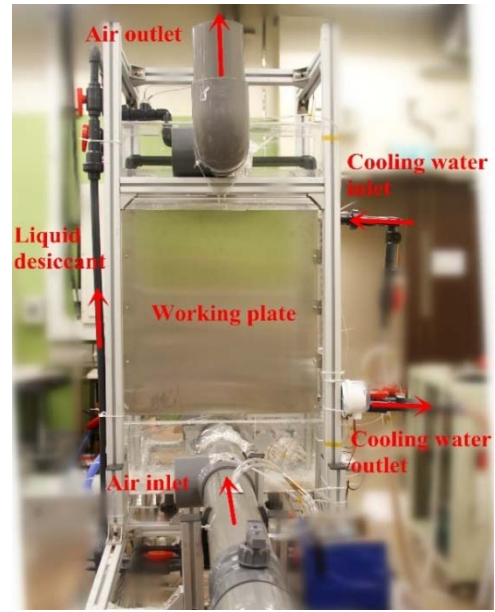


Fig. 5.2 Photographs of the experimental setup

Two stainless steel plates were selected as the substrate plates regarding their good heat conductivity and corrosion resistance. Lithium Chloride (LiCl) aqueous was chosen as the absorption medium in this experiment. In Channel I, the substrate plate was just cleaned with ethanol, while in Channel II, the substrate plate was firstly cleaned with ethanol and then coated with nanoscale TiO_2 superhydrophilic particles. The size of the plate dehumidifier was $550 \times 100 \times 600 \text{ mm}$ ($L \times W \times H$). The real photographs of the working channels are provided in Fig. 5.3.



(a) Side view



(b) Front view

Fig. 5.3 Photograph of the working channels

As shown in Fig. 5.1, the red line represents the circulation of liquid desiccant aqueous solution. The desiccant solution was stored in the solution tank and pumped to the inlet of the plate dehumidifier. After interacting with the processed air, the weak desiccant aqueous solution was collected and returned to the solution tank. The green line represents the flow of processed air. The air, supplied by a fan, was firstly heated and humidified to the test condition, and then interacted with the liquid desiccant falling film. The sampling devices were fixed at both inlet and outlet of the air channel to measure the temperature and humidity of the process air. The blue line stands for the circulation of the cooling water. The cooling water was provided by a chiller and used to remove the latent heat released during the absorption process and therefore to prevent the temperature increase of desiccant solution. In addition, the whole channel

was well insulated to prevent the heat exchange between the dehumidifiers and the surroundings. The experiments of these two single-channel plate dehumidifiers were conducted simultaneously to ensure the same experimental conditions.

As the measuring and controlling devices in this experiment are same as those in Chapter 3, the specifications can be referenced from Table 3.1.

5.3 Performance indices and uncertainty analysis

In the experiment, the extra moisture is removed from processed air to liquid desiccant due to the surficial vapor pressure difference. To evaluate the dehumidification performance of the plate dehumidifiers, three performance indices, i.e., the moisture removal rate, m_ω , the dehumidification efficiency, η_ω , and the mass transfer coefficient, h_D , were introduced. Besides, the performance enhancing ratio ε was proposed to compare the dehumidification performance of the coated and uncoated plate dehumidifiers.

The moisture removal rate, m_ω , represents the moisture handling capacity of the plate dehumidifier, defined as follows.

$$m_\omega = m_a (\omega_{a,in} - \omega_{a,out}) \quad (5.1)$$

where m_a is the mass flow rate of air, kg/s. $\omega_{a,in}$ and $\omega_{a,out}$ represent inlet and outlet air humidity, g/kg dry air, respectively.

The dehumidification efficiency, η_{ω} , is defined as the ratio of the actual moisture change between process air and liquid desiccant to the maximum possible change. η_{ω} is defined as follows:

$$\eta_{\omega} = \frac{\omega_{a,in} - \omega_{a,out}}{\omega_{a,in} - \omega_{equ,in}} \quad (5.2)$$

where $\omega_{equ,in}$ represents the air absolute humidity in equilibrium with the inlet solution at its temperature and concentration, g/kg dry air.

The mass transfer coefficient h_D represents the mass transfer rate between processed air and liquid desiccant solution, g/(m² · s).

$$h_D = \frac{m_a (\omega_{a,in} - \omega_{a,out})}{A \Delta \omega} \quad (5.3)$$

where A is the wetting area of the falling film, m², and $\Delta \omega$ is the mean humidity difference between process air and desiccant solution, g/kg dry air.

The performance enhancing ratio is defined as the ratio of the dehumidification performance, including moisture removal rate and dehumidification efficiency, of the coated plate dehumidifier to that of the uncoated one.

$$\varepsilon_{\omega} = \frac{m_{\omega, coated}}{m_{\omega, uncoated}} \quad (5.4)$$

$$\varepsilon_{\eta} = \frac{\eta_{\omega, coated}}{\eta_{\omega, uncoated}} \quad (5.5)$$

where ε_{ω} and ε_{η} represent the enhancing ratios of moisture removal rate and

dehumidification efficiency.

5.4 Results and discussion

5.4.1 Energy conservation and results validation analysis

In the experiment, more than 200 experimental conditions were selected based on Hong Kong climate to investigate the dehumidification performance enhancement with TiO₂ coating. The detailed ranges of the experimental conditions are listed in Table 5.1 and part of the experimental conditions are listed in Table 5.2.

Table 5.1 Ranges of the inlet experimental parameters

Parameter	Symbol	Unit	Range
Air temperature	$T_{a,in}$	°C	23.6-38.7
Air humidity	$\omega_{a,in}$	g/kg dry air	10.9-26.2
Air flow rate	$m_{a,in}$	g/kg	0.027-0.07

Solution flow rate	$m_{s,in}$	g/kg	0.01-0.049
Solution temperature	$T_{s,in}$	°C	23.1-30.5
Solution concentration	X_s	%	38%
Cooling water flow rate	m_f	g/kg	0.03-0.10
Cooling water temperature	$T_{f,in}$	°C	15.6-24.9

Table 5.2 Part of the experimental conditions

No.	$T_{a,in}$ (°C)	$\omega_{a,in}$ (g/kg)	$T_{s,in}$ (°C)	$T_{f,in}$ (°C)	m_a (kg/s)	$T_{a,out}$ (°C)	$\omega_{a,out}$ (g/kg)	$T_{s,out}$ (°C)	$T_{f,out}$ (°C)	m_s (kg/s)
1	26.5	19.4	26.4	16.5	0.062	26.8	14.7	28	17.2	0.044
2	29.0	19.4	26.3	16.4	0.062	28.0	15.0	27.9	17.3	0.045
3	30.1	23.6	25.8	15.7	0.061	28.9	17.5	28.1	17.0	0.044
4	33.8	23.8	25.9	16.0	0.061	30.4	18.3	28.3	17.3	0.044
5	29.7	13.5	23.9	15.8	0.063	28.0	11.0	27.3	16.5	0.015
6	29.6	13.6	23.8	16.1	0.063	28.2	11.8	29.4	16.6	0.010
7	29.5	17.6	27.0	16.8	0.063	29.0	14.5	30.5	17.5	0.016
8	29.5	17.7	27.4	15.9	0.063	29.0	15.6	32.6	17.0	0.010
9	30.1	22.6	26.3	16.8	0.057	28.9	17.3	28.9	18.3	0.047
10	30.3	22.7	26.7	16.1	0.049	28.6	17.5	28.2	17.2	0.045
11	29.7	20.2	25.2	20.2	0.061	26.3	15.5	27.2	20.8	0.043
12	30.1	19.9	25.8	23.0	0.061	26.2	16.0	27.2	23.3	0.048

Before the experimental results analysis, the energy conservation analysis should be conducted to verify the reliability of the experimental results. Due to the temperature difference between liquid desiccant and process air as well as the phase change during the dehumidification process, heat transfer occurred between processed air, liquid desiccant and cooling water. Therefore, the energy conservation equation are defined as follows:

$$m_a(h_{a,in} - h_{a,out}) = (m_{s,out}h_{s,out} - m_{s,in}h_{s,in}) + m_f C_{pf}(T_{f,out} - T_{f,in}) \quad (5.6)$$

Fig. 5.4 shows the energy conservation conditions of the plate dehumidifier. It can be observed that most of the results evenly fall within $\pm 30\%$ error band with the mean deviation of 4.9%, validating the accuracy of the experimental results. Besides, the heat released by the process air is a little higher than that absorbed by the liquid desiccant and the cooling water from Fig. 5.4. It could be explained that part of the heat is released to the surroundings despite the good thermal insulation of the system.

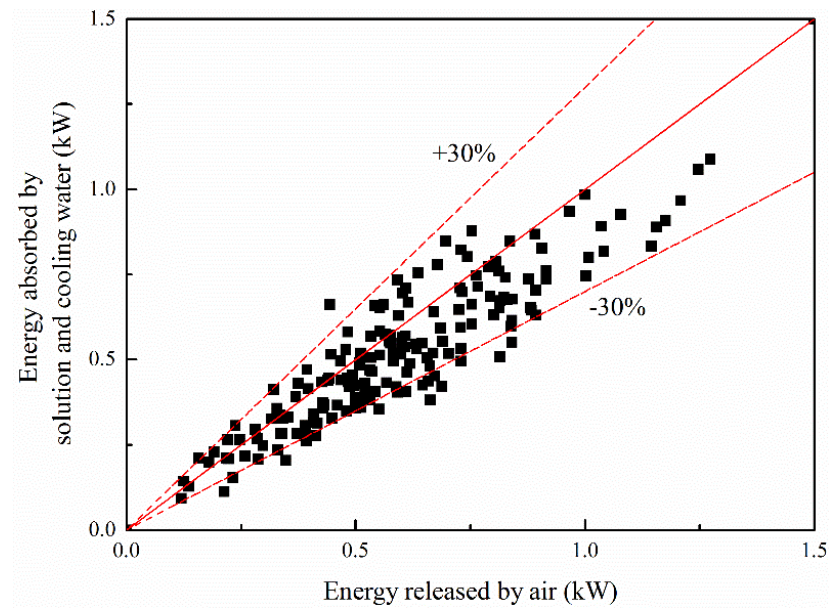


Fig. 5.4 Energy conservation of the experimental results

5.4.2 Flow characteristics of falling film

5.4.2.1 Surface wettability

The development and characterization of the nanoscale TiO_2 super-hydrophilic coating is conducted in Chapter 3. To investigate the effect of TiO_2 super-hydrophilic coating on dehumidification performance, an experimental setup with two single-channel internally-cooled liquid desiccant dehumidifiers is fabricated, as shown in Fig. 5.1. The substrate plate in Channel I was just cleaned with ethanol, while in Channel II, the substrate plate was firstly cleaned with ethanol and then coated with nanoscale TiO_2 super-hydrophilic particles. To investigate the effect of surface wettability on dehumidification performance, the contact angles of liquid desiccant solution on

coated and uncoated plate dehumidifiers were conducted, as shown in Fig. 5.5. The contact angle of the liquid desiccant drops significantly from 84.6° on the uncoated plate to 8.8° on the coated one. The test results indicated that the wettability of the solid surface was effectively improved with the TiO_2 superhydrophilic coating.

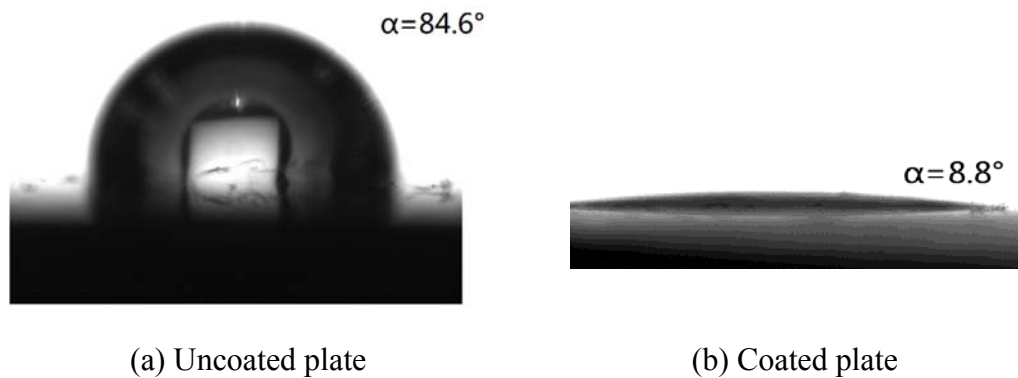


Fig. 5.5 Contact angles of LiCl aqueous solution on coated and uncoated plates

5.4.2.2 Wetting ratio

As the TiO_2 super-hydrophilic coating needs to be activated by UV light, the coated plate was periodically illuminated by UV light in the experiment. Fig. 5.6 shows the variation of the contact angles for the coated plates under temporary and periodical activation. It was observed that the contact angles of the coated plate under temporary activation increased little during the first 48 hours but afterwards increased rapidly. However, for the coated plate under periodical activation, the contact angle remained almost constant and the super-hydrophilicity was effectively maintained due to the UV

activation.

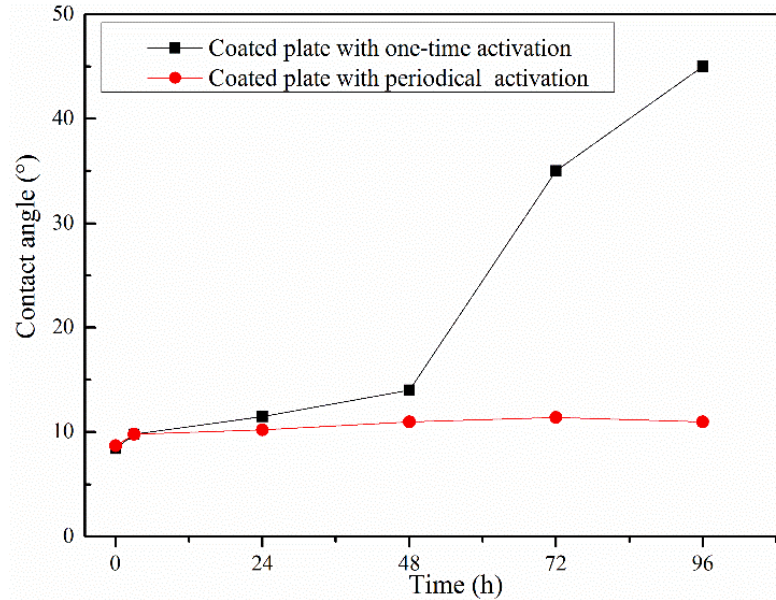
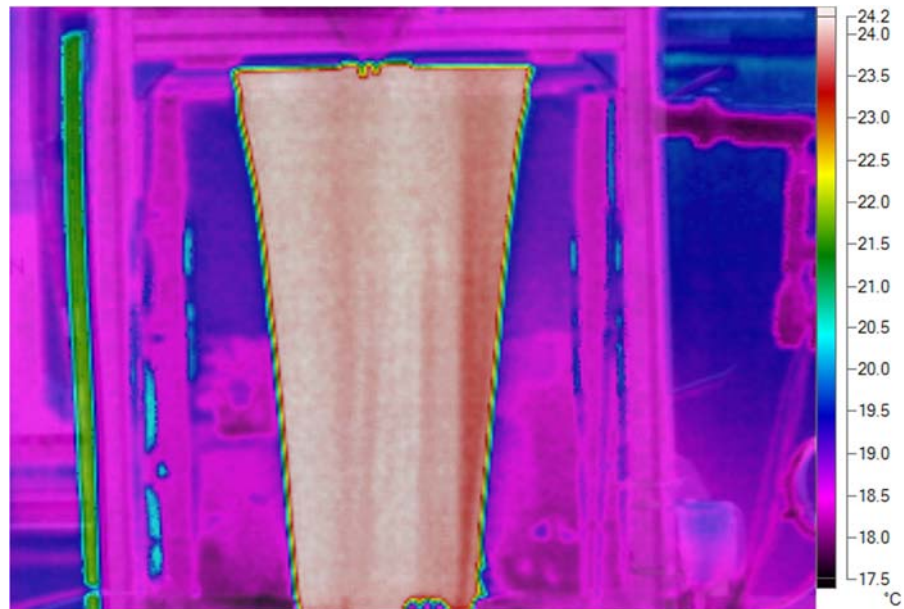


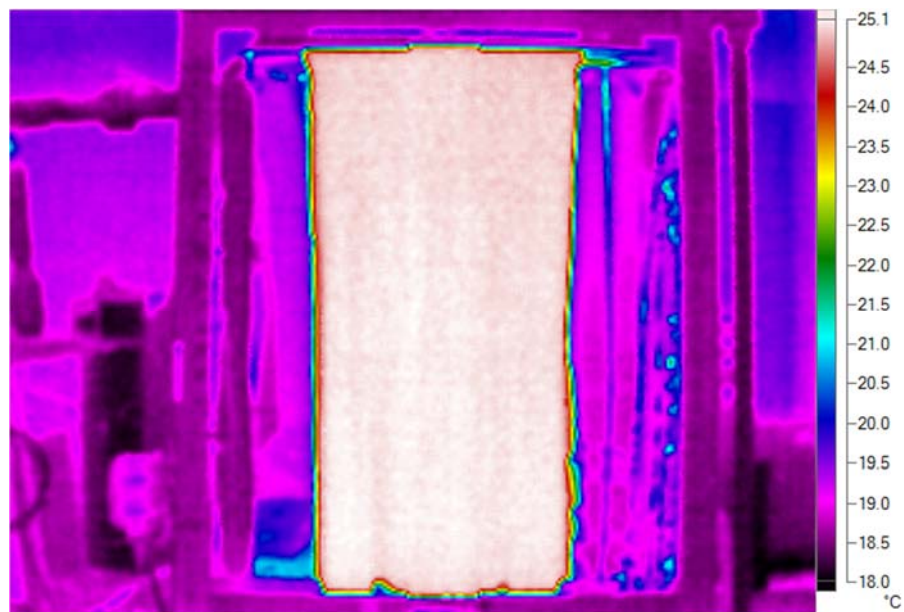
Fig. 5.6 Contact angles of coated plates under one-time and periodical activation

As the heat and mass transfer during dehumidification process depends heavily on the contact area between processed air and liquid desiccant solution, the wetting area of liquid desiccant solution on working plates is one of the key parameters in liquid desiccant dehumidifiers. In this experiment, the wetting area was captured by a thermal image camera (Fluke Ti 200). Fig. 5.7 shows the thermal images of the fall film on the coated and uncoated plate dehumidifiers. The falling film on the uncoated plate dehumidifier shrinks seriously along the flow direction due to the repellence between desiccant solution and the working plate, while little shrinkage of falling film occurs in the surface-modified plate dehumidifier. The huge difference of the falling film distribution can be attributed to the significant increment of the surface wettability

caused by the nanoscale TiO₂ super-hydrophilic coating.



(a) Uncoated plate dehumidifier



(b) Coated plate dehumidifier

Fig. 5.7 Thermal images of falling film on coated and uncoated plate dehumidifiers

To better investigate the wetting area in surface-modified plate dehumidifier, wetting ratio, φ_A , is introduced in the thesis. The wetting ratio, φ_A , represents the ratio of the actual wetting area to the maximum possible one. Fig. 5.8 presents the variation of the wetting ratios with the desiccant flow rates for coated and uncoated plate dehumidifiers. The wetting ratio on coated plate was much higher than that on the uncoated one. Due to the shrinkage of the falling film, the maximum wetting ratio on the uncoated plate was around 75%. However, the coated plate was easy to be completely or almost completely wetted by the desiccant solution. That was because the TiO₂ super-hydrophilic coating on coated plate could significantly improve surface wettability and reduce the shrinkage of the falling film. Both the wetting ratios on the coated and uncoated plate firstly increased rapidly and then slightly with the solution flow rates. In addition, falling film breakdown occurred at low solution flow rates and increasing the flow rates could effectively reduce the breakdown and therefore significantly increase the wetting ratios. One interesting finding was that the minimum wetting flow rate on the coated plate was 0.015 kg/s which was lower than that on the uncoated plate with the value of 0.020 kg/s. The minimum wetting flow rate represents the minimum required solution flow rate to avoid the falling film breakdown. The difference was attributed to the higher surface wettability on the coated plate.

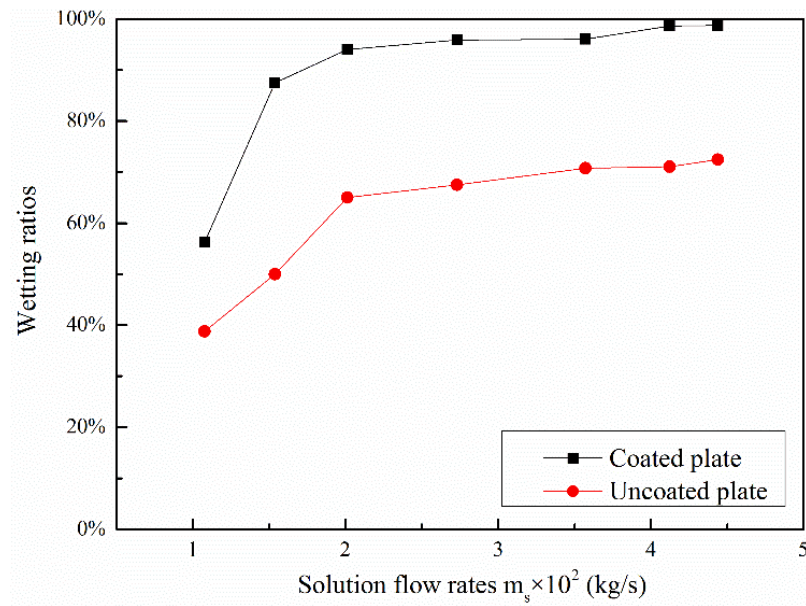


Fig. 5.8 Effect of solution flow rates on wetting ratios on coated and uncoated plates

5.4.2.3 Falling film thickness and fluctuation

As discussed in Chapter 3, several correlations of mean falling film thickness have been proposed. The detailed correlations can be referenced in Table. 3.7. Fig. 5.9 shows the variation of both measured and calculated mean falling film thickness with liquid desiccant flow rates. The mean falling film thicknesses on both coated and uncoated plates increases with the liquid desiccant flow rate. One interesting finding is that the mean film thickness on uncoated plate is a little higher than that on coated plate, which results from the different wetting conditions of liquid desiccant, as shown in Fig. 5.9. The falling film shrinks obviously along flowing direction in uncoated plate dehumidifier, while little shrinkage occurs in coated plate dehumidifier.

Therefore, the mean falling film thickness in coated plate dehumidifier is higher than that in coated plate dehumidifier. Besides, the measured mean falling film thickness was compared with the measured values by Nusselt equation [118], as shown in Fig. 5.9. It is found that the mean falling film thickness in coated plate dehumidifier agrees well with Nusselt equation [118], while that in uncoated plate dehumidifier is a bit higher than the calculated values. The reason is that Nusselt equation [118] was developed based on the experimental data in tubes, in which no shrinkage was considered. Therefore, Nusselt equation [118] could accurately estimate the mean falling film thickness in coated plate dehumidifiers but underestimate the values in uncoated plate dehumidifiers.

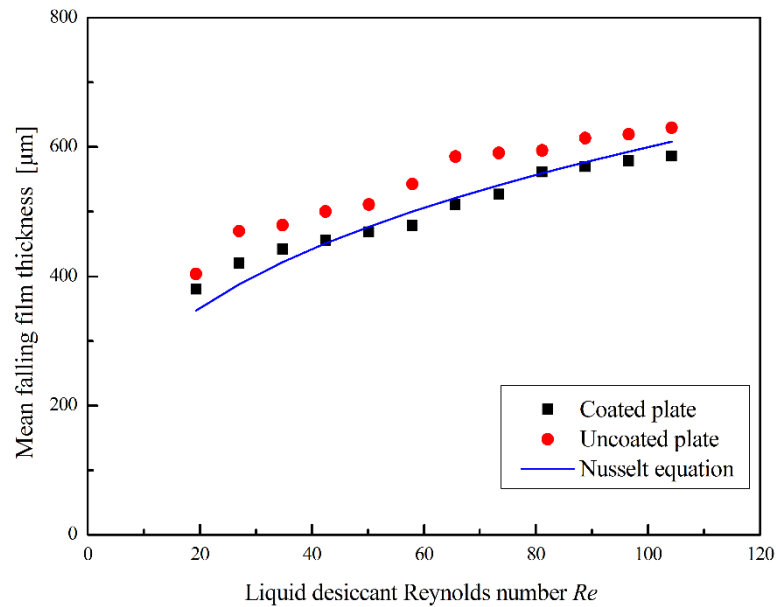


Fig. 5.9 Mean falling film thickness in coated and uncoated plate dehumidifiers

The fluctuation of falling film is another influencing factor affecting dehumidification

performance. Fig. 5.10 presents the instantaneous falling film thickness in both coated and uncoated plate dehumidifiers. The liquid desiccant flow rates demonstrate positive effect on fluctuation of falling film. It is observed that the falling film fluctuates periodically and the amplitude is mainly determined by liquid flow rates. In uncoated plate dehumidifier, the average amplitude increased from 6.6 μm to 25.9 μm with the liquid Reynolds number increased from 19.3 to 104.2, while the average amplitude increased from 3.3 μm to 27.7 μm in coated plate dehumidifiers. To estimate the fluctuation of falling film thickness, a novel and simplified empirical correlation of instantaneous falling film thickness is developed based on the experimental results.

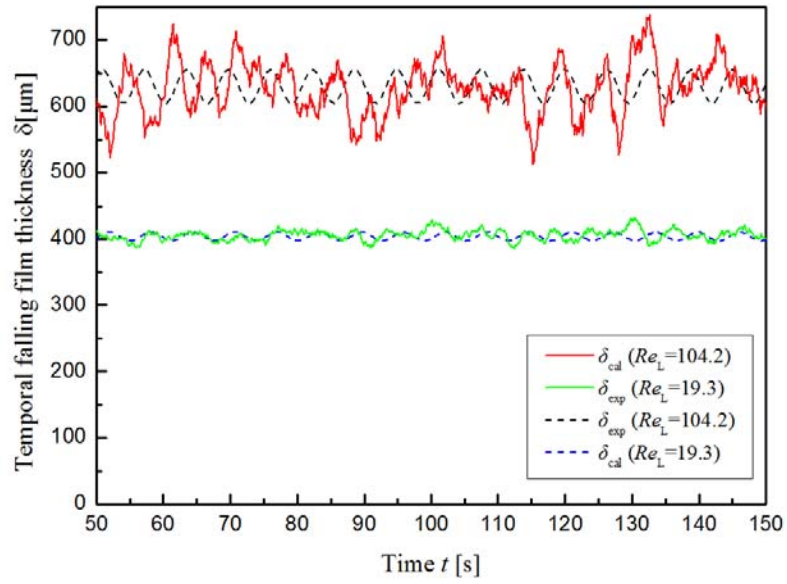
In coated plate dehumidifier,

$$\delta = (0.287 Re_L - 1.80) \sin(1.04t) + 0.909 \left(\frac{v^2}{g} \right)^{1/3} Re_L^{1/3} \quad (5.7)$$

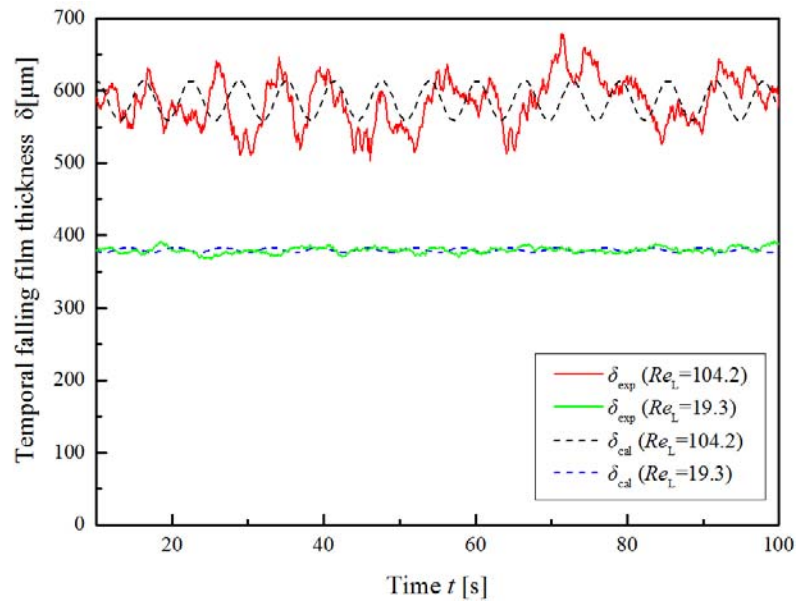
In uncoated plate dehumidifier,

$$\delta = (0.227 Re_L - 2.40) \sin(1.02t) + 1.01 \left(\frac{v^2}{g} \right)^{1/3} Re_L^{1/3} \quad (5.8)$$

The comparison between measured and calculated instantaneous falling film thickness in coated and uncoated plate dehumidifiers is shown in Fig. 5.10. The R^2 values for Eqs. (5.7) and (5.8) are 0.95 and 0.96, respectively. Although the newly-developed correlation cannot accurately predict the falling film thickness all the time, the overall agreement between calculated and measured falling film thickness is acceptable.



(a) Uncoated plate dehumidifier



(b) Coated plate dehumidifier

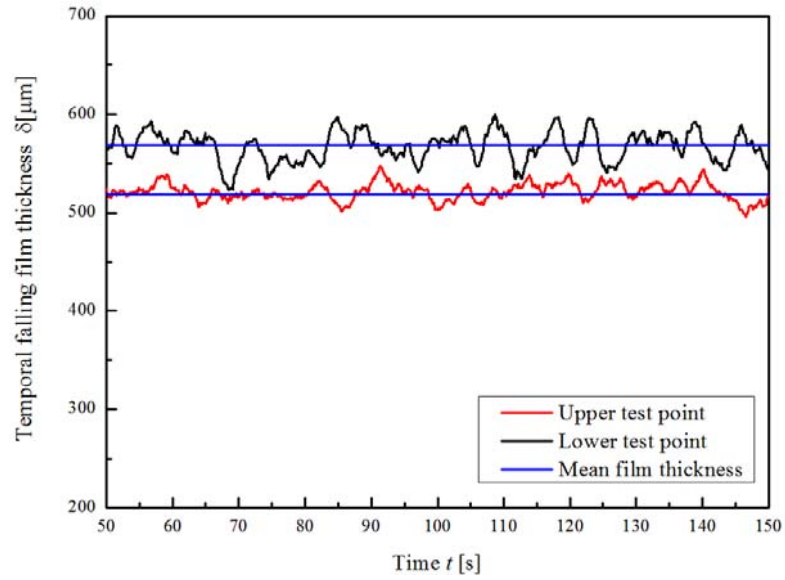
Fig. 5.10 Comparison between measured and calculated falling film thickness for both coated and uncoated plate dehumidifier

Fig 5.11 presents the instantaneous falling film thickness at lower and upper test points for both coated and uncoated plate dehumidifiers. It is clearly observed that the falling

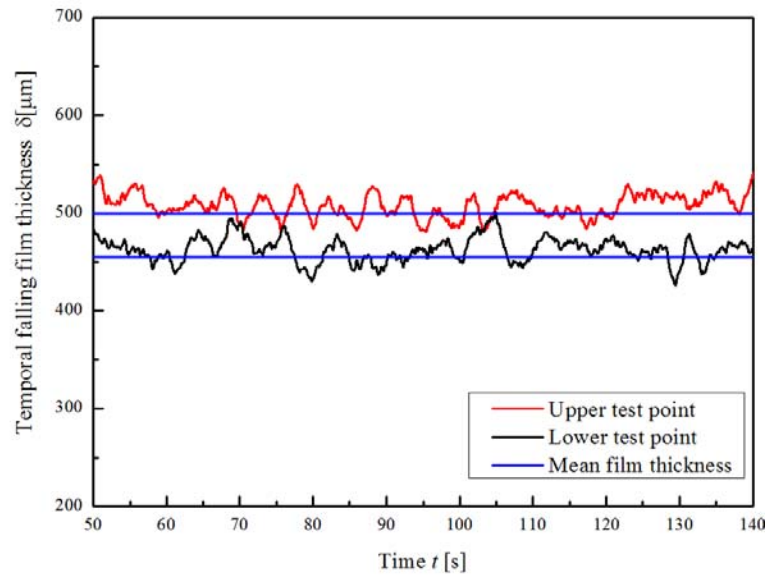
film fluctuates periodically at both lower and upper test points. Further analysis indicates that the fluctuation at the lower test point is more intense than that at the upper test point in terms of both frequency and amplitude. Three development stages of falling film were observed in the experiment. At first stage, the falling film just spread out from the distributor and flowed as flat film. Then, two-dimensional waves occurred and the flow fluctuation increased. Quickly, three-dimensional waves were developed and the fluctuation of falling film turned more intense. Another interesting finding is that the film thickness at the upper test point was higher than that at the lower test point in uncoated plate dehumidifier, but the opposite phenomenon occurred in coated plate dehumidifier. According to mass conservation, the falling film thickness is determined by liquid velocity and wetting length. These two factors demonstrate opposite effect on falling film thickness. As the wetting length at the lower section is smaller than that at the upper section in uncoated plate dehumidifier due to the film shrinkage, the falling film thickness at the lower section is a bit higher than that at the upper section. However, as little shrinkage occurs in coated plate dehumidifier, the increasing liquid velocity due to gravity along flow direction could reduce the film thickness.

Better understanding of the falling film fluctuation or waves can help estimate the actual interfacial area between processed air and desiccant accurately. The new

correlation of falling film wave can also applied in other falling film applications to improve the predicative accuracy.



(a) Uncoated plate dehumidifier

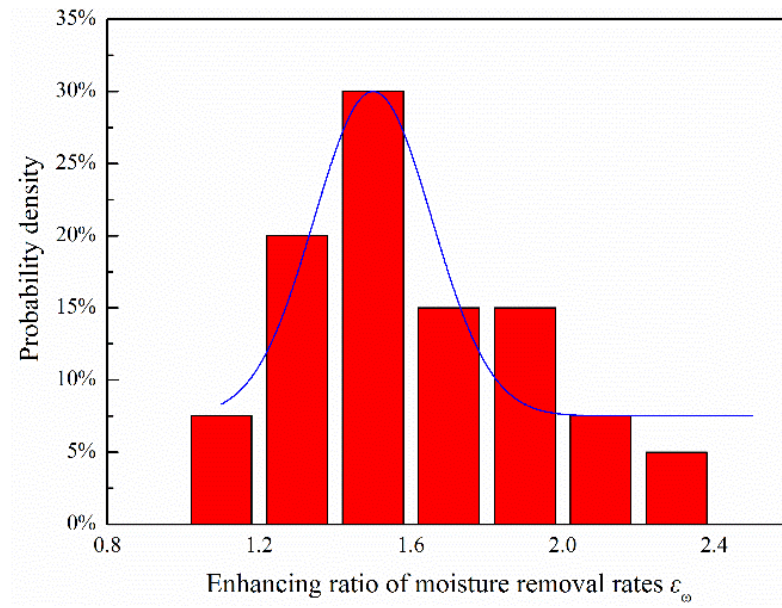


(b) Coated plate dehumidifier

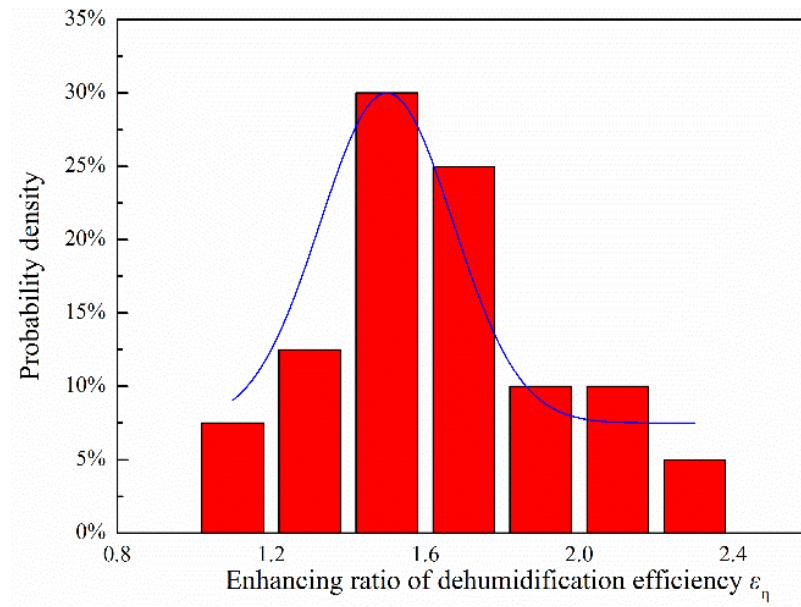
Fig. 5.11 Instantaneous falling film thickness at both lower and upper test point for both coated and uncoated plate dehumidifier ($Re_s=57.9$, $T_s=25^\circ\text{C}$)

5.4.3 Dehumidification performance enhancement

Fig. 5.12 presents the probability density of the performance enhancing ratios of the coated dehumidifier. The dehumidification performance was significantly enhanced by the TiO₂ super-hydrophilic coating. Both enhancing ratios increased from 1.0 to 2.4 with the mean values of 1.60 and 1.63 for ε_w and ε_η , respectively. To further analyze the data, Gauss curves were fitted in the figure. The results demonstrated that the highest probability for the enhancing ratios lied in 1.5. The performance enhancement of the coated plate dehumidifier can be attributed to the increase of the wetting area and the decrease of the falling film thickness caused by the TiO₂ super-hydrophilic coating. As discussed above, the contact angle of the liquid desiccant on the working plates was significantly reduced by the coating, which could effectively prevent the shrinkage of the falling film and therefore increase the wetting area. In addition, the falling film thickness on the coated plate also decreased with the increase of the surface wettability. The decrease of the falling film thickness could benefit the dehumidification performance by reducing the heat transfer resistance between the falling film and the cooling water. Besides, the mass transfer resistance inside the falling film could also be reduced by accelerating the replenishment of the surficial liquid desiccant.



(a) Enhancing ratio of moisture removal rate ε_{ω}



(b) Enhancing ratio of dehumidification efficiency ε_{η}

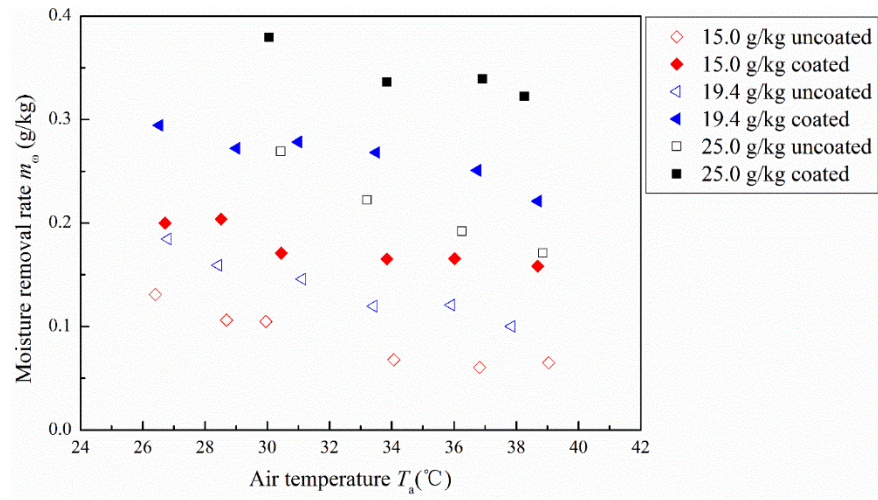
Fig. 5.12 Probability density of the performance enhancing ratio for the coated plate dehumidifier

5.4.4 Influencing factors analysis of dehumidification performance

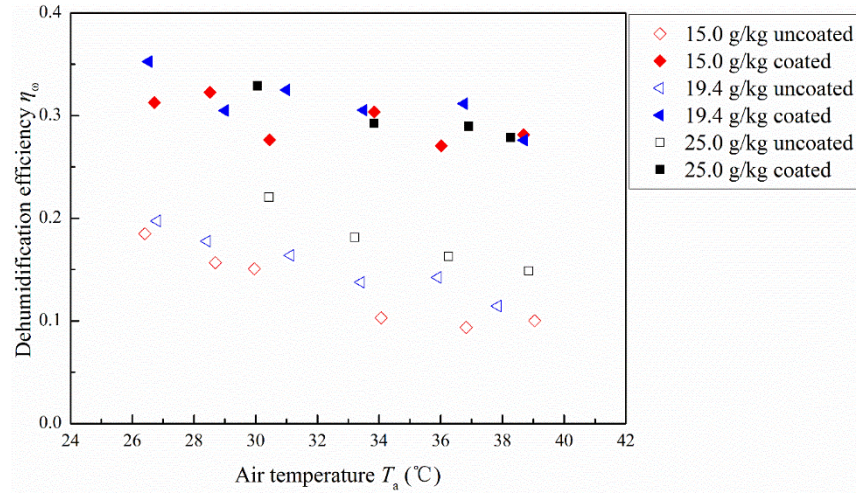
The influence of the inlet parameters (including air temperature, air humidity and air flow rate, desiccant flow rate and cooling water temperature) on the dehumidification performance for the coated and uncoated plate dehumidifiers was investigated comprehensively in this section.

5.4.4.1 Air temperature

Fig. 5.13 shows the variation of dehumidification performance with air temperature at different inlet air humidity for the coated and uncoated plate dehumidifiers. It can be clearly observed that dehumidification performance of the coated plate dehumidifier was much better than that of the uncoated plate dehumidifier. Both the moisture removal rate and the dehumidification efficiency decreased with the increase of air temperature. As air temperature increased, more heat was exchanged from the air to the liquid desiccant. The temperature increase of the liquid desiccant could reduce the driving force of the dehumidification process and therefore deteriorate the dehumidification performance.



(a) Moisture removal rate m_{ω}



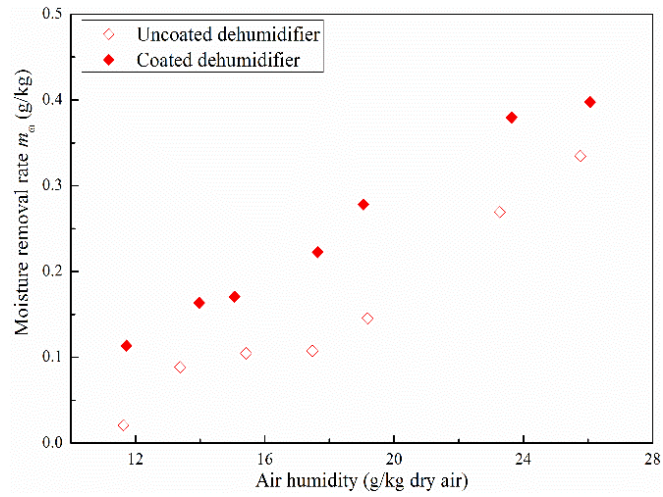
(b) Dehumidification efficiency η_{ω}

$T_{a,in}$	$\omega_{a,in}$	$m_{a,in}$	$T_{s,in}$	$m_{s,in}$	T_{fin}	m_f
(°C)	(g/kg)	(kg/s)	(°C)	(kg/s)	(°C)	(kg/s)
26.4-38.7	15.0, 19.4, 25.0	0.06	26.4	0.043	20.0	0.050

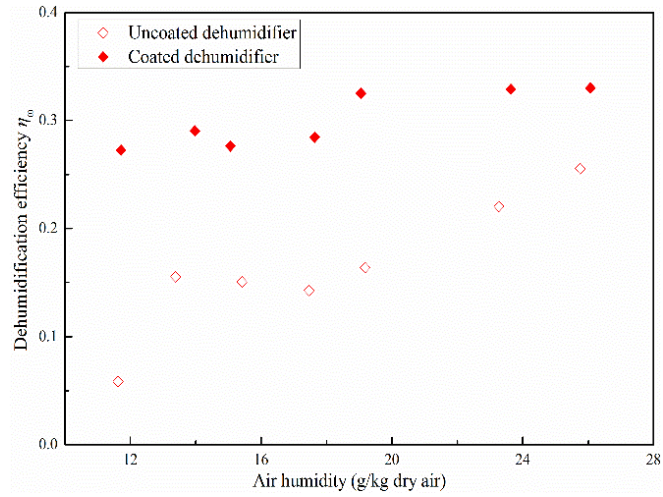
Fig. 5.13 Effect of air temperature on dehumidification performance of coated and uncoated plate dehumidifiers

5.4.4.2 Air humidity

Fig. 5.14 demonstrates the effect of air humidity on dehumidification performance. As the air humidity varies a lot during the whole year, it is necessary to investigate the effect of air humidity on dehumidification performance. As shown in Fig. 5.14(a), the moisture removal rate increased rapidly with the air humidity. The driving force of the vapor absorption increased significantly with the air humidity, which led to obvious increase of the moisture removal rate. However, as shown in Fig. 5.14(b), the dehumidification efficiency of the coated plate dehumidifier just increased slightly with air humidity. As air humidity increased, both the actual moisture absorption rate and the maximum possible one increased accordingly. The compromising results led to a slight increase of the dehumidification efficiency. However, the dehumidification efficiency of the uncoated plate dehumidifier increased rapidly with air humidity, especially under higher air humidity conditions. As part of the working plate was unwetted by the liquid desiccant solution in the uncoated plate dehumidifier, the water moisture might condense on the unwetted surface due to the low temperature of the working plate. The moisture condensation could partly increase the dehumidification efficiency. However, as the coated plate was almost completely wetted by the liquid desiccant, little moisture condensation occurred in the coated plate dehumidifier. Thus the difference in dehumidification efficiency between coated and uncoated plates becomes smaller with higher air humidity.



(a) Moisture removal rate m_{ω}



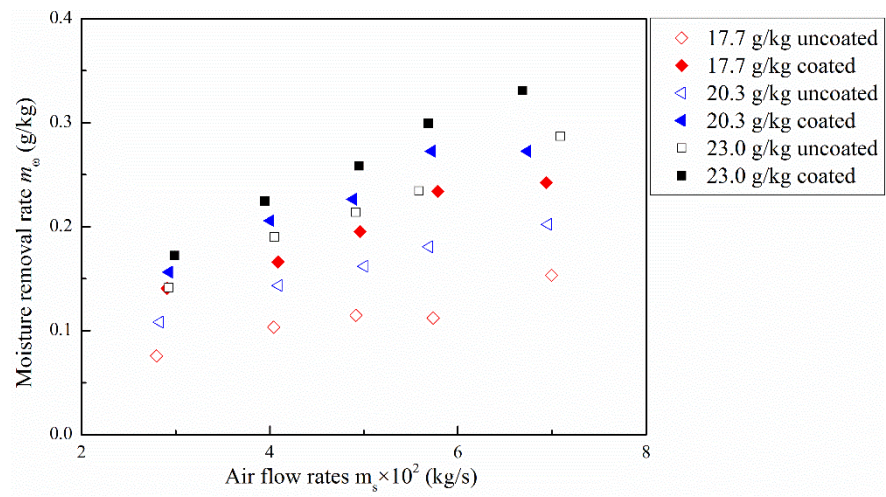
(b) Dehumidification efficiency η_{ω}

$T_{a,in}$	$\omega_{a,in}$	$m_{a,in}$	$T_{s,in}$	$m_{s,in}$	$T_{f,in}$	m_f
(°C)	(g/kg)	(kg/s)	(°C)	(kg/s)	(°C)	(kg/s)
30.5	11.7-26.2	0.06	26.1	0.043	20.0	0.050

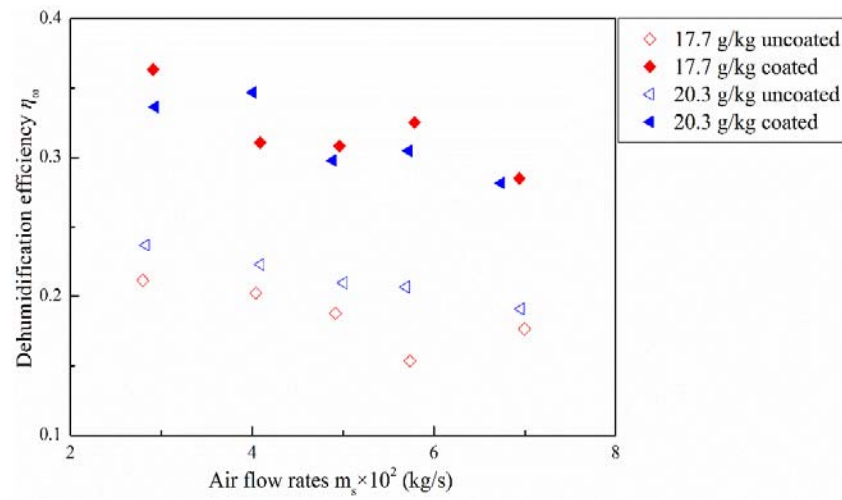
Fig. 5.14 Effect of air humidity on dehumidification performance of coated and uncoated plate dehumidifiers.

5.4.4.3 Air flow rate

The influence of air flow rate on dehumidification performance for the coated and uncoated plate dehumidifier is shown in Fig. 5.15. As shown in Fig. 5.15(a), the moisture removal rates increased rapidly with the air flow rates, which could be attributed to the reduction of the concentration polarization. The concentration polarization in dehumidification process referred to the depletion of the water moisture in the boundary layer of the process air and the accumulation of the water moisture in the boundary layer of the liquid desiccant solution. The existence of the concentration polarization could prevent the moisture exchange from the process air to the liquid desiccant and therefore affect the dehumidification performance. It was found that increasing the air flow rate could thin the boundary layers and reduce the concentration polarization as well, which could effectively increase the moisture removal rates. However, as the length of the plate dehumidifier was limited, the increase of air flow rate might lead to insufficient contact time for the air and liquid desiccant. Therefore, the dehumidification efficiency dropped with air flow rates



(a) Moisture removal rate m_{ω}



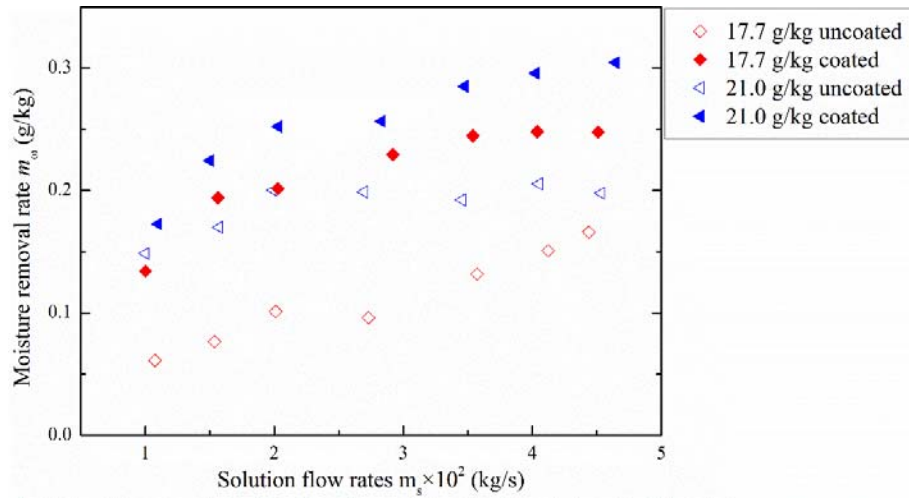
(b) Dehumidification efficiency η_{ω}

$T_{a,in}$	$\omega_{a,in}$	$m_{a,in}$	$T_{s,in}$	$m_{s,in}$	T_{fin}	m_f
(°C)	(g/kg)	(kg/s)	(°C)	(kg/s)	(°C)	(kg/s)
30.5	17.7, 20.3, 23	0.029-0.069	26.0	0.043	20.0	0.050

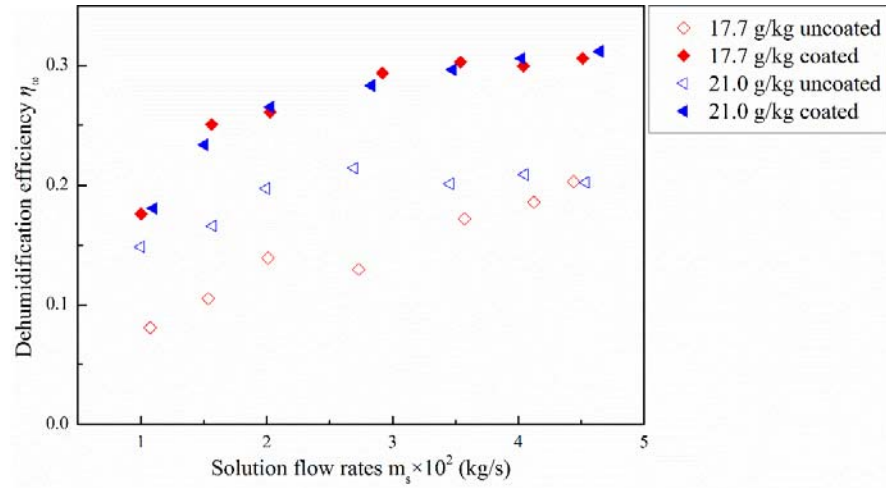
Fig. 5.15 Effect of air flow rate on dehumidification performance of coated and uncoated plate dehumidifiers

5.4.4.4 Desiccant solution flow rate

As shown in Fig. 5.16, both the moisture removal rate and the dehumidification efficiency increased with desiccant flow rates. Firstly, the wetting area of the liquid desiccant increased with desiccant flow rates, which could directly improve the dehumidification performance. Secondly, the fluctuation of the liquid desiccant falling film was also enhanced with higher desiccant flow rates. The higher fluctuation could accelerate the replenishment of the surficial liquid desiccant and reduce the mass transfer resistance inside the falling film. Lastly, the temperature increase of the liquid desiccant was reduced with higher desiccant flow rates. The experimental results indicated that the temperature increase of the liquid desiccant was reduced from 3.6 °C to 1.7 °C as the desiccant flow rate increased from 0.16 g/kg to 0.045 g/kg. One interesting finding from Fig. 5.16(a) is that the moisture removal rate firstly increased rapidly then slightly with desiccant flow rates, which can be explained by the variation of the wetting area with the solution flow rates, as shown in Fig. 5.8. The increase of desiccant flow rate could significantly increase the wetting area and therefore significantly increase the dehumidification performance with lower desiccant flow rates. As desiccant flow rate increased above the minimum wetting flow rate, the wetting area increased slightly, leading to a slight increase of the dehumidification performance



(a) Moisture removal rate m_ω



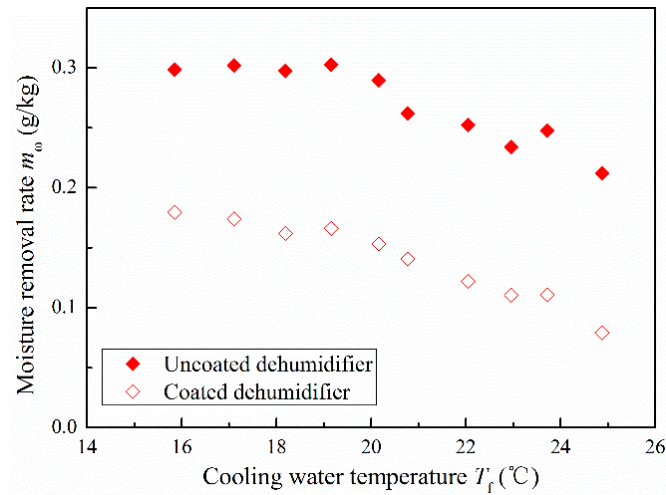
(b) Dehumidification efficiency η_ω

$T_{a,in}$	$\omega_{a,in}$	$m_{a,in}$	$T_{s,in}$	$m_{s,in}$	$T_{f,in}$	m_f
(°C)	(g/kg)	(kg/s)	(°C)	(kg/s)	(°C)	(kg/s)
30.3	17.7, 21.0	0.06	25.9	0.01-0.049	20.1	0.050

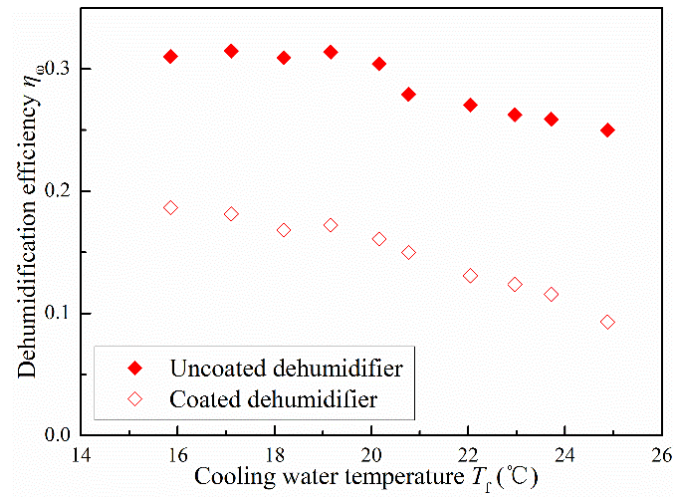
Fig. 5.16 Effect of desiccant solution flow rate on dehumidification performance of coated and uncoated plate dehumidifiers

5.4.4.5 Cooling water temperature

In internally-colded liquid desiccant dehumidifier, the cooling water is used to remove the latent heat released during the absorption process and to prevent the temperature increase of the liquid desiccant. Therefore, the cooling water temperature is very important to dehumidification performance. Fig. 5.17 illustrates the effect of cooling water temperature on dehumidification performance of coated and uncoated plate dehumidifiers. Both the moisture removal rate and the dehumidification efficiency decreased with increase of the cooling water temperature. The temperature increase deteriorated the heat transfer between the cooling water and the desiccant solution and therefore affected the dehumidification performance. In addition, vapor condensation might occur on the exposed surface in some experimental conditions with high humidity and low cooling water temperature, which could also enlarge the dehumidification rate, as shown in Fig. 5.18.



(a) Moisture removal rate m_w



(b) Dehumidification efficiency η_{ω}

$T_{a,in}$	$\omega_{a,in}$	$m_{a,in}$	$T_{s,in}$	$m_{s,in}$	$T_{f,in}$	m_f
(°C)	(g/kg)	(kg/s)	(°C)	(kg/s)	(°C)	(kg/s)
30.1	20.2	0.06	26	0.043	15.8-24.9	0.050

Fig. 5.17 Effect of cooling water temperature on dehumidification performance of coated and uncoated plate dehumidifiers



Fig. 5.18 Condensation of vapor on exposed surfaces

5.4.5 Development of mass transfer coefficient considering solid-liquid interaction effect

Mass transfer coefficient, representing the mass transfer rate between liquid desiccant solution and processed air, is one of the critical index in liquid desiccant dehumidifiers. Therefore, it is very important to accurately estimate the mass transfer coefficient under various operating conditions. To non-dimensionalize the mass transfer coefficient, Sherwood (Sh) number is proposed. The relationship between mass transfer coefficient and Sherwood (Sh) number is expressed as follows.

$$h_D = \frac{D_a Sh}{d} \quad (5.9)$$

where D_a is the diffusion coefficient and d is the width of the air channel. Several mass transfer correlations of liquid desiccant dehumidifiers have been proposed in

terms of Sherwood (Sh) number. The existing correlations are summarized as follows.

Table 5.3 Summary of mass transfer correlations

Sources	Correlations	Flow patterns
Reker et al. [129]	$Sh_G = 0.0065 Re_G^{0.83} Sc_G^{0.15}$	Counter-current
Onda et al [130]	$Sh_G = 5.23 Re_G^{0.7} Sc_G^{0.33}$	Counter-current
Chung and Wu [47]	$Sh_G = 4 \times 10^{-5} Re_G^{1.73} Sc_G^{0.33} \left(\frac{P_{TEG}}{P_{total}} \right)^{-0.5}$	Counter-current
	$\times \left(\frac{L}{G} \right)^{1.15}$	(With fin coils)
	$Sh_G = 2 \times 10^{-5} Re_G^{1.74} Sc_G^{0.33} \left(\frac{P_{TEG}}{P_{total}} \right)^{-0.51}$	(Without fin coils)
Nielsen et al. [131]	$Sh_G = 3.1 \times 10^{-4} Re_G^{1.05} Re_L^{0.207} Sc_G^{0.5}$	Co-current
	$Sh_G = 5.59 \times 10^{-6} Re_G^{1.546} Sc_G^{0.333} \left(\frac{F_s}{F_a} \right)^{0.617}$	Cross-flow
Liu et al. [132]	$\times (1 - \xi)^{-5.353}$	
Qi [133]	$Sh = 3.2 \times 10^{-4} Re_G^{0.37} Sc_G^{0.33} Re_s^{0.47} Sc_s^{0.33}$	Co-current
Yin et al. [68]	$Sh = 4.513 \times 10^{-3} k Re_G^{1.56} Sc_G^{0.33}$	Co-current
	$k = 76.456 T_s^{-2.991}$	

As presented in Table 5.3, the mass transfer coefficient is mainly determined by Reynolds number and Schmidt number of processed air and liquid desiccant solution. However, the surface property, especially the surface wettability, has not been

considered in the existing mass transfer correlations. As discussed above, the surface property plays an important role in mass transfer between the processed air and liquid desiccant solution. Therefore, a novel mass transfer correlation considering the effect of surface wettability on dehumidification performance is developed in this section. The original form of the new mass transfer correlation is given as follows.

$$Sh_G = Af(\gamma) Re_G^{B_1} Sc_G^{B_2} Re_S^{B_3} \quad (5.8)$$

where $f(\gamma)$ is the function of surface free energy, γ .

$$f(\gamma) = C - D\gamma^E \quad (5.9)$$

where $A-E$ are coefficients and need to be identified. Non-linear regression method is adopted in this section to identify the unknown coefficients based on the experimental results. The coefficient $A-E$ are identified as follows.

Table 5.4 Summary of coefficients in the new mass transfer correlation

Coefficient	A	B_1	B_2	B_3	C	D	E
Value	-0.716	0.800	16.1	0.167	12.2	12.3	0.00233

Therefore, the new empirical mass transfer correlation is expressed as follows.

$$Sh_G = -0.716f(\gamma) Re_G^{0.800} Sc_G^{16.1} Re_L^{0.167} \quad (5.10)$$

$$f(\gamma) = 12.2 - 12.3\gamma^{0.00233} \quad (5.11)$$

To verify the new mass transfer correlation, the comparison between the calculated and experimental mass transfer coefficients are shown in Fig. 5.19. 93% of the calculated mass transfer coefficient fell within $\pm 20\%$ errors of the experimental results with the average relative deviation (ARD) of 0.7%, validating the newly-developed mass transfer correlation.

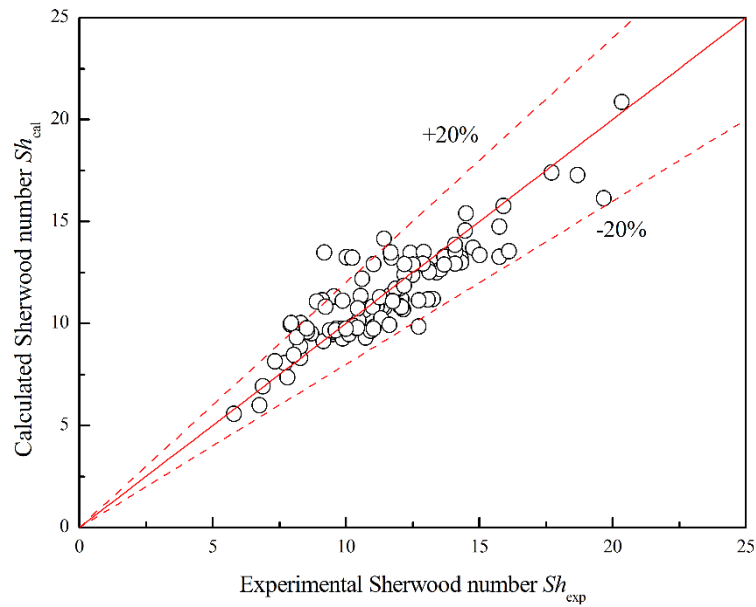


Fig. 5.19 Comparison between calculated and experimental mass transfer coefficient

In the existing mass transfer correlations, the liquid desiccant dehumidifiers were assumed to be completely wetted by liquid desiccant solution, which did not accord with the practical case. Therefore, $f(\gamma)$, a function of surface free energy, is newly introduced to account for the effect of surface wettability on dehumidification performance in the newly-developed mass transfer coefficient and improve the

prediction accuracy. Fig. 5.20 presents the comparison of the calculated mass transfer coefficient by present correlation, Nielsen et al. [131] correlation and Yin et al. [68] correlation, respectively. The calculated mass transfer coefficients by present correlation agree well with the experimental results. However, Nielsen et al. [131] correlation overestimates the mass transfer coefficient a bit, while Yin et al. [68] correlation underestimates the mass transfer coefficient. This difference might result from different geometric structures of the liquid desiccant dehumidifiers.

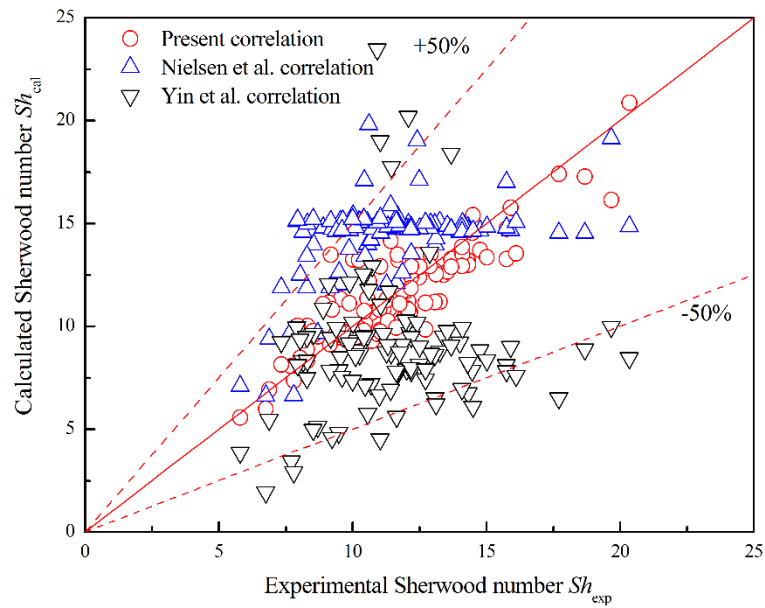


Fig. 5.20 Comparison of the calculated mass transfer coefficients by present correlation, Nielsen et al. [131] correlation and Yin et al. [68] correlation.

5.5 Summary

In this chapter, an experimental setup with two single-channel internally-cooled liquid desiccant dehumidifiers was fabricated to investigate the flow and heat/mass transfer

characteristics of the surface-modified plate dehumidifier. The main conclusions are summarized as follows.

(1) Surface-modification technology was adopted in this chapter to increase the surface wettability of plate dehumidifiers. A double layer TiO_2 super-hydrophilic coating was developed and the characterization of the coating was conducted. The test results showed that the contact angle of the liquid desiccant was significantly reduced from 84.6° to 8.8° and the adhesion between surface and liquid desiccant was effectively enhanced by the super-hydrophilic coating.

(2) The flow characteristics of falling film is influenced by surface wettability. The wetting ratio of liquid desiccant solution was significantly improved with surface treatment. The falling film on uncoated plate dehumidifier shrank seriously along the flow direction due to the repulsion between desiccant solution and the working plate, while little shrinkage of falling film occurred in the surface-modified plate dehumidifier. The maximum wetting ratio was increased from 75% to 100% by TiO_2 super-hydrophilic coating. The mean falling film thickness in coated plate dehumidifier was a bit lower than that in the uncoated plate dehumidifier. A novel and simplified correlation of instantaneous falling film thickness is developed to simulate the fluctuation of falling film.

(4) The dehumidification ability, including moisture removal rate ε_w and dehumidification efficiency ε_η , was significantly improved with the TiO₂ super-hydrophilic coating. The average enhancing ratios for moisture removal rate and dehumidification efficiency were 60% and 63%, respectively. The performance enhancement was mainly attributed to the increase of wetting area.

(5) The influencing factors of the dehumidification performance were investigated in detail. The air temperature shows negative effect on dehumidification performance, while the air flow rate, humid ratio and liquid desiccant flow rate demonstrate positive effect on dehumidification performance.

(6) A novel empirical correlation of mass transfer correlation considering solid-liquid interaction effect was developed using non-linear regression method based on the experimental results. The surface free energy was considered in the correlation to account for solid-liquid interaction effect on dehumidification performance. The comparison between calculated results by present model and other existing models indicated that the new correlation demonstrated superior prediction accuracy.

CHAPTER 6

ANALYTICAL MODEL OF HEAT AND MASS TRANSFER PERFORMANCE CONSIDERING THE SOLID-LIQUID INTERACTION EFFECT

6.1 Introduction

As summarized in Chapter 2, several simulation models of liquid desiccant dehumidifiers have been developed. However, most of existing models do not consider the incomplete wetting conditions or actual wetting area of liquid desiccant solution, so they cannot be applied accurately in actual conditions. Therefore, this chapter aims to develop an improved heat and mass transfer model of internally-cold liquid desiccant dehumidifiers considering actual wetting area. The main academic contributions in this chapter are summarized as follows.

- (1) A falling film shrinkage model is developed to accurately estimate the actual wetting area of liquid desiccant solution in plate dehumidifiers considering solid-liquid interaction effect. The shrinkage model is well validated by experimental results.
- (2) An improved heat and mass transfer model of an internally-cold liquid desiccant dehumidifier considering the actual wetting conditions is developed to investigate the heat and mass transfer characteristics of liquid desiccant plate dehumidifiers.

(3) The effect of surface wettability on flow characteristics is numerically investigated using the newly-developed model. The actual wetting areas of liquid desiccant in plate dehumidifiers with different contact angles are simulated. Besides, the effect of surface wettability on mean falling film thickness and the distribution of falling film thickness along the flow direction are also investigated.

(4) The effect of surface wettability on dehumidification performance are comprehensively investigated. The distributions of processed air and liquid desiccant parameters along the flow direction are simulated to investigate the heat and mass transfer characteristics of liquid desiccant dehumidifiers.

6.2 Numerical model development

6.2.1 Model development of falling film shrinkage with different contact angles

According to Zhang et al. [134], the falling film shrinks rapidly along the flow direction and the shrinkage varies considerably depending on the surface wettability of working surface. In this chapter, the model was extended to very low contact angles of around 10° , which can be achieved with super-hydrophilic coating. As shown in Fig. 6.1 (a), the falling film can be divided into two parts, i.e., the central part and the rim part. The shrinkage is caused by the surface tension gradient between these parts.

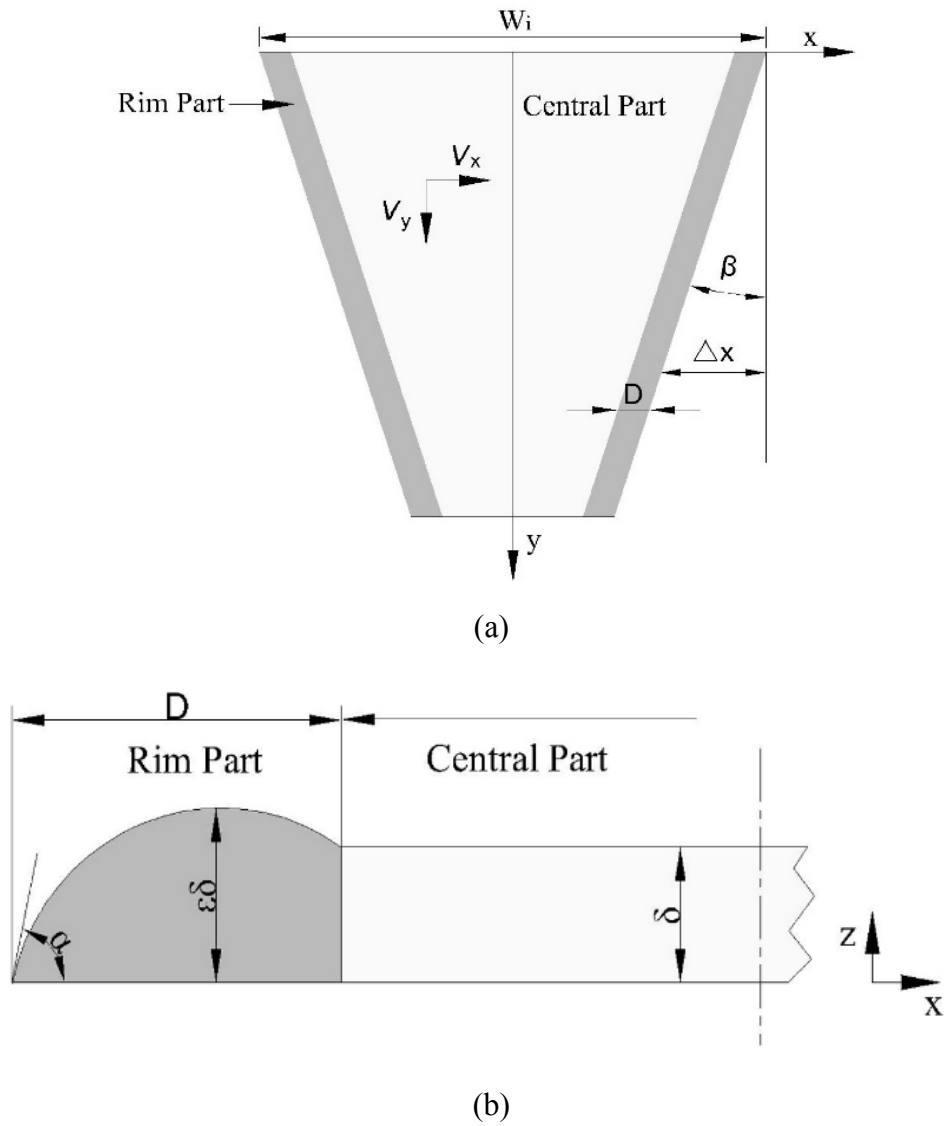


Fig. 6.1 Schematic of (a) falling film and (b) rim part

The shrinkage width Δx can be calculated from the velocity component in the transverse direction V_x . The transverse velocity component can be obtained by momentum equations in the rim part:

$$\mu_s \frac{\partial^2 V_x}{\partial z^2} = 0 \quad (6.1)$$

where μ_s is the dynamic viscosity of the desiccant solution. The boundary conditions can be calculated as below:

$$z = 0, V_x = 0; \quad z = \delta, \mu_s \frac{\partial V_x}{\partial z} = \frac{\partial \sigma}{\partial x} \cos \beta$$

where σ is the surface tension of the desiccant solution, and β , as shown in Fig. 6.1(b), is the angle between the shrinkage line and the y -axis, which can be calculated as below:

$$\beta = \frac{V_{y,m}}{\sqrt{V_{y,m}^2 + V_x^2}} \quad (6.2)$$

δ is the thickness of the falling film, which can be calculated as below:

$$\delta = \left(\frac{3m_s \mu_s}{W(y) \rho_s^2 g} \right)^{1/3} \quad (6.3)$$

where $W(y)$ represents the width of the falling film at a given position on the y -axis. Therefore, by combining the equations above, the transverse velocity V_x can be expressed as below:

$$V_x = \frac{\sqrt{2}}{2} V_{y,m} \left[\left(1 + \frac{4 \left(\frac{\delta(\sigma_{cen} - \sigma_{rim})}{4\mu_s D} \right)^2}{V_{y,m}^2} \right)^{0.5} - 1 \right]^{0.5} \quad (6.4)$$

where σ_{cen} and σ_{rim} refer to the surface tensions of the desiccant solution at the central part and the rim part, respectively. The surface tension of LiCl was taken from Conde [34]. In Eqs. (6.2) and (6.4), $V_{y,m}$ stands for the maximum velocity of the falling film at the y -axis, which can be calculated by Eq. (6.5):

$$V_{y,m} = \frac{1}{2} \frac{\rho_s g}{\mu_s} \delta^2 \quad (6.5)$$

In Eq. (6.4), D stands for the width of the rim part, as shown in Fig. 6.1(b). By geometrical analysis, the value of D can be obtained as below [134]:

$$D = \frac{\varepsilon \delta \sin \alpha}{(1 - \cos \alpha)} + \delta \sqrt{\frac{2\varepsilon}{(1 - \cos \alpha)} (\varepsilon - 1) - (\varepsilon - 1)^2} \quad (6.6)$$

where ε is a deformation factor, which is related to the physical properties and the flow rate of the desiccant solution as well as the temperature difference between the desiccant solution and the working surface.

As the falling film flows down along the y -axis in the plate dehumidifier, the shrinkage width Δx at the y_0 position on the y -axis can be obtained by integrating the transverse velocity from the top of the falling film to the y_0 position:

$$\Delta x = \int_0^{y_0/V_{y,m}} V_x dt = \frac{\sqrt{2}}{2} V_{y,m} \frac{|\sigma_{rim} - \sigma_{cen}|}{\sigma_{rim} - \sigma_{cen}} \int_0^{y_0} \left[\left(1 + \frac{\delta^2 (\sigma_{rim} - \sigma_{cen})^2}{4 V_{y,m}^2 \mu_s^2 D^2} \right)^{0.5} - 1 \right]^{0.5} dy \quad (6.7)$$

Then, the wetting length at the y_0 position is calculated as below:

$$W_{y_0} = W_i - 2\Delta x = W_i - \sqrt{2} V_{y,m} \frac{|\sigma_{rim} - \sigma_{cen}|}{\sigma_{rim} - \sigma_{cen}} \int_0^{y_0} \left[\left(1 + \frac{\delta^2 (\sigma_{rim} - \sigma_{cen})^2}{4 V_{y,m}^2 \mu_s^2 D^2} \right)^{0.5} - 1 \right]^{0.5} dy \quad (6.8)$$

where W_i is the initial wetting length at the inlet of the plate dehumidifier.

Finally, the total wetting area of the falling film can be calculated by integrating the wetting length from the top to the bottom:

$$A = \int_0^H W(y) dy \quad (6.9)$$

where A is the total wetting area of the desiccant solution and H is the height of the working plate.

6.2.2 Model development of heat and mass transfer with variable film thickness

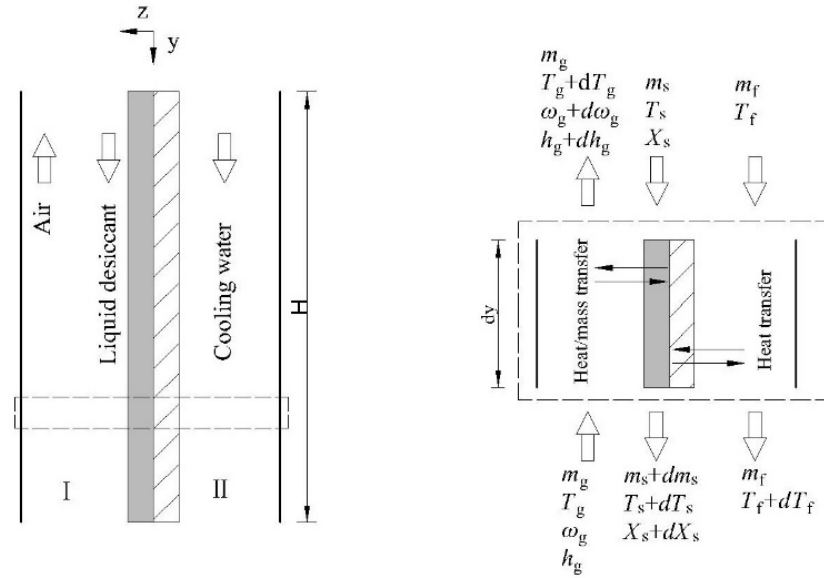


Fig. 6.2 Schematic of the internally cooled plate dehumidifier

Fig. 6.2 shows the schematic of the internally cooled plate dehumidifier. Heat and mass transfer occurred between air flowing upward and desiccant solution flowing downward in Channel I while the latent heat released during the absorption process was removed by the cooling water in Channel II, which could prevent the temperature increasing of the desiccant solution and therefore the driving force of moisture

exchange could be maintained nearly constant.

To simplify the heat and mass transfer model of the internally cooled plate dehumidifier, several assumptions are adopted in the present model.

(1) The properties of desiccant solution, air and cooling water are considered constant within the control volume.

(2) The desiccant solution, air and cooling water are considered well mixed in the cross-section.

(3) The plate dehumidifier is assumed to be well insulated and no heat is transferred to the surroundings.

(4) Due to the high heat conductivity of the working plate, the local wall temperature is set equal to the local cooling water temperature.

A control volume with the width of dy , as showed in Fig. 6.2, is presented to illustrate the heat and mass transfer in plate dehumidifier. The mass and energy balance equations of the control volume are listed below.

Heat transfer equation of between air and desiccant solution:

$$m_g C_{pg} dT_g = h_c (T_s - T_a) W(y) dy \quad (6.10)$$

Mass conservation equation of air:

$$m_g d\omega_g = dm_s = h_d (\omega_{sat} - \omega_g) W(y) dy \quad (6.11)$$

Energy conservation equation of air:

$$dh_g = (C_{pg} + C_{pv} \omega_g) dT_g + (\gamma + C_{pv} T_g) d\omega_g \quad (6.12)$$

Energy conservation equation of desiccant solution:

$$m_f C_{pf} dT_f + d(m_s h_s) + m_g dh_g = 0 \quad (6.13)$$

where $d(m_s h_s)$ can be calculated below.

$$d(m_s h_s) = m_s dh_s + h_s dm_s = m_s C_{ps} dT_s + h_s dm_s \quad (6.14)$$

Therefore, the energy conservation equation of desiccant solution can be rewritten as below.

$$dT_s = -\frac{1}{C_{ps}} \left(\frac{m_g}{m_s} dh_g + \frac{m_g}{m_s} C_{ps} T_s d\omega_g + \frac{m_f}{m_s} C_{pf} dT_f \right) \quad (6.15)$$

Mass conservation equation of desiccant solution:

$$dX_s = \frac{-dm_s}{m_s - m_g d\omega_g} X_s \quad (6.16)$$

Energy conservation equation of cooling water:

$$m_f C_{pf} dT_f = h_f (T_s - T_w) W(y) dz \quad (6.17)$$

In the above equations, ω_{sat} means the moisture content of air which is in equilibrium with the desiccant solution and h_f represents the overall heat transfer coefficient between cooling water and desiccant solution. h_c and h_d refer to the heat and mass transfer coefficients between air and desiccant solution, respectively. The relationship between h_c and h_d is expressed as below.

$$Le = \frac{h_c}{h_d C_{pg}} \quad (6.18)$$

where Le is Lewis number. In the present model, the mass transfer coefficient is calculated using the new mass transfer correlation developed in Chapter 5.

$$Sh_G = -0.716 f(\gamma) Re_G^{0.800} Sc_G^{16.1} Re_L^{0.167} \quad (6.19)$$

$$f(\gamma) = 12.2 - 12.3 \gamma^{0.00233} \quad (6.20)$$

6.2.3 Discretization and calculation of the new model

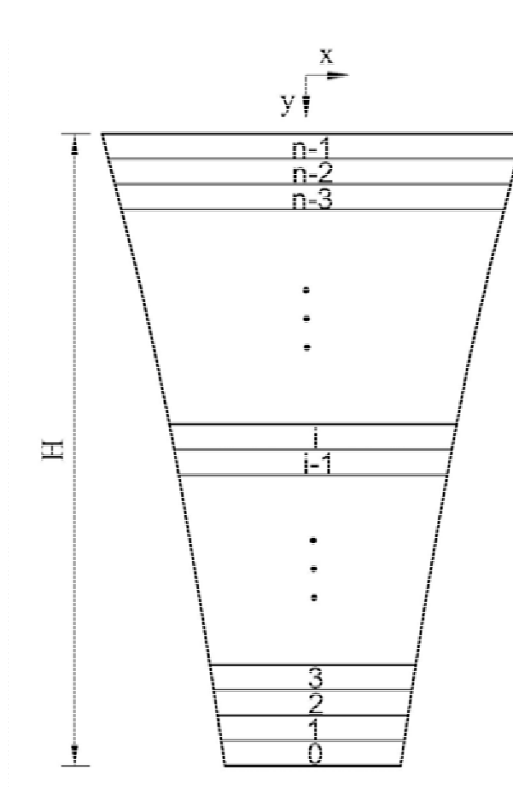


Fig. 6.3 Numerical model of plate dehumidifier with variable wetting length

The finite difference method (FDM) is adopted to solve the equations in the present model. As shown in Fig. 6.3, the plate dehumidifier can be divided into n differential

elements with variable wetting length. Based on FDM, the heat and mass transfer equations in Section 6.2.2 can be discretized as below.

Heat transfer equation between air and desiccant solution:

$$\frac{(T_{g,i+1} - T_{g,i})}{\Delta y} = \frac{h_c (T_{s,i} - T_{a,i}) W (i \Delta y)}{m_{g,i} C_{pg,i}} \quad (6.21)$$

Mass conservation equation of air:

$$\frac{(\omega_{g,i+1} - \omega_{g,i})}{\Delta y} = \frac{h_d (\omega_{sat,i} - \omega_{sat,i}) W (i \Delta y)}{m_{g,i}} \quad (6.22)$$

Energy conservation equation of air:

$$h_{g,i+1} - h_{g,i} = (C_{pg,i} + C_{pv,i} \omega_{g,i}) (T_{g,i+1} - T_{g,i}) + (\gamma_i + C_{pv,i} T_{g,i}) (\omega_{g,i+1} - \omega_{g,i}) \quad (6.23)$$

Energy conservation equation of cooling water:

$$\frac{(T_{f,i+1} - T_{f,i})}{\Delta y} = \frac{h_f (T_{s,i} - T_{f,i}) W (i \Delta y)}{m_f C_{pf,i}} \quad (6.24)$$

Energy conservation equation of desiccant solution:

$$\begin{aligned} T_{s,i+1} - T_{s,i} = & -\frac{1}{C_{ps,i}} \left[\frac{m_{g,i}}{m_{s,i}} (h_{g,i+1} - h_{g,i}) + \frac{m_{g,i}}{m_{s,i}} C_{ps,i} T_{s,i} (\omega_{g,i+1} - \omega_{g,i}) \right. \\ & \left. + \frac{m_{f,i}}{m_{s,i}} C_{pf,i} (T_{f,i+1} - T_{f,i}) \right] \end{aligned} \quad (6.25)$$

Mass conservation equation of desiccant solution:

$$X_{s,i+1} - X_{s,i} = \frac{m_{g,i} (\omega_{g,i+1} - \omega_{g,i})}{m_{s,i} - m_{g,i} (\omega_{g,i+1} - \omega_{g,i})} X_{s,i} \quad (6.26)$$

In the present model, the parameters of inlet air, desiccant solution and cooling water

are given. The calculation starts from $i=0$ to $i=n-1$ with Eqs. (6.21) to (6.26). The thickness of falling film is recalculated at each step by incorporating with variable wetting length and moisture removal between desiccant solution and air. The calculation process is shown in Fig. 6.4. If the simulating results do not meet the accuracy requirement, the supposed outlet parameters of desiccant solution and cooling water should be changed and the calculation should be repeated until the accuracy requirement is satisfied.

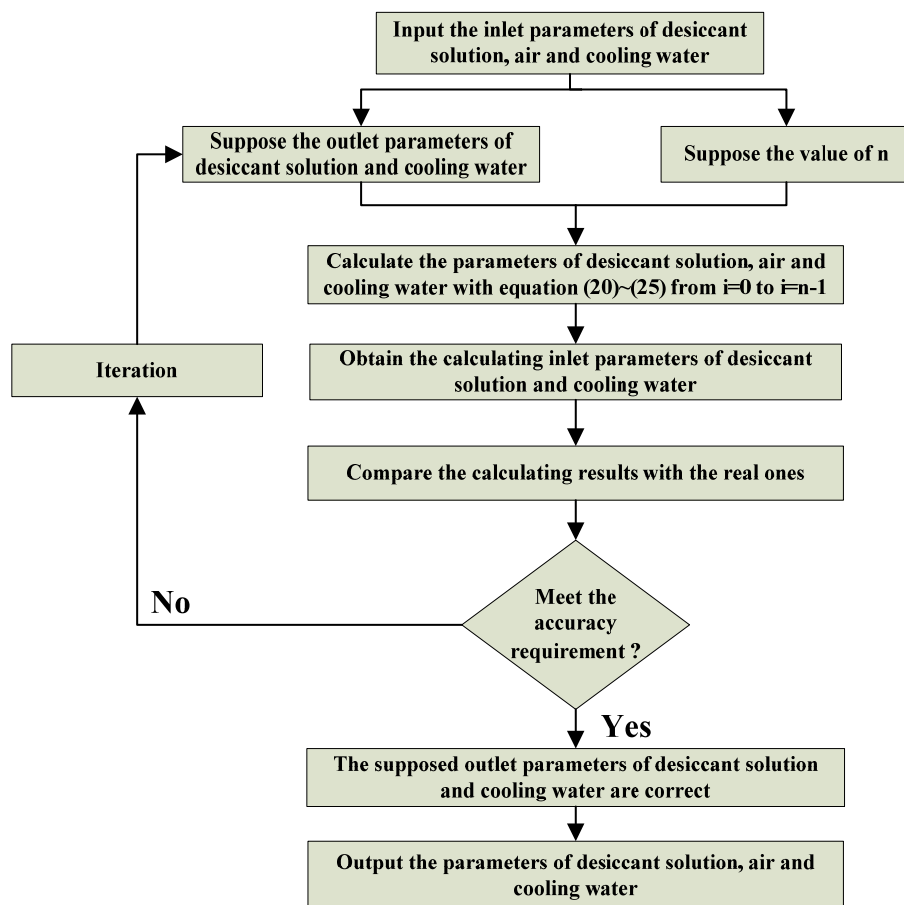


Fig. 6.4 Flow chart of calculation process

6.3 Model validation and uncertainty analysis

6.3.1 Model validation

To validate the new heat and mass transfer model with variable wetting length, the simulation results were compared with the existing experimental results. The uncertainties of the experimental results were 8.32%. The Average Relative Deviation (*ARD*) between the simulation and the experimental results was proposed as below:

$$ARD = \frac{1}{num} \sum_{i=1}^{num} \left| \frac{\varepsilon_{exp,i} - \varepsilon_{cal,i}}{\varepsilon_{exp,i}} \right| \times 100\% \quad (6.27)$$

where *num* is the number of simulation results.

Fig. 6.5 presents the comparison of the simulation moisture removal rates and the experimental results. Most of the simulation results fell within the $\pm 20\%$ error band of the experimental results with the *ARD* of 4.23%, which proves that the simulation results are reliable.

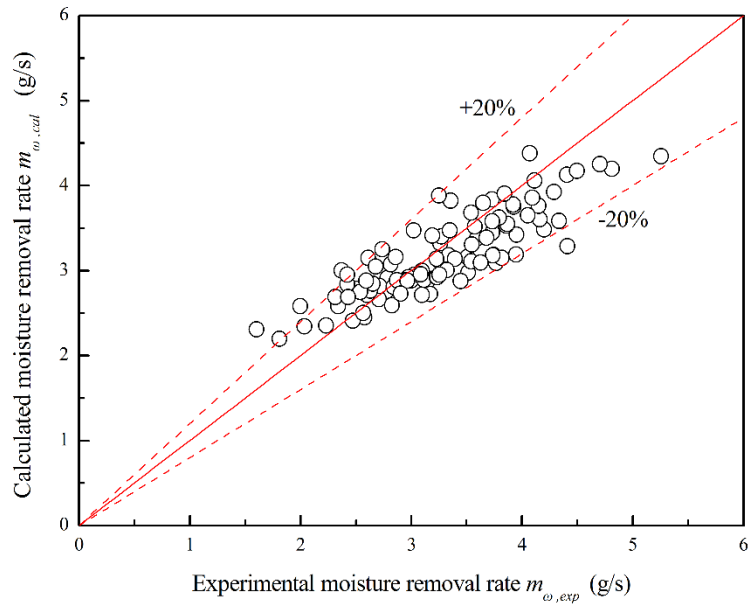
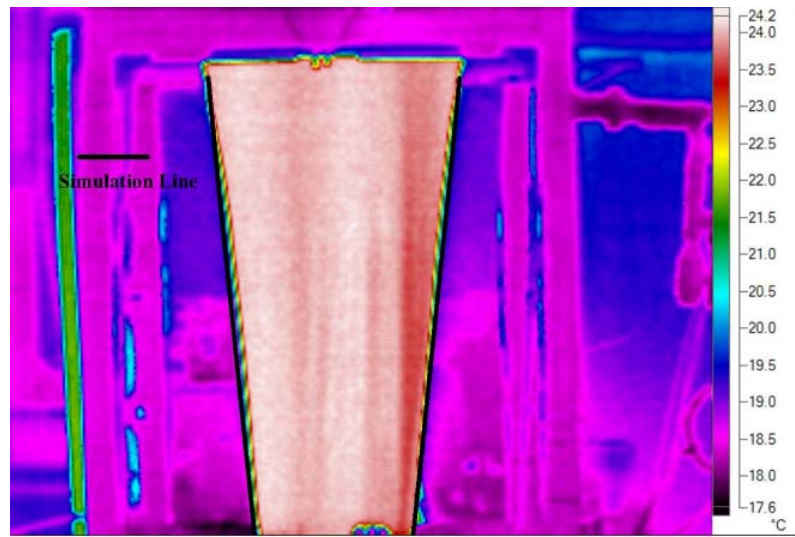
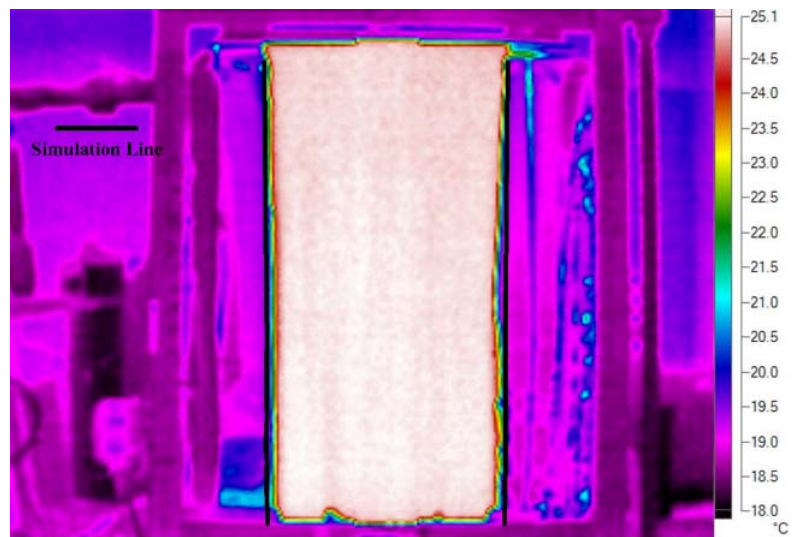


Fig. 6.5 Comparison of the simulation results with the experimental data

The comparison of the simulated film boundaries with the corresponding experimental ones at different contact angles is presented in Fig. 6.6. The simulation results are in good agreement with the measured boundaries, which indicates that the present model can accurately predict the shrinkage of the falling film and the influence of contact angles on the falling film shrinkage. Besides, it can be clearly observed that the shrinkage of the falling film is more pronounced with larger contact angles.



(a) $\alpha=84.6^\circ$



(b) $\alpha=8.8^\circ$

Fig. 6.6 Comparison of the simulated and experimental film boundaries with different contact angles

6.3.2 Uncertainty analysis

To further validate the new model, uncertainty analysis is also conducted, as shown in Table 6.1. The outlet air humidity ratio was selected as the index in the analysis. In

addition, a dimensionless sensitivity coefficient, SC , was introduced to investigate the influence of the input parameters on the outlet results [135]. SC can be obtained as below:

$$SC = \frac{\left| \omega_{p_0+\Delta p} - \omega_{p_0} \right| + \left| \omega_{p_0-\Delta p} - \omega_{p_0} \right|}{2\Delta p} \times \frac{p_0}{\omega_{p_0}} \quad (6.28)$$

where p_0 and Δp represent the base values and uncertainty of the input parameters, respectively. It can be inferred from the analysis that the simulation results were heavily affected by the inlet desiccant solution parameters, such as the temperature and concentration, and as well as the inlet air humidity ratio. In addition, as the contact angles of the desiccant solution on the working surfaces differed significantly among the various plates, the influence of the contact angles on the simulation results was also important despite the small sensitivity coefficient of the contact angle.

Table 6.1 Uncertainty and sensitivity analysis of present model

Input parameters	T_g	ω_g	m_g	T_s	m_s	X_s	T_f	α
	[°C]	[g/kg]	[kg/s]	[°C]	[kg/s]	[%]	[°C]	[°]
Base values	31	15	0.09	25	0.15	38%	22	45
Input uncertainty	±10%	±10%	±10%	±10%	±10%	±5.3%	±10%	±10%
Results uncertainty	0.11%	8.7%	1.6%	10.6%	0.17%	2.17%	3.78%	0.27%
SC	0.009	0.861	0.170	1.102	0.017	0.456	0.073	0.025

6.4 Results and discussion

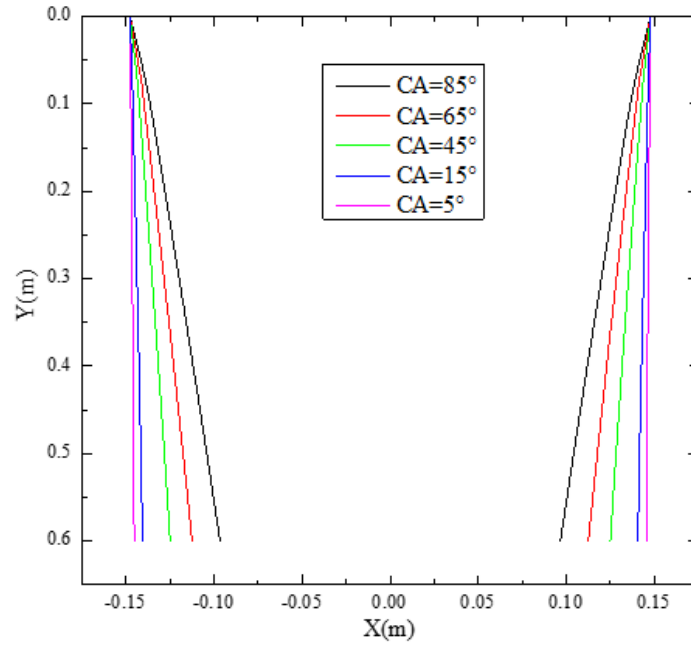
6.4.1 Effect of surface wettability on wetting area

Fig. 6.7 plots the shrinkage of the falling film along the flow direction with different contact angles. It is apparent that the falling film contracts intensively and becomes very narrow with larger contact angles, but only shows very slight shrinkage with lower contact angles. As the contact angle decreases from 85° to 5° , the wetting length at the outlet of the plate dehumidifier increases from 0.193 m to 0.291 m with the same initial wetting length of 0.296 m at the inlet of the dehumidifier. It can be calculated that the total wetting area increases significantly from 0.145 m^2 to 0.176 m^2 . This phenomenon can be explained by the fact that the surface tension gradient is reduced at lower contact angles. According to Young equation [98], the contact angle depends on the relationship between the solid–gas interfacial tension $\sigma_{s,g}$, solid–liquid interfacial tension $\sigma_{s,l}$ and liquid–gas interfacial tension $\sigma_{l,g}$, as follows:

$$\cos \alpha = (\sigma_{s,g} - \sigma_{s,l}) / \sigma_{l,g} \quad (6.29)$$

The decrease in the contact angles implies the decrease in the solid–liquid interfacial tension and reduces the contraction of the falling film. In addition, as the surface tension gradient $(\sigma_{cen} - \sigma_{rim})/D$ decreases with the increase of D , and D increases with the decrease of the contact angles, the surface tension gradient decreases with the decrease of the contact angles and the Marangoni effect in the transverse direction

becomes weaker accordingly.

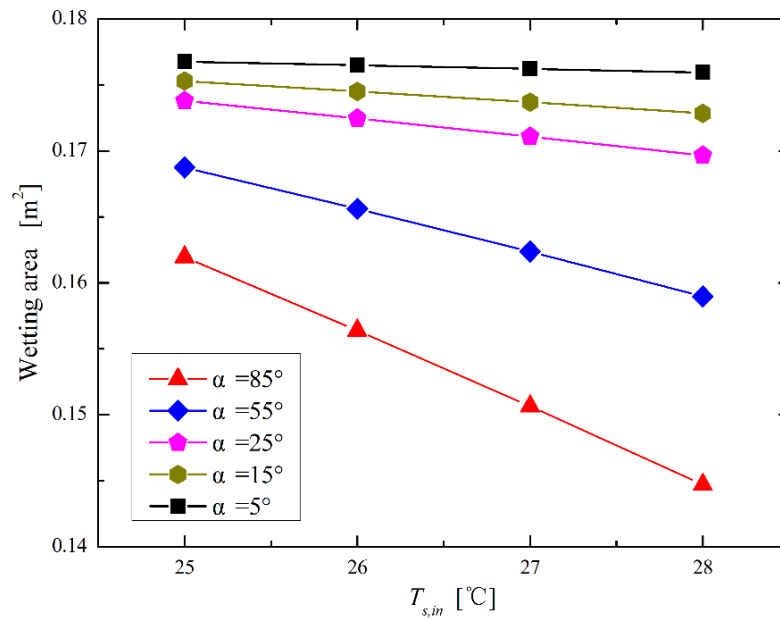


T_g	ω_g	m_g	T_s	m_s	X_s	T_f
[°C]	[g/kg]	[kg/s]	[°C]	[kg/s]	[%]	[°C]
31	15	0.09	28	0.15	38.8	20

Fig. 6.7 Shrinkage of the falling film with different contact angles

Fig. 6.8 shows the variation of the wetting area with the desiccant solution temperature at different contact angles. It can be observed that the wetting area decreases with the increase of the desiccant solution temperature. As $T_{s,in}$ increases, the liquid falling film contracts and becomes narrower. This contraction occurs because the surface tension gradient in the transverse direction increases with the increase of the desiccant solution temperature and the shrinkage along the flow direction turns out more intensive. Another interesting finding is that the negative gradient differs considerably

with the contact angle. The negative gradient decreases from $5.75 \times 10^{-3} \text{ m}^2/\text{°C}$ with the contact angle of 85° to $0.27 \times 10^{-3} \text{ m}^2/\text{°C}$ with the contact angle of 5° . A possible reason for this trend is that the width of the rim part, D , increases rapidly with the decrease of the contact angles which would weaken the effect of the desiccant solution temperature on the surface tension gradient.

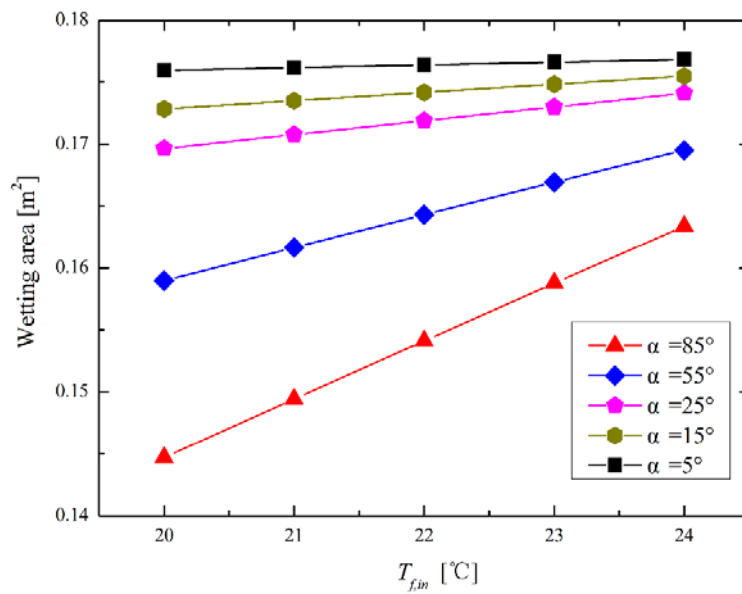


T_g	ω_g	m_g	T_s	m_s	X_s	T_f
[°C]	[g/kg]	[kg/s]	[°C]	[kg/s]	[%]	[°C]
31	15	0.09	25~28	0.15	38.8	20

Fig. 6.8 Effect of desiccant solution temperature on wetting area with different contact angles

The effect of cooling water temperature on the wetting area at different contact angles is presented in Fig. 6.9, which resembles the trend for the desiccant solution

temperature. The wetting area increases with the increase of cooling water temperature, but the rate of this increase depends on the contact angles. The positive gradient decreases from $4.67 \times 10^{-3} \text{ m}^2/\text{°C}$ with the contact angle of 85° to $0.22 \times 10^{-3} \text{ m}^2/\text{°C}$ with the contact angle of 5° , from which it can be inferred that increasing the cooling water temperature effectively reduces the surface tension gradient in the transverse direction at constant desiccant solution temperature.

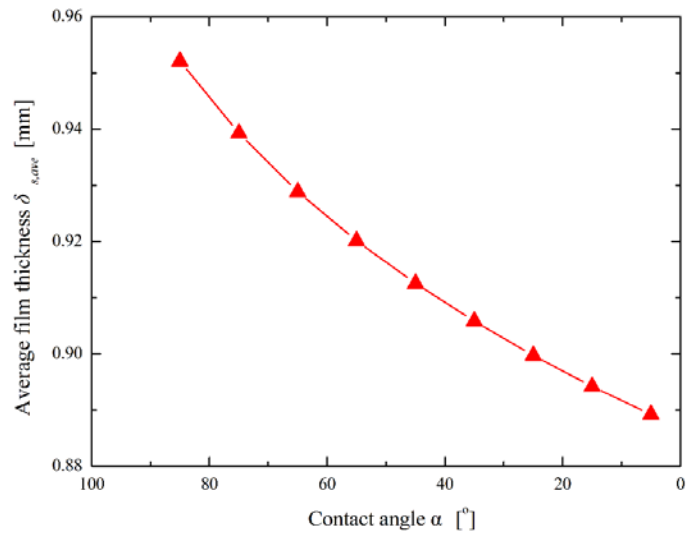


T_g	ω_g	m_g	T_s	m_s	X_s	T_f
[°C]	[g/kg]	[kg/s]	[°C]	[kg/s]	[%]	[°C]
31	15	0.09	28	0.15	38.8	20~24

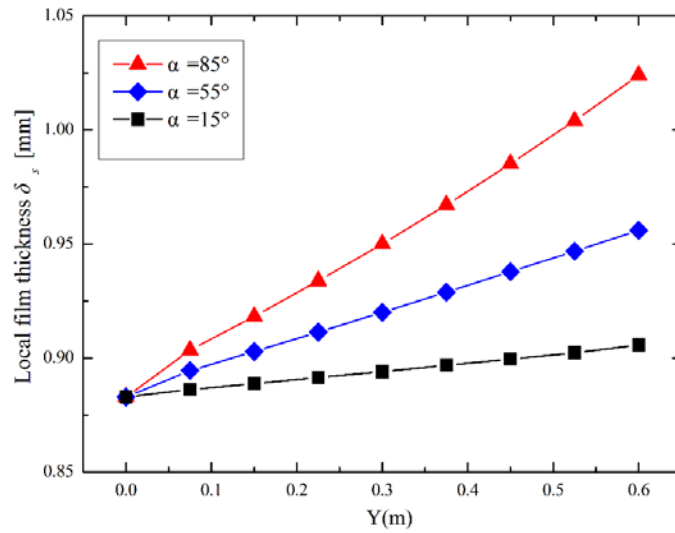
Fig. 6.9 Effect of desiccant solution temperature on wetting area with different contact angles

6.4.2 Effect of surface wettability on film thickness

Fig. 6.10(a) shows the variation of average falling film thickness with contact angles. The average falling film thickness is calculated based on the local falling film thickness at each differential element. It can be observed that the average falling film thickness $\delta_{s,ave}$ decreases rapidly from 0.952 mm to 0.889 mm as the contact angles decreases from 85° to 5°. This decrease occurs because of the marked increase in the wetting area at lower contact angles, as shown in Fig. 6.7. In addition, the distribution of the local falling film thickness along the flow direction with different contact angles is presented in Fig. 6.10(b). $Y = 0$ represents the inlet of the plate dehumidifier and $Y = 0.6$ m represents the outlet. It can be observed that the local falling film thickness increases along the flow direction. The falling film thickness is related to both the wetting length and the film velocity. On one hand, the wetting length is reduced along the flow direction, which acts to increase the falling film thickness. On the other hand, the film velocity increases along the flow direction, which acts, conversely, to thin the falling film. The decrease of wetting length is larger than the increase of film velocity, so the net effect is to increase the local falling film thickness. Another interesting observation in Fig. 6.10(b) is that the positive gradient of the local film thickness is determined by the contact angles. It can be observed that the positive gradient of local film thickness along the flow direction drops rapidly from 0.235mm/m to 0.0197mm/m as the contact angle decreases from 85° to 5°. Lower contact angles lead to reduced shrinkage of the falling film, which weakens the effect of the wetting length on the increase of film thickness.



(a) Average falling film thickness



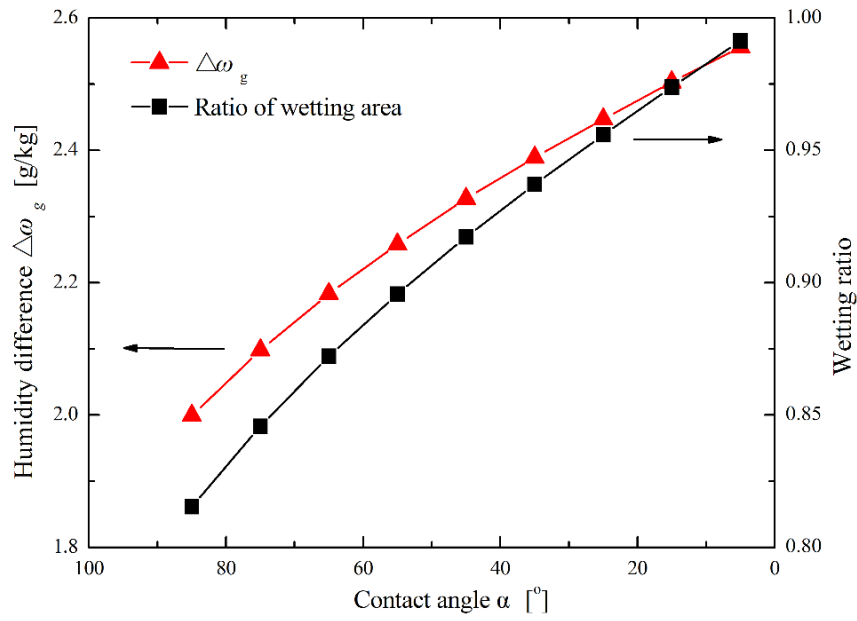
(b) Distribution of falling film thickness along the flow direction

T_g	ω_g	m_g	T_s	m_s	X_s	T_f
[°C]	[g/kg]	[kg/s]	[°C]	[kg/s]	[%]	[°C]
31	15	0.09	28	0.15	38.8	20

Fig. 6.10 Variation of the falling film thickness with different contact angles

6.4.3 Effect of surface wettability on dehumidification performance

The variation of both the moisture removal rate and the ratio of the wetting area with contact angles are shown in Fig. 6.11. The ratio of the wetting area represents the ratio of the actual wetting area to the maximum wetting area of the plate dehumidifier. As the contact angle decreases from 85° to 5° , the moisture removal rate increases from 2.0 g/kg to 2.56 g/kg, i.e., by a factor of 1.28. Meanwhile, the ratio of the wetting area increases from 0.815 to 0.991, i.e., by a factor of 1.21. The increase in the wetting area effectively increases the contact area between the desiccant solution and the process air, as well as increasing the moisture removal rate. Another interesting observation in Fig. 6.11 is that the increasing ratio of moisture removal rate is greater than that of the wetting area. One possible explanation for this is that at lower contact angles, the average falling film thickness is also lower, as shown in Fig. 6.10(a), which effectively reduces the heat transfer resistance between the cooling water and the desiccant solution and accelerates the replenishment of the superficial desiccant solution. Therefore, both the increase of the wetting area and the decrease of the falling film thickness benefit the heat and mass transfer performance of the internally cooled plate dehumidifier.

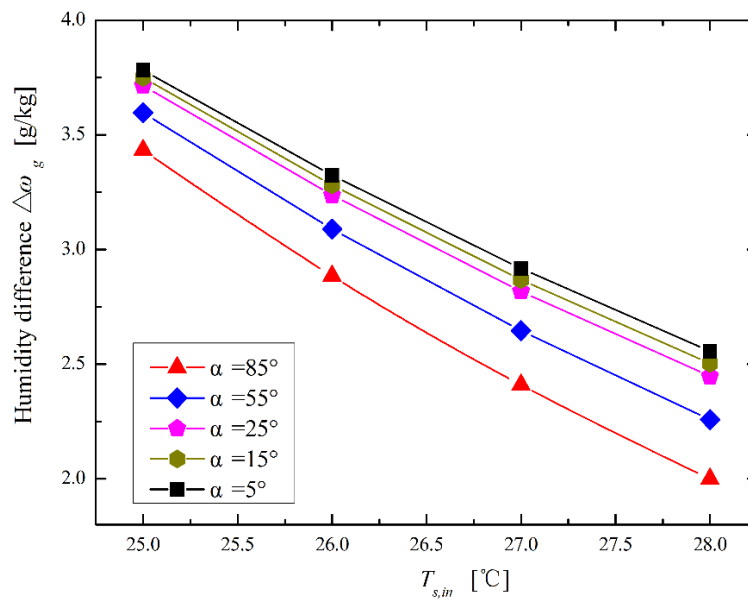


T_g	ω_g	m_g	T_s	m_s	X_s	T_f
[°C]	[g/kg]	[kg/s]	[°C]	[kg/s]	[%]	[°C]
31	15	0.09	28	0.15	38.8	20

Fig. 6.11 Effect of desiccant solution temperature on wetting area with different contact angles

The effect of the desiccant solution temperature on the moisture removal rate with different contact angles is presented in Fig. 6.12. The moisture removal rate decreases rapidly with the increase of the desiccant temperature. This trend is related to the surface vapour pressure of the desiccant solution, which, at a given concentration, increases exponentially with the temperature. This in turn markedly reduces the driving force of mass transfer between the desiccant solution and the process air, thus significantly reducing the moisture removal rate at higher temperature. In addition, it can be observed in Fig. 6.12 that the effect of the contact angles on the moisture

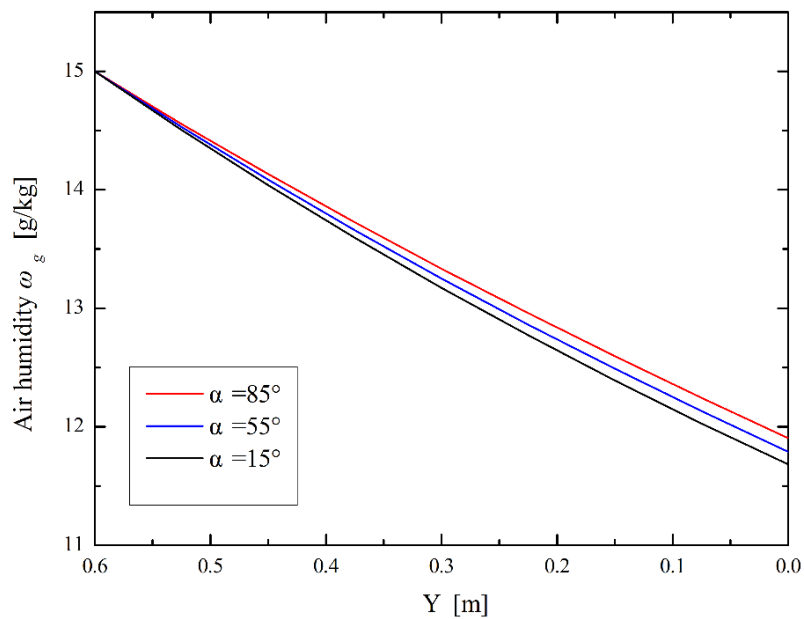
removal rate differs in desiccant solution temperature. As the contact angle decreases from 85° to 5°, the moisture removal rate at 25°C increases from 3.43 g/kg to 3.78 g/kg, i.e., with an increment of 0.35 g/kg, whereas at 28°C it increases from 2.0 g/kg to 2.56 g/kg, i.e., with an increment of 0.56 g/kg. One possible reason is that the effect of contact angles on wetting area is more intensive at higher desiccant solution temperature, as shown in Fig. 6.8, and therefore the contact angles shows bigger impact on heat and mass transfer at higher desiccant solution temperature.



T_g	ω_g	m_g	T_s	m_s	X_s	T_f
[°C]	[g/kg]	[kg/s]	[°C]	[kg/s]	[%]	[°C]
31	15	0.09	25~28	0.15	38.8	20

Fig. 6.12 Effect of desiccant solution temperature on wetting area with different contact angles

Fig. 6.13 shows the distribution of the humidity ratio of the process air along the flow direction with different contact angles. $Y = 0.6$ m represents the inlet of the process air and $Y = 0$ represents the outlet. It can be observed that the humidity ratio decreases from the inlet to the outlet of the plate dehumidifier. The negative gradient increases with the decrease of the contact angles.



T_g	ω_g	m_g	T_s	m_s	X_s	T_f
[°C]	[g/kg]	[kg/s]	[°C]	[kg/s]	[%]	[°C]
31	15	0.09	26	0.15	38.8	22

Fig. 6.13 Effect of desiccant solution temperature on wetting area with different contact angles

6.5 Summary

This chapter reports an improved heat and mass transfer model of an internally-cooled

liquid desiccant plate dehumidifier considering the actual wetting area. The effect of surface wettability on dehumidification performance is investigated in this chapter. The main conclusions are summarized as follows.

(1) An improved heat and mass transfer model of a liquid desiccant dehumidifier is developed considering solid-liquid interaction effect. The shrinkage of falling film in plate dehumidifier is accurately simulated in the new model.

(2) The effect of surface wettability on flow characteristics of falling film in a plate dehumidifier is investigated. As the contact angle decreases from 85° to 5° , the total wetting area increases significantly from 0.145 m^2 to 0.176 m^2 with the ratio of 21.4%, while the mean falling film thickness decreases from 0.952 mm to 0.889 mm. Besides, the variation of local falling film thickness along the flow direction is also investigated.

(3) The effect of surface wettability on dehumidification performance is also investigated in this chapter. As the contact angle decreases from 85° to 5° , the moisture removal rate increases from 2.0 g/kg to 2.56 g/kg, i.e., by a factor of 1.28. The performance enhancement is attributed to the increase of the wetting area and the decrease of the falling film thickness. Besides, the variations of processed air parameters along the flow direction are simulated using the new model.

Besides, this model can be applied in other falling applications, such as evaporators, condensers and chemical columns.

CHAPTER 7

ENERGY CONSUMPTION ANALYSIS OF SOLAR- ASSISTED LIQUID DESICCANT AIR-CONDITIONING SYSTEM CONSIDERING SOLID-LIQUID INTERACTION EFFECT

7.1 Introduction

As discussed above, the effect of solid-liquid interaction effect on dehumidification performance is comprehensively investigated. This chapter aims to develop a dynamic system model of solar-assisted liquid desiccant air-conditioning system to estimate the energy consumption of air-conditioning system and to investigate the effect of surface wettability on energy consumption of the whole system. A commercial building in Hong Kong is selected as the case building. The main academic contributions in this chapter are summarized as follows.

(1) A dynamic model of solar-assisted liquid desiccant air-conditioning system is developed to investigate solid-liquid interaction effect on energy consumption. The system consists of an internally-cold liquid desiccant dehumidifier, an internally-heated liquid desiccant regenerator, a solar collector and auxiliary heater system, a cooling coil system and several heat exchangers system. Three iteration loops, i.e.,

iteration loop of liquid desiccant solution, iteration loop of heating water and iteration loop of cooling water, are adopted to estimate the energy consumption.

(2) The energy consumption of the solar-assisted liquid desiccant air-conditioning system in a commercial building is simulated to investigate the effect of surface wettability on energy consumption. The simulation results indicate that improving surface wettability of falling film dehumidifiers could reduce the energy consumption. Around 9.1% ($100 \text{ MW} \cdot \text{h}$) of total energy consumption could be saved for solar-assisted liquid desiccant air-conditioning system with the surface contact angle reducing from 110° to 10° . Besides, the monthly energy consumption of chilling system in liquid desiccant air-conditioning system with different falling film dehumidifiers is simulated.

(3) The effect of solar collection system on energy consumption of the whole air-conditioning system is investigated. The introduction of solar energy could save around 15.4% ($200 \text{ MW} \cdot \text{h}$) of electricity consumption for liquid desiccant air-conditioning system.

7.2 Model development of solar-assisted liquid desiccant air-conditioning system considering solid-liquid interaction effect

7.2.1 Description of solar-assisted liquid desiccant air-conditioning system

To estimate the energy consumption of solar-assisted liquid desiccant air-conditioning system, a dynamic model composing of an internally-cold liquid desiccant dehumidifier, an internally-heated liquid desiccant regenerator, a solar collector and auxiliary heater, a cooling coil and several heat exchangers is developed, as shown in Fig. 7.1.

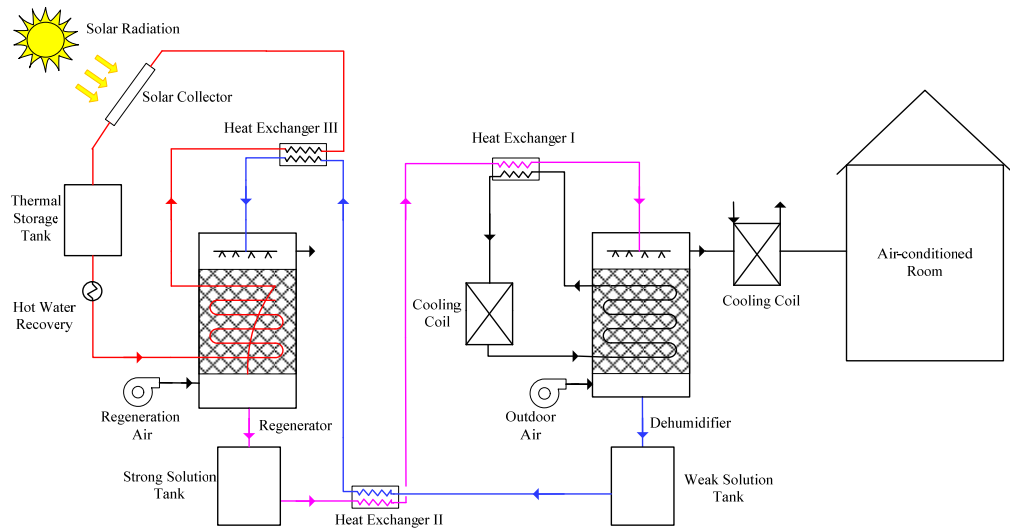


Fig. 7.1 Schematic diagram of solar-assisted liquid desiccant air-conditioning system

As shown in Fig. 7.1, the outdoor fresh air, supplied by air fans, is dehumidified by the internally-cold liquid desiccant dehumidifier and then cooled to indoor set point

by the cooling coil. Then, the dry and cool air is supplied to the air-conditioned rooms. During this process, the latent heat and part of the sensible heat of the outdoor air are handled by the liquid desiccant dehumidifier, while the rest of the sensible heat is handled by the cooling coil. Due to the separate handling of latent heat and sensible heat, less energy will be consumed by employing liquid desiccant air-conditioning system.

To maintain the desiccant solution temperature and improve the dehumidification performance, the internally-cold water is adopted in the liquid desiccant dehumidifier to remove the latent heat released during dehumidification process. After absorbing the extra moisture of liquid desiccant, the liquid desiccant solution becomes weak. To recycle the liquid desiccant solution, a liquid desiccant regenerator is equipped in the system. To remove the latent heat released during the regeneration process, an internally-heated devices is fixed in the regenerator. To reduce the energy consumption, solar energy is utilized as the heat sources of internally-heated water. Besides, the weak liquid desiccant solution is pre-heated by solar energy before flowing into the regenerator. As the equilibrium vapor pressure of desiccant solution, increasing the solution temperature could effectively improve the regeneration performance.

The solar energy collection system consists of a solar collector, thermal storage tank

and an auxiliary heater. To improve the efficiency of solar collection system, the evacuated-tube solar collector is adopted. Besides, the auxiliary heater acts as a supplement in case of inadequate solar energy.

Besides, several heat exchangers are adopted in the system to improve the operating efficiency of the system. Pre-cooling and pre-heating heat exchangers are fixed at the inlet of both liquid desiccant dehumidifier and regenerator. Besides, to recover the heat from the concentrated liquid desiccant solution and improve the operating efficiency, a heat exchanger is fixed between the weak desiccant solution and the concentrated desiccant solution. Therefore, the weak desiccant solution is heated, while the concentrated desiccant solution is cooled.

7.2.2 Models of individual components

As discussed above, the solar-assisted liquid desiccant air-conditioning system is composed of an internally-cold air dehumidifier, an internally-heated regenerator, a solar collection system, a coiling coil, a cooling tower and several heat exchangers. To estimate the whole energy consumption, the model development of each component is necessary.

7.2.2.1 Internally-cold/heated liquid desiccant dehumidifier/regenerator

The liquid desiccant dehumidifier acts as an absorber to remove the extra moisture of processed air. The moisture exchanges from humid air to liquid desiccant solution. As discussed in Chapter 5, the mass transfer coefficient of liquid desiccant plate dehumidifiers was developed. Therefore, the moisture removal rate of the internally-cold liquid desiccant plate dehumidifier is given as follows.

$$m_{\omega,de} = m_{a,de} (\omega_{a,in} - \omega_{a,out}) = h_{D,de} A \Delta \omega \quad (7.1)$$

where m is mass flow rate, g/kg, and ω is the air humidity, g/kg dry air. h_D represents mass transfer coefficient, $\text{g}/(\text{m}^2 \cdot \text{s})$. A is the contact area between liquid desiccant solution and processed air. $\Delta \omega$ is the humid different between the processed air and the air in equilibrium with the solution at its temperature and concentration, g/kg dry air.

As opposite process occurs in liquid desiccant regenerator, the moisture removal rate of internally-heated liquid desiccant plate regenerator is given as follows.

$$m_{\omega,re} = m_{a,re} (\omega_{a,in} - \omega_{a,out}) = h_{D,re} A \Delta \omega \quad (7.2)$$

7.2.2.2 Solar collection system

An evacuated-tube solar collector, acting as a heat source, is employed in the system. The water, heated in the evacuated-tube solar collector, is used to pre-heat the liquid

desiccant solution and provide the latent heat during the regeneration process. As the solar energy collected in the evacuated-tube solar collector is determined by several factors, such as area of collector, climate conditions and the water temperature, the overall solar energy is estimated as follows.

$$Q_{solar} = IA_c \eta_{solar} = \tau IA_c - U_c A_c (t_{f,in} - t_{amb}) \quad (7.3)$$

where Q is the heat collected in the evacuated-tube solar collector, kW. I represents the solar radiation, W/m^2 . τ is the transmissivity of the glass above the evacuated-tube solar collector, %. A_c is the working area of the evacuated-tube solar collector, m^2 . U_c represents the heat loss coefficient of the solar collector to the surroundings, $W/(m^2 \cdot K)$. Besides, $t_{f,in}$ and t_{amb} refer to the temperature of the inlet water and the surrounding air, respectively, $^{\circ}C$. η_{solar} represents the efficiency of the evacuated-tube solar collector.

The rated efficiency of the evacuated-tube solar collector is 0.84. As η_{solar} is influenced by the inlet water temperature and the surrounding air temperature, the formula of η_{solar} can be expressed as follows [133].

$$\eta_{solar} = 0.84 - 2.02(T_{in} - T_{amb}) / I + 0.0046I[(T_{in} - T_{amb}) / I]^2 \quad (7.4)$$

Besides, an auxiliary electrical heater is fixed in the solar collection system to act as a supplement to the solar collector in case of inadequate solar energy. The rated efficiency of the auxiliary electrical heater is 0.9.

7.2.2.3 Cooling coil

As discussed above, the latent load and part of the sensible load of the processed air are handled by the internally-cold liquid desiccant dehumidifier. The rest of the sensible load is handled by the cooling coil fixed after the dehumidifier in air-conditioning system. Therefore, the cooling load handled by the cooling coil is expressed as follows.

$$Q_{cc} = Q_c - Q_{de} = Q_c - m_{da}(h_a - h_{a,cc}) \quad (7.5)$$

where Q_{cc} is the cooling load handled by the cooling coil, kW. Q_c is the total cooling load of the air-conditioned room, kW, and Q_{de} is the cooling load handled by the liquid desiccant dehumidifier, kW. h_a is the enthalpy of ambient air, J/kg, and $h_{a,cc}$ is the enthalpy of inlet air to cooling coil, J/kg.

In the solar-assisted liquid desiccant air-conditioning system, the cooling coil is driven by a vapor compressor with the average COP of 3.3. Therefore, the electricity consumption can be estimated using the cooling load and COP.

7.2.2.4 Cooling tower

In the internally-cold liquid desiccant dehumidifier, the cooling water is used to maintain the desiccant solution temperature and improve the dehumidification efficiency. Besides, the cooling water is also used to pre-cool the concentrated liquid

desiccant solution. A cooling tower with the efficiency of 0.45 is adopted as the cooling sources. The efficiency of the cooling tower is defined as follows.

$$\eta_{ct} = \frac{T_{w,in} - T_{w,out}}{T_{w,in} - T_{a,wb}} \quad (7.6)$$

where η_{ct} is the efficiency of the cooling tower. $T_{w,in}$ and $T_{w,out}$ represent the inlet and outlet cooling water temperature of the cooling tower, °C. $T_{a,wb}$ is the wet-bulb temperature of the ambient air, °C, which presents negative effect on the outlet cooling water temperature at certain operating efficiency .

7.2.2.5 Heat exchanger

To improve the system efficiency, several heat exchangers are fixed in solar-assisted liquid desiccant air-conditioning system. One heat exchanger is fixed at the inlet of liquid desiccant dehumidifier/regenerator to cool/heat the desiccant solution. Besides, to recycle the thermal energy of concentrated liquid desiccant solution and the cooling energy of weak liquid desiccant solution, a heat exchanger is fixed between the concentrated and weak desiccant solution. The efficiency of the heat exchanger is defined as follows.

$$\begin{aligned} \eta_{ex} &= \frac{m_{hot} c_{p,hot} (T_{hot,in} - T_{hot,out})}{\min(m_{hot} c_{p,hot}, m_{cold} c_{p,cold}) (T_{hot,in} - T_{cold,in})} \\ &= \frac{m_{cold} c_{p,cold} (T_{cold,in} - T_{cold,out})}{\min(m_{hot} c_{p,hot}, m_{cold} c_{p,cold}) (T_{hot,in} - T_{cold,in})} \end{aligned} \quad (7.7)$$

where η_{ex} is the efficiency of the heat exchanger. m_{hot} and m_{cold} represent the mass

flow rates of hot and cold fluids, kg/s, respectively. T_{hot} and T_{cold} refer to the temperature of hot and cold fluid, °C, respectively. The subscripts of *in* and *out* represent the inlet and outlet fluids. The rated efficiency of the heat exchanger I and II is 0.93 and that of the heat exchanger II is 0.54.

7.2.2.6 Air fan

Air fans are used in the air-conditioning system to drive the processed air. The power consumed by air fans is determined by air flow volume, air pressure and efficiency of air fans, as expressed as follows.

$$P_{fan} = \frac{Q_a \Delta p}{\eta_{fan}} \quad (7.8)$$

where P_{fan} is the power consumption of air fans, W, and Q_a is the volume flow rate of air, m³/s. Δp represents the pressure increase of air, Pa. η_{fan} is the efficiency of air fans. In this study, the rated efficiency of air fans is assumed to be 0.7.

7.2.2.7 Pumps

The pumps in solar-assisted liquid desiccant air-conditioning system are used to drive the liquid desiccant solution during dehumidification and regeneration process. The power consumption of pumps is determined by flow rates of desiccant solution, pressure increase of liquid and efficiency of pumps, as defined as follows.

$$P_{pump} = \frac{\rho_{water} g H Q_s}{\eta_p} \quad (7.9)$$

where P_{pump} refers to the power consumption of pumps, W. ρ_{water} is the density of water, kg/m³, which is assumed as 1000 kg/m³ in the system. H is the hydraulic head of the pump, m, and Q_s is the volume flow rate of the working fluids, m³/s. η_p is the rated efficiency of pumps, which is assumed as 0.65 in the model.

The specifications of each component are present as follows.

Table 7.1 Specifications of main equipment

Dehumidifier/regenerator	Size	550×600 mm
Solar collector	Rated efficiency	0.84
	Angle	22.5°
Auxiliary electrical heater	Rated efficiency	0.90
Coiling coil	COP	3.3
Cooling tower	Rated efficiency	0.45
Heater exchanger	Rated efficiency	0.93 (I and III)
		0.54 (II)
Air fan	Rated efficiency	0.70
Pump	Rated efficiency	0.65

7.2.3 Model iterations

The model of each component is developed, as discussed above. To calculate the energy consumption of each component, the input and output parameters of each component need to be identified during the simulation process. The input and output parameters of each component are shown in Fig. 7.2.

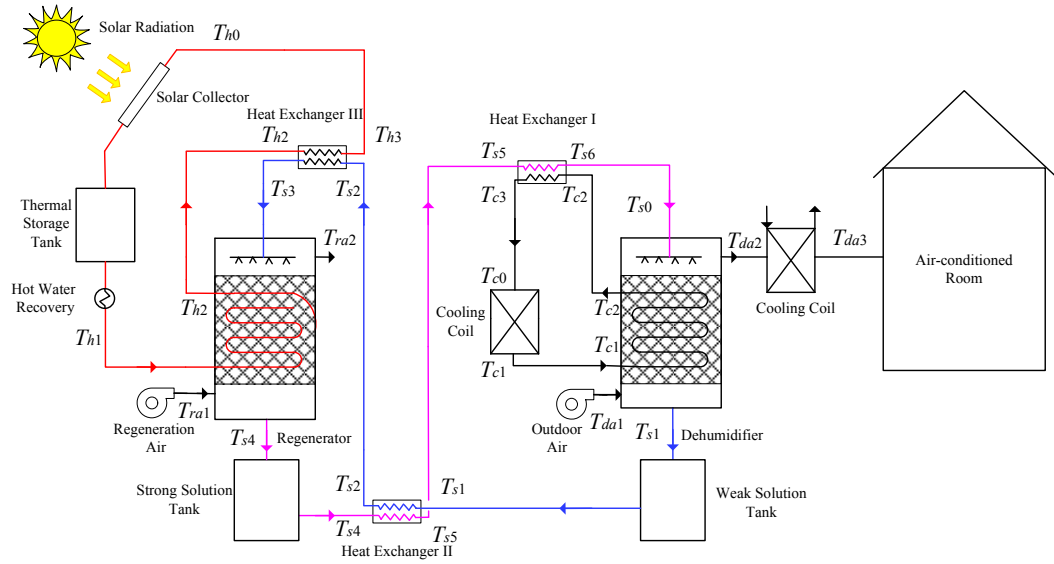


Fig. 7.2 Schematic diagram of input and output parameters of each component

As the liquid desiccant solution, cooling water and heating water are recycled in the system, three iteration loops are adopted in the simulation model to identify the accurate inlet and outlet parameters.

7.2.3.1 Iteration of liquid desiccant solution

As shown in Fig.7.2, the liquid desiccant solution is recycled between the dehumidifier and the regenerator. Firstly, the liquid desiccant solution (T_{s0}, X_{s0}) enters the air dehumidifier to absorb the extra moisture of the processed air. Heat and mass transfer occurs between the liquid desiccant solution and processed air. Then, the liquid desiccant solution (T_{s1}, X_{s1}) flows out of the dehumidifier and is pre-heated by the concentrated desiccant solution. The pre-heated weak desiccant solution (T_{s2}, X_{s1}) is further heated by the heating water from the solar collector. Then, the weak and hot desiccant solution (T_{s3}, X_{s1}) is re-concentrated in the regenerator. After the regenerator, the concentrated desiccant solution (T_{s4}, X_{s2}) is stored in the strong solution tank and supplied to the air dehumidifier. To recover the heat energy of the concentrated desiccant solution, a heat exchanger is fixed between the concentrated and weak desiccant solution. After the heat exchanger, the desiccant solution (T_{s5}, X_{s2}) is further cooled by the cooling water to improve the absorption capacity. Finally, the desiccant solution (T_{s6}, X_{s2}) enters the air dehumidifier. Therefore, T_{s6} and X_{s2} should be equal to T_{s0} and X_{s0} , respectively.

7.2.3.2 Iteration of heating water

The heating water is used to heat the weak desiccant solution before the regenerator

and maintain the temperature of the desiccant solution during the regeneration process. The initial heating water (T_{h0}) is heated by solar radiation and then stored in the thermal storage tank. Then, the heating water (T_{h1}) enters the regenerator and the heat transfer occurs between the heating water and the liquid desiccant solution. After flowing out of the regenerator, the heating water (T_{h2}) is used to heat the weak desiccant solution through Heat Exchanger III. Finally, the heating water (T_{h3}) re-enters the solar collector. Therefore, the temperature of heating water T_{h3} should be equal to T_{h0} .

7.2.3.3 Iteration of cooling water

The cooling water is used to cool the concentrated desiccant solution before the dehumidifier to improve the absorption capacity and maintain the temperature of the desiccant solution during the dehumidification process. The cooling water in solar-assisted liquid desiccant air-conditioning system is supplied by a cooling tower. The initial cooling water (T_{c0}) is cooled by the cooling tower and then supplied to the dehumidifier. The latent heat released during dehumidification process is removed by the cooling water (T_{c1}). Then, the cooling water (T_{c2}) flows out of the dehumidifier and is used to cool the concentrated desiccant solution. Finally, the cooling water (T_{c3}) re-enters the cooling tower. Therefore, the temperature of cooling water T_{c3} should be equal to T_{c0} .

The relationship between inlet and outlet parameters is identified using the models discussed in Section 7.2.2. Therefore, the dynamic simulation model of solar-assisted liquid desiccant air-conditioning system is developed. To estimate the energy consumption of the solar-assisted liquid desiccant air-conditioning system, the assumption of the initial parameters is necessary. The detailed initial values of the parameters are assumed in Table 7.2.

Table 7.2 Assumed initial values of the parameters

Fluid	Parameter	Component	Value
Desiccant	Mass flow rate [kg/s]	Dehumidifier	0.5
		Regenerator	0.5
	Temperature [°C]	Dehumidifier	25
	Concentration [wt.%]	Dehumidifier	34.5
Air	Mass flow rate [kg/s]	Dehumidifier	Standard ventilation rate
Cooling water	Mass flow rate [kg/s]	Heat exchanger I	0.5
		Dehumidifier	0.5
	Temperature [°C]	Cooling tower	30
Heating water	Mass flow rate [kg/s]	Heat exchanger III	0.5
	Temperature [°C]	Solar collector	60

7.2.4 Description of the case building

A dynamic system model is developed to estimate the energy consumption of solar-assisted liquid desiccant air-conditioning system. A typical commercial building is selected as the case building in this study [133]. The layout of the building is shown in Fig. 7.3.

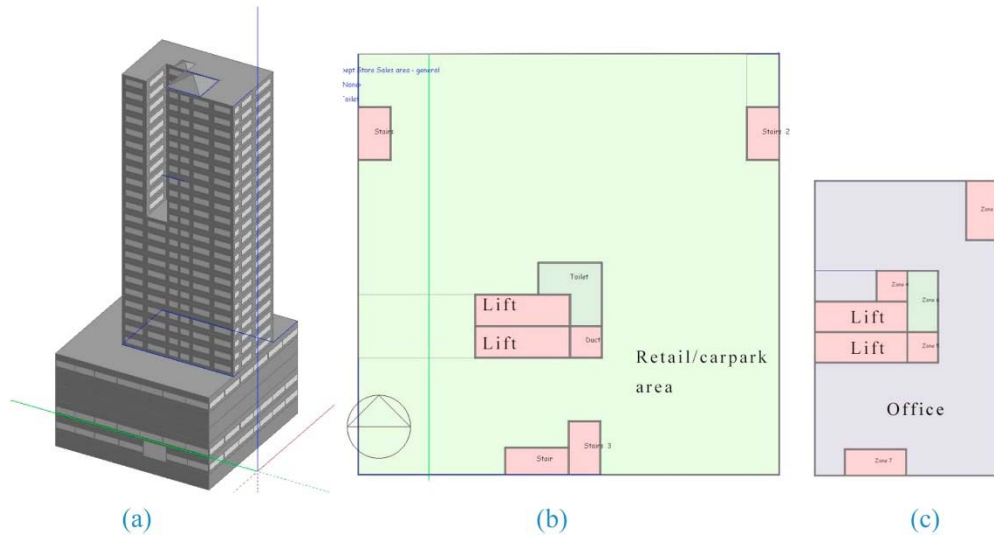


Fig. 7.3 Layout of the typical commercial building in Hong Kong

The case building is north-south orientation. As shown in Fig. 7.3, the building is composed of five floors of the retail/car-park ($1600 \text{ m}^2/\text{f}$) and 24 floor of offices ($545 \text{ m}^2/\text{f}$ from Floor 5-15 and $515 \text{ m}^2/\text{f}$ from Floor 16-26).

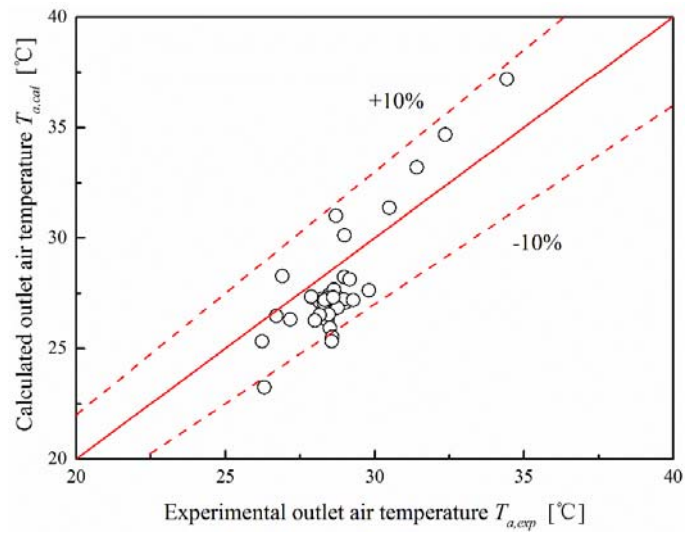
The thermal properties of the building components, including windows, walls and roofs, are referenced from the energy code by the Hong Kong Government [136].

Besides, the indoor air temperature in cooling season is selected as 23°C [137].

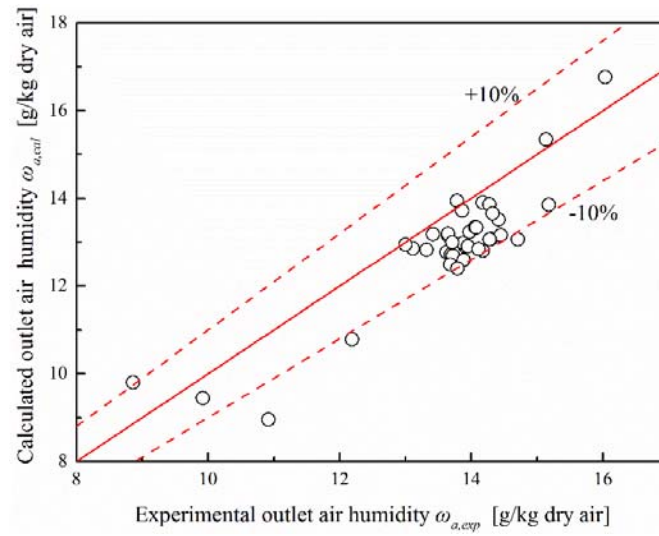
7.3 Results and discussion

7.3.1 Model validation

Before the simulation analysis of the energy consumption, model validation is necessary. Fig. 7.4 presents the comparison between the simulated and experimental outlet parameters of the processed air from the dehumidifier. Most of the simulated results fell within $\pm 10\%$ error of the experimental results, validating the model of solar-assisted liquid desiccant air-conditioning system.



(a) Air temperature



(b) Air humidity

Fig. 7.4 Comparison between simulated and experimental results

7.3.2 Energy consumption of solar-assisted liquid desiccant air-conditioning system

The dynamic model of solar-assisted liquid desiccant air-conditioning system is developed and the weather data and the cooling load of the case building are imported into the model. The time interval in the simulation process is 1 hour and the simulation period is from May to October.

Fig. 7.5 presents the comparison of the energy consumption between solar-assisted liquid desiccant air-conditioning system (SLDACS), liquid desiccant air-conditioning system (LDACS) and traditional vapor-compression air-conditioning system

(VCACS). Without the solar collection system, the energy consumption of the liquid desiccant air-conditioning system is much higher than that of the traditional vapor-compression air-conditioning system. The reason is that a large amount of electricity is consumed to drive the regeneration process of the desiccant solution. To reduce the energy consumption, a solar collection system is adopted and the regeneration process of the weak desiccant solution is driven by solar energy. Therefore, the energy consumption of solar-assisted liquid desiccant air-conditioning system is rapidly reduced due to the less energy consumption for regenerators. The introduction of solar energy could save around 15.4% (200 MW · h) of electricity consumption for liquid desiccant air-conditioning system.

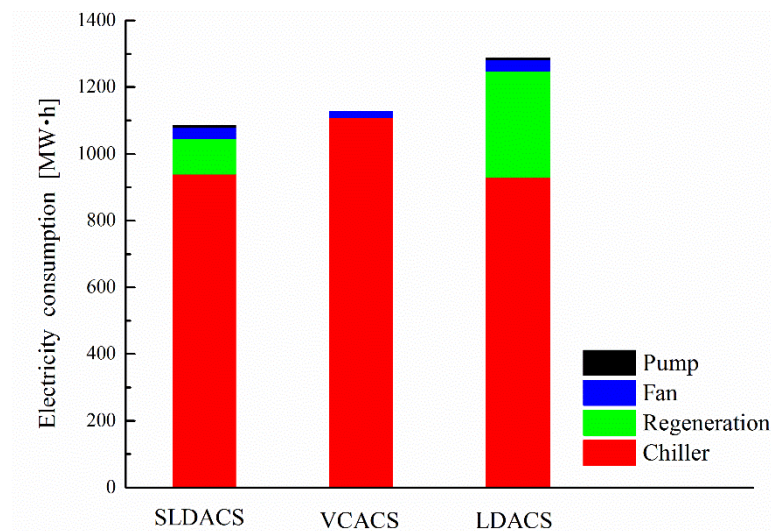


Fig. 7.5 Comparison of electricity consumption between different systems

7.3.3 Effect of surface wettability on energy consumption

As investigated above, surface wettability is one of the key influencing factors of dehumidification performance. The air dehumidifier/regenerator is the core component in liquid desiccant air-conditioning system. Therefore, it is necessary to investigate the effect of surface wettability on energy consumption of air-conditioning system.

Fig. 7.6 shows the electricity consumption of solar-assisted liquid desiccant air-conditioning system with liquid desiccant dehumidifiers using different plate dehumidifiers. Three plate dehumidifiers with the contact angle of 110° , 85° and 10° are adopted in the simulation. It is observed that the surface wettability present effective effect on energy consumption. The energy consumption decreases with the increasing of the surface wettability. Around 9.1% ($100 \text{ MW} \cdot \text{h}$) of electricity could be saved for solar-assisted liquid desiccant air-conditioning system with the surface contact angle reducing from 110° to 10° . The reason is that increasing the surface wettability could improve the dehumidification performance and then reduce the energy consumption of the air dehumidifier. Therefore, it is necessary to improve the surface wettability of liquid desiccant dehumidifiers in the point of energy consumption.

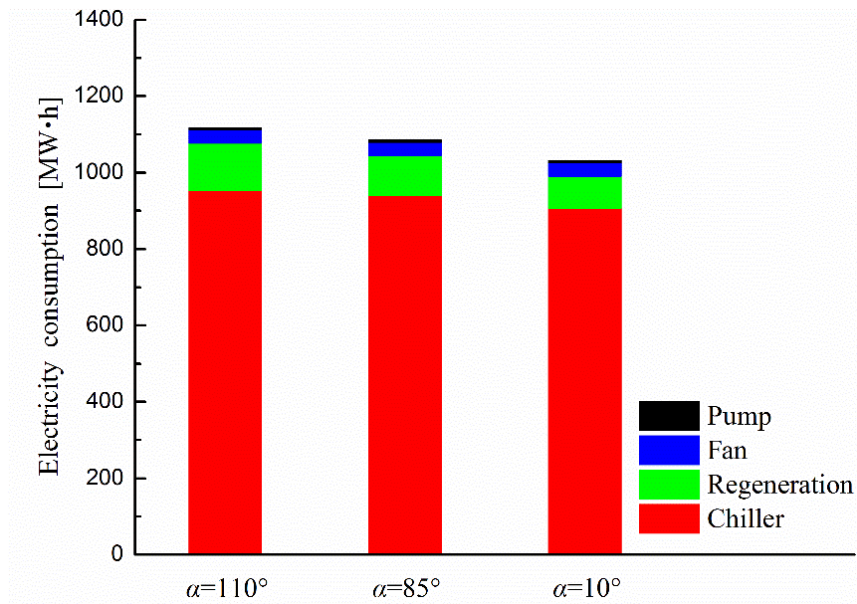


Fig. 7.6 Comparison of electricity consumption of SLDACS

To further investigate the effect of surface wettability on energy consumption, the energy consumption of chiller, which includes the cooling coil and cooling tower, during the cooling seasons is simulated. Fig. 7.7 presents the monthly electricity consumption of the chiller in SLDACS with different plate dehumidifiers. Same trends of the monthly electricity consumption are observed for different plate dehumidifiers. The monthly electricity consumption of the chiller with higher surface wettability is slightly lower than that with lower surface wettability. The lower energy consumption is attributed to the higher dehumidification performance improved by the higher surface wettability.

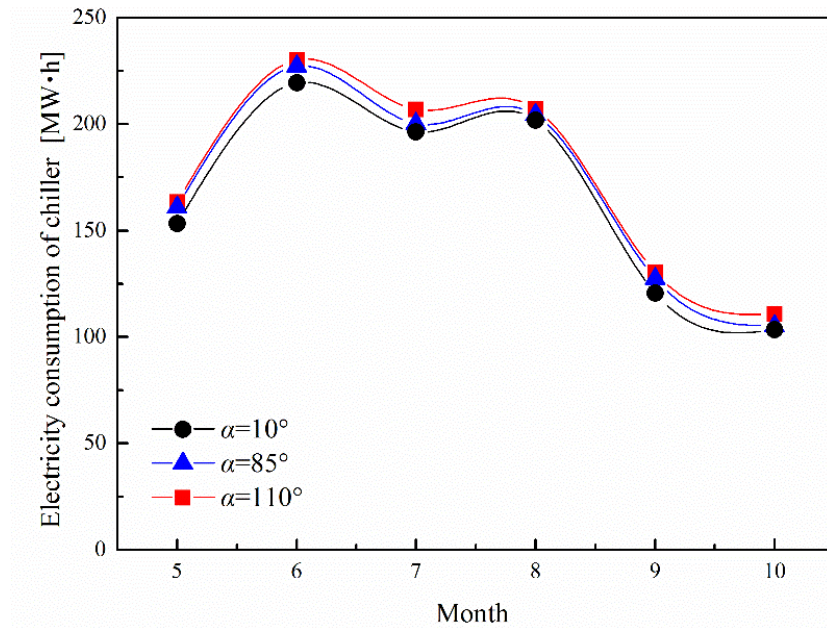


Fig. 7.7 Monthly electricity consumption of chillers

7.4 Summary

This chapter develops a dynamic model to estimate the energy consumption of solar-assisted liquid desiccant air-conditioning system. The effect of surface wettability on energy consumption is analyzed. The main conclusions are summarized as follows.

(1) A dynamic model of solar-assisted liquid desiccant air-conditioning system for a commercial building in Hong Kong is developed. The simulation model of each component in the system is developed using mass and energy balance equations. To estimate the energy consumption, three iteration loops, i.e., iteration loop of liquid desiccant solution, iteration loop of heating water and iteration loop of cooling water, are considered.

(2) The energy consumption of liquid desiccant air-conditioning system with and without solar collection system is simulated. The introduction of solar energy could save around 15.4 % (200 MW · h) of electricity consumption for liquid desiccant air-conditioning system.

(3) The effect of surface wettability on energy consumption is analyzed. Increasing the surface wettability of plate dehumidifiers could reduce the energy consumption accordingly. Around 9.1% (100 MW · h) of total energy consumption could be saved for solar-assisted liquid desiccant air-conditioning system with the surface contact angle reducing from 110° to 10°. The energy saving is attributed to the dehumidification performance enhancement by higher surface wettability.

The simulation results in this chapter indicated that improving surface wettability could effectively reduce the energy consumption of liquid desiccant air-conditioning system. The findings in this chapter provides an effective approach to reducing the building energy consumption.

CHAPTER 8

CONCLUSIONS AND RECOMMENDATIONS FOR FUTURE WORK

This research investigates the importance of surface properties in falling film dehumidifiers and analyzed the enhanced heat and mass transfer performance by surface treatment of applying TiO₂ super-hydrophilic coating experimentally and theoretically. A novel TiO₂ super-hydrophilic coating is developed to improve the surface wettability and the dehumidification performance as well. Besides, the solid-liquid interaction effect on dehumidification performance is comprehensively investigated and a new mass transfer correlation considering solid-liquid interaction effect is established. Besides, an improved heat and mass transfer model of liquid desiccant dehumidifier is developed and the solid-liquid interaction effect is considered in the new model. Finally, a dynamic model of solar-assisted liquid desiccant air-conditioning system is developed to estimate the energy consumption and investigate the effect of surface wettability on energy consumption. The main conclusions and recommendations are summarized as follows.

8.1 Conclusions

Surface property is one of the key influencing factors in falling film liquid desiccant

dehumidifiers. To investigate the effect of surface properties on dehumidification performance, three commonly-used plate dehumidifiers, i.e., Stainless plate dehumidifier, Titanium plate dehumidifier and Polytetrafluoroethylene (PTFE) plate dehumidifier, with distinctive surface properties are adopted, as discussed in Chapter 3. The characterization test of different working plates is conducted and the surface free energy of Titanium plate, Stainless plate and PTFE plate are 50.61 mJ/m², 36.98 mJ/m² and 30.34 mJ/m², respectively, indicating that Titanium plate possesses the superior wettability compared with the other plates. The falling film shrinks seriously along the flow direction in PTFE plate dehumidifier while a little shrinkage occurs in Titanium plate dehumidifier due to the strong adhesion between liquid desiccant and solid surface. The experimental results prove that the plate dehumidifiers with higher surface wettability demonstrates superior dehumidification performance.

Based on the findings in Chapter 3, a novel super-hydrophilic coating is fabricated onto the dehumidifier plate using nanoscale anatase TiO₂ particles, as discussed in Chapter 4. The characteristics of the TiO₂ super-hydrophilic particles and coating are investigated through XRD and FESEM and HRTEM test. The test results indicate that pure and highly dispersive TiO₂ super-hydrophilic coating is well developed. Besides, the surface free energy of TiO₂ coating before and after UV activation is identified using Young-Good-Girifalco-Fowke approach [125]. The super-hydrophilicity of

TiO₂ coating is effectively activated by UV illumination and the surface free energy is significantly improved 15.71 mJ/m² 90.15 mJ/m².

The experimental setup is reconstructed with two single-channel internally-cooled plate dehumidifiers to investigate the heat and mass transfer characteristics in surface-modified plate dehumidifier by applying TiO₂ coating, as shown in Chapter 5. One plate dehumidifier is treated with TiO₂ super-hydrophilic coating and the other is only cleaned by ethanol. The contact angle test results show that the contact angle of the liquid desiccant is significantly reduced from 84.6° to 8.8° and the surface wettability is effectively enhanced by the super-hydrophilic coating. Besides, the flow characteristics of falling film on coated and uncoated plate dehumidifiers are investigated experimentally. Severe shrinkage of falling film along the flow direction occurs in uncoated plate dehumidifier, while little shrinkage occurs in the coated one. The maximum wetting ratio is increased from 75% to 100% by super-hydrophilic coating. More than 200 experimental conditions are adopted in the experiment. The dehumidification performance is significantly improved with the average enhancing ratios of around 60%. Finally, the influencing factors of the dehumidification performance are investigated experimentally in detail. The air temperature shows negative effect on dehumidification performance, while the air flow rate, humid ratio and liquid desiccant flow rate demonstrate positive effect on dehumidification

performance. A novel empirical correlation of mass transfer coefficient was developed using non-linear regression method based on the experimental results. The surface free energy was considered in the correlation to account for solid-liquid interaction effect on dehumidification performance.

Based on the experimental study in Chapter 5, an improved heat and mass transfer model of internally-cold liquid desiccant dehumidifier is developed considering solid-liquid interaction effect, as discussed in Chapter 6. The actual wetting area is considered in the new model. A shrinkage model of falling film considering solid-liquid interaction effect is proposed to accurately estimate the wetting area of liquid desiccant solution in different plate dehumidifier. The effect of surface wettability on dehumidification performance is theoretically investigated. Improving surface wettability could significantly improve the dehumidification performance. The simulation results indicates that the enhancing ratio in dehumidification performance could be achieved around 30% with the contact angle decreasing from 85° to 5° . The performance enhancement is attributed to the increase of the wetting area and the decrease of the falling film thickness. The total wetting area increases significantly from 0.145 m^2 to 0.176 m^2 with the ratio of 21.4%, while the mean falling film thickness decreases from 0.952 mm to 0.889 mm.

Based on both experimental and theoretical investigation above, a dynamic model of solar-assisted liquid desiccant air-conditioning system considering solid-liquid interaction effect is developed, as discussed in Chapter 7. The effect of surface wettability in falling film dehumidifiers on energy consumption is analyzed. Increasing the surface wettability of falling film dehumidifiers could effectively reduce the energy consumption. Around 9.1% ($100 \text{ MW} \cdot \text{h}$) of total energy consumption could be saved for solar-assisted liquid desiccant air-conditioning system with the surface contact angle reducing from 110° to 10° . The energy saving is attributed to the dehumidification performance enhancement by higher surface wettability. Besides, the simulation results shows that the introduction of solar energy could save around 15.4 % ($200 \text{ MW} \cdot \text{h}$) of electricity consumption for liquid desiccant air-conditioning system.

This research is very useful to other falling film applications and the findings in this research could provide guidance to improve the operating performance to other falling applications, such as evaporators, condensers and chemical columns.

8.2 Recommendations for Future Work

Following the completion of the research work reported in this thesis, several recommendations for Future Work are proposed as follows.

The basic principle of the super-hydrophilicity for TiO_2 coating is still not clear and the microscopic interaction between liquid and solid surface need to be further investigated.

As the falling film in plate dehumidifier is time-varying and also spatial, the flow characteristics of falling film is very complex. Besides, the effect of falling film fluctuation on dehumidification performance is unclear. Therefore, to further understand the flow characteristics of falling film and its effect on dehumidification, 3-D model need to be developed.

Additionally, as heat and mass transfer occurs simultaneously during dehumidification process, the coupled characteristics of heat and mass transfer is still not clear. In the existing models, the coupled relationship between heat and mass transfer is treated by assuming certain Lewis number, which do not accord with the actual situations. Therefore, it is recommended to further analyze the coupled relationship between heat and mass transfer and develop a model to describe the coupled characteristics.

The condensation of humid air on the unwetted surface was observed in the experiment. However, this phenomenon is not considered in the existing models of heat and mass transfer in falling film dehumidifiers, which might affect the estimation accuracy. Therefore, a new heat and mass transfer model considering the effect of vapor

condensation is necessary.

References

- [1] P. Tuominen, R. Holopainen, L. Eskola, J. Jokisalo, M. Airaksinen. Calculation method and tool for assessing energy consumption in the building stock, *Building and Environment* 75 (2014): 153-160.
- [2] L. Perez-Lombard, J. Ortiz, J.F. Coronel, I.R. Maestre. A review of HVAC systems requirements in building energy regulations, *Energy and Buildings* 43(2-3) (2011): 255-268.
- [3] Hong Kong Energy End Use Data, Electrical and Mechanical Services, Department of Hong Kong Special Administrative Region, 2017.
- [4] I. Blom, L. Itard, A. Meijer. Environmental impact of building-related and user-related energy consumption in dwellings, *Building and Environment* 46(8) (2011): 1657-1669.
- [5] G.W. Brundrett. Hand Book of Dehumidification technology, *Drying Technology*. 1989 7:1 (1989) 143-147, DOI: 10.1080/07373938908916580.
- [6] G.M. Ge, F. Xiao, X.F. Niu. Control strategies for a liquid desiccant air-conditioning system. *Energy and buildings*, 43(6) (2011): 1499-1507.
- [7] A.S.A. Mohamed , M.S. Ahmed, A.A.M. Hassan, M. Salah Hassan, Performance evaluation of gauze packing for liquid desiccant dehumidification system, *Case Studies in Thermal Engineering* 8 (2016) 260-276.
- [8] M.S. Park, J.R. Howell, G.C. Vliet, J. Peterson. Numerical and experimental

results for coupled heat and mass transfer between a desiccant film and air in cross flow, *International Journal of Heat and Mass Transfer* 37 (1994): 395-402.

[9] A. Ali, K. Vafai, A.R.A. Khaled. Analysis of heat and mass transfer between air and falling film in a cross flow configuration. *International Journal of Heat and Mass Transfer* 47 (2004): 743-755.

[10] G. Karimi, M Kawaji. Flow characteristics and circulatory motion in wavy falling films with and without counter-current gas flow. *International Journal of Multiphase Flow* 25(6-7) (1999): 1305-1319.

[11] R.H. Qi, L. Lu, H.X. Yang, F. Qin. Investigation on wetted area and film thickness for falling film liquid desiccant regeneration system. *Applied Energy*, 112 (2013): 93-101.

[12] Y.G. Yin, X.S. Zhang, G. Wang, L. Luo. Experimental study on a new internally cooled/heated dehumidifier/regenerator of liquid desiccant systems. *International Journal of Refrigeration* 31(5) (2008): 857-866.

[13] S. Jain, P.K. Bansal. Performance analysis of liquid desiccant dehumidification systems. *International Journal of Refrigeration*, 30(5) (2007): 861-872.

[14] M.S. Buker, S.B. Riffat. Recent developments in solar assisted liquid desiccant evaporative cooling technology-a review. *Energy and Buildings* 96 (2015): 95-108.

[15] J.K. Kim, C. W. Park, Y. T. Kang. The effect of micro-scale surface treatment on heat and mass transfer performance for a falling film H₂O/LiBr absorber. *International*

Journal of Refrigeration 26 (2003): 575-585.

[16] X.M. Ye, H. X, S.D. Ma. Review on experimental research on wetting of surfactant solutions. Journal of North China Electric Power University, 38(3) (2011): 72-77.

[17] H. Fujita, T. Ueda. Falling liquid films in absorption machines. International Journal of Refrigeration 16(1993): 281-292.

[18] J. F. Roques, V. Dupont, J. R. Thome. Falling film transitions on plain and enhanced tubes. Journal of Heat Transfer 124(2002):491-499.

[19] Y. T. Kang, T. Kashiwagi. Heat transfer enhancement by Marangoni convection process. Proceeding of the International Sorption Heat Pump Conference, Shanghai, China, 2002, 283-288.

[20] M. R. Islam, N. E. Wijesundera, J. C. Ho. Performance study of a falling-film absorber with a film-inverting configuration. International Journal of Refrigeration 26(8) (2003): 909-917.

[21] X. Y. Cui, J. Z. Shi, C. Tan, Z. P. Xu. Investigation of plate falling film absorber with film-inverting configuration. Journal of Heat Transfer 131(2009): 072001-1-9.

[22] J.K. Kim, J.Y. Jung, Y.T. Kang. The effect of nano-particles on the bubble absorption performance in a binary nanofluid. International Journal of Refrigeration, 29(1) (2006): 22-29.

[23] X.H. Ma, F.M. Su, J.B. Chen. Heat and mass transfer enhancement of the bubble

absorption for a binary nanofluid. *Journal of Mechanical Science and Technology* 21(2007): 1338-1343.

[24] L. Mei, Y.J. Dai. A technical review on use of liquid-desiccant dehumidification for air-conditioning application. *Renewable and Sustainable Energy Reviews* 12 (2008): 662-689.

[25] P. Mazzei, F. Minichiello, D. Palma. HVAC dehumidification systems for thermal comfort: a critical review. *Applied Thermal Engineering* 25 (2005): 677-707.

[26] Y. Jiang, Z. Li, X.L. Chen, X.H. Liu. Liquid desiccant air conditioning system and its applications. *Journal of HV&AC* 34 (2004): 88-98.

[27] Z. Li. Liquid desiccant air conditioning and independent humidity control air conditioning systems. *Journal of HV&A* 33 (2003): 26-31.

[28] Y. Yang, X.G. Li, W.Y. Li, C.C. Fang, X.L., Qi. Experimental study on the characteristics of solar powered liquid dehumidification system. *Acta Energiae Solaris Sinica* 21 (2) (2000): 155-159.

[29] G.O.G. Lof. Cooling with solar energy. *Congress on Solar Energy*, Tucson, USA, 1955, 171-189.

[30] E. Elsarrag. Dehumidification of air by chemical liquid desiccant in a packed column and its heat and mass transfer effectiveness. *HVAC&R Research* 12 (1) (2006): 3-16.

[31] M. M. Rafique, P. Gandhidasan, H.M.S. Bahaidarah. Liquid desiccant materials

and dehumidifiers-A review. *Renewable and Sustainable Energy Reviews* 56 (2016): 179-195.

[32] A. Lowenstein, K.E. Slyzak. A zero carry over liquid desiccant air conditioner for solar applications. *ASME International Solar Energy Conference (ISEC 2006)*, 2006, Denver, Colorado.

[33] T.W. Chung, C.M. Luo. Vapor Pressures of the Aqueous Desiccants. *Journal of Chemical & Engineering Data* 44 (5) (1999): 1024-1027.

[34] M.R. Conde. Properties of aqueous solutions of lithium and calcium chlorides: formulations for use in air conditioning equipment design. *International Journal of Thermal Sciences* 43 (2004):367-82.

[35] L. McNelly. Thermodynamic properties of aqueous solutions of lithium bromide. *ASHRAE Transactions* 85 (1979):412-34.

[36] Y. Kaita. Thermodynamic properties of lithium bromide-water solutions at high temperatures. *International Journal of Refrigeration* 24 (2001):371-90.

[37] A.A. Ertas, E.E. Anderson, I. Kiris. Properties of a new liquid desiccant solution- lithium chloride and calcium chloride mixture. *Solar Energy* 49(3) (1992):205-12.

[38] J.W. Studak, J.L.Peterson. A preliminary evaluation of alternative liquid desiccants for a hybrid desiccant air conditioner. *Proceedings of the Fifth Symposium on Improving Building Systems in Hot and Humid Climates*, Houston, TX, 1988.

[39] W. Kessling, E. Laevemann, C. Kapfhammer. Energy storage for desiccant

cooling systems component development. *Solar Energy* 64(4-6) (1998): 209-21.

[40] A.A. Pesaran, Y.O. Parent, M. Meckler, D. Novosel. Evaluation of liquid desiccant-enhanced heat pipe air preconditioner, *ASHRAE Transactions* 101 (1995) 713-724.

[41] S. Jain, P.L. Dhar, S.C. Kaushik. Experimental study on the dehumidifier and regenerator of a liquid desiccant cooling system. *Applied Thermal Engineering* 20 (2000): 253-267.

[42] W.Y. Saman, S. Alizadeh. An experimental study on a cross-flow type plate heat exchanger for dehumidification/cooling. *Solar Energy* 73 (2002): 59-71.

[43] W. Kessling, E. Laevemann, C. Kapfhammer. Energy storage for desiccant cooling systems component development. *Solar Energy* 64(4-6) (1998): 209-21.

[44] J. Liu, T. Zhang, X.H. Liu, J.J. Jiang. Experimental analysis of an internally-cooled/heated liquid desiccant dehumidifier/regenerator made of thermally conductive plastic. *Energy and Buildings* 99 (2015): 75-86.

[45] J. Liu, T. Zhang, X.H. Liu, J.J. Jiang. Experimental analysis of an internally-cooled/heated liquid desiccant dehumidifier/regenerator made of thermally conductive plastic. *Energy and Buildings* 99 (2015): 75-86.

[46] T. Zhang, X.H. Liu, J.J. Jiang, X.M. Chang, Y. Jiang, Experimental analysis of an internally cooled liquid desiccant dehumidifier, *Building and Environment* 63 (2013) 1-10.

- [47] T.W. Chung, H. Wu, Comparison between spray towers with and without fin coils for air dehumidification using triethylene glycol solutions and development of the mass-transfer correlations, *Industrial & Engineering Chemistry Research* 39 (2000) 2076-2084.
- [48] A.G. Queiroz, A.F. Orlando, F.E.M. Saboya. Performance Analysis of an Air Drier for a Liquid Dehumidifier Solar Air Conditioning System. *Journal of Solar Energy Engineering* 110(2) (1998): 120-124.
- [49] H.M. Hellmann, G. Grossman. Simulation and analysis of an open-cycle dehumidifier-evaporator-regenerator (DER) absorption chiller for low-grade heat utilization. *International Journal of Refrigeration* 18(3) (1995): 177-189.
- [50] C.Q. Ren, M. Tu, H.H. Wang. An analytical model for heat and mass transfer processes in internally cooled or heated liquid desiccant-air contact units. *International Journal of Heat and Mass Transfer* 50(17) (2007): 3545-3555.
- [51] L.C.S. Mesquita. S.J. Harrison, D. Thomey. Modeling of heat and mass transfer in parallel plate liquid-desiccant dehumidifiers. *Solar Energy* 80 (2006): 1475-1482.
- [52] R.E. Treybal, *Mass Transfer Operations*, 3rd ed., McGraw-Hill, New York, 1981.
- [53] W.F. Stoecker, *Design of Thermal Systems*, 3rd ed., McGraw-Hill, New York, 1989.
- [54] V.H. Ramm, Absorption of gases, in: *Israel Program for Scientific Translations*, Jerusalem, 1968.

- [55] D.Q. Kern, Process Heat Transfer, McGraw-Hill, Japan, 1950.
- [56] D.I. Stevens, J.E. Braun, S.A. Klein. An effectiveness model of liquid-desiccant system heat/mass exchangers. *Solar Energy* 142(6) (1989): 449-55.
- [57] A.Y. Khan, H.D. Ball. Development of a generalized model for performance evaluation of packed-type liquid sorbent dehumidifiers and regenerators. *ASHRAE Transactions* 98 (1992): 525-33.
- [58] R.H. Qi, L. Lu, H.X. Yang. Development of simplified prediction model for internally cooled/heated liquid desiccant dehumidification system. *Energy and Buildings* 59 (2013): 133-142.
- [59] X.H. Liu, X.M. Chang, J.J. Xia, Y. Jiang. Performance analysis on the internally cooled dehumidifier using liquid desiccant. *Building and Environment* 44 (2008):299-308.
- [60] Y.G. Yin, X.S. Zhang, D.G. Peng, X.W. Li. Model validation and case study on internally cooled/heated dehumidifier/regenerator of liquid desiccant systems. *International Journal of Thermal Science* 48(2009):1664-71.
- [61] Y.J. Dai, H.F. Zhang. Numerical simulation and theoretical analysis of heat and mass transfer in a cross flow liquid desiccant air dehumidifier packed with honeycomb paper. *Energy Conversion and Management* 45 (2004):1343-56.
- [62] S.W. Peng, Z.M. Pan. Heat and mass transfer in liquid desiccant air-conditioning process at low flow conditions. *Communications in Nonlinear Science and Numerical*

Simulation 14 (2009):3599-3607

[63] A. K. Hueffed, L.M. Chamra, P.J. Mago. A simplified model of heat and mass transfer between air and falling-film desiccant in a parallel-plate dehumidifier. *Journal of Heat Transfer* 131(5) (2009):052001-1-7.

[64] X.H. Liu, Y. Jiang, K.Y. Qu. Analytical solution of combined heat and mass transfer performance in a cross-flow packed bed liquid desiccant air dehumidifier. *International Journal of Heat and Mass Transfer* 51 (2008):4563-72.

[65] X.Y. Chen, Z. Li, Y. Jiang, K.Y. Qu. Analytical solution of adiabatic heat and mass transfer process in packed-type liquid desiccant equipment and its application. *Solar Energy* 80 (2006):1509-16.

[66] Y.M. Luo Study on the coupled flow, heat and mass transfer processes in a liquid desiccant dehumidifier. PhD Thesis. The Hong Kong Polytechnic University, Hong Kong, China, 2015.

[67] J.R. Howell, E.C.H. Bantel, Design of liquid desiccant dehumidification and cooling systems. *Solar Energy Utilization* 129 (1987): 374-386.

[68] Y.G. Yin, X.S. Zhang, Z.Q. Chen, Experimental study on dehumidifier and regenerator of liquid desiccant cooling air conditioning system, *Building and Environment*, 42 (2007): 2505-2511.

[69] D. Pietruschka, U. Eicker, M. Huber, Schumacher J. Experimental performance analysis and modelling of liquid desiccant cooling systems for air conditioning in

residential buildings. *International Journal of Refrigeration* 29(1) (2006): 110-124.

[70] X.H. Liu, Y. Jiang, K.Y. Qu. Heat and mass transfer model of cross flow liquid desiccant air dehumidifier/regenerator. *Energy Conversion and Management* 48 (2) (2007): 546-554.

[71] O.A. Kabov, B. Scheid, I.A. Sharina, J.C. Legros. Heat transfer and rivulet structures formation in a falling thin liquid film locally heated. *International Journal of Thermal Science* 427 (2002): 664-672.

[72] P.N. Yoshimura, T. Nosoko, T. Nagata. Enhancement of mass transfer into a falling laminar liquid film by two-dimensional surface waves-some experimental observations and modeling. *Chemical Engineering Science*, 51(8) (1996): 1231-1240.

[73] J. Geng. Influence of Marangoni Effect on Distillation in Packing Tower. PhD Dissertation. : Nanjing University, Nanjing, China, 2002.

[74] F. Zhang, D.L. Tang, J. Geng, Z.X. Wang, Z.B. Zhang. Study on the temperature distribution of heated falling liquid films. *Physica D: Nonlinear Phenomena*, 237(7) (2008): 867-872.

[75] S.R. Broome. Liquid Distribution And Falling Film Wetting In Dairy Evapourators. Master Dissertation. University of Canterbury, Christchurch, New Zealand, 2005.

[76] K.R. Morison, Q.A.G. Worth, N.P. O’dea. Minimum Wetting and Distribution Rates in Falling Film Evapourators. *Food and Bioproducts Processing* 84 (4) (2006):

302-310.

[77] A.A. Farayedhi, A.P. Gandhidasan, et al. Regeneration of liquid desiccants using membrane technology. *Energy Conversion and Management* 40(13) (1999): 1405-1411.

[78] R.H. Qi, Y. Hu, Y.H. Wang, L. Lu. A new approach to enhance the heat and mass transfer of liquid desiccant dehumidification with a titanium dioxide super-hydrophilic self-cleaning coating. *Journal of Cleaner Production* 112 (2016): 3555-3561.

[79] A.T. Conlisk. Semi-analytical design of a falling film absorber. *Journal of heat transfer* 116 (1994):1055-1058.

[80] R. Yang, D. Jou. Heat and mass transfer of absorption process for the falling film flow inside a porous medium. *International Journal of Heat and Mass Transfer* 38(6) (1995):1121-1126.

[81] K. Nakao, E. Ozaki, G. Yamanaka. Study on vertical type heat exchanger for absorption heat transformer. *National Heat Transfer Symposium of Japan*, 1986: 367-369.

[82] J.K. Kim, Y.T. Kang, C.W. Park. The effect of micro-scale surface treatment on heat and mass transfer performance for a falling film H₂O/LiBr absorber. *Proceeding of the International Sorption Heat Pump Conference*, Shanghai, China, 2002, 277-282.

[83] H.C. Cho, Y.T. Kang, C.D. Kim. Effect of surface roughness of micro-scale hatched tubes on the absorption performance. *Proceeding of the International Sorption*

Heat Pump Conference, Shanghai, China, 2002, 300-304.

[84] P. Chen. Investigation on the heat-mass transfer on vertical tube of falling film of water vapor absorption aqueous lithium bromide. Dalian University of Technology, Dalian, China, 2002. (In Chinese)

[85] M. Yin, J.B. Chen, P. Chen, X.H. Ma, S.P. Li. Study on the heat-mass transfer in falling film outside the vertical tube for water vapor absorption into aqueous lithium bromide. Journal of Chemical Engineering of Chinese Universities 16(6) (2002): 604-607. (In Chinese)

[86] Y.T. Kang, T. Kashiwagi. Heat transfer enhancement by Marangoni convection in $\text{NH}_3\text{-H}_2\text{O}$ absorption process. International Journal of Refrigeration 25 (2002): 780-788.

[87] N. Nishimura, T. Nomura, H. Lyota. Investigation of absorption enhancement by a surfactant. Proceeding of the International Sorption Heat Pump Conference, Shanghai, China, 2002, 373-377.

[88] E. Hihara, T. Saito. Effect of surfactant on falling film absorption. International Journal of Refrigeration 16(5) (1993): 339-346.

[89] W.L. Cheng, R. Zhao, C. Liu, S.L. Jiang, Z.S. Chen. Experimental study of influence of additives on ammonia bubble absorption. Journal of Refrigeration 27(3) (2006): 35-40. (In Chinese)

[90] W.L. Cheng, Z.S. Chen. Experimental study of steam absorption into aqueous

lithium bromide with vapor of additive. Fluid Machinery 30(12) (2002): 40-43. (In Chinese)

[91] M.R. Islam, N.E. Wijesundera, J.C. Ho. Performance study of a falling-film absorber with a film-inverting configuration. International Journal of Refrigeration, 26(8) (2003): 909-917.

[92] M.R. Islam, J.C. Ho, N.E. Wijesundera. A study of heat and mass transfer in falling films of film-inverting absorbers. 13th International Heat Transfer Conference, 2006, Sydney, Australia.

[93] X.Y. Cui, J.Z. Shi, C. Tan. Investigation of plate falling film absorber with film-inverting configuration. Journal of Heat Transfer 131(2009): 072001-9.

[94] J.K. Kim, J.Y. Jung, Y.T. Kang. Mass transfer enhancement of a binary nano-fluid for absorption application. The 13th International Heat Conference, Australia, 2006.

[95] K.I. Lee, H.J. Kim, J.H. Jung. An experimental study on the falling film heat transfer for binary nano-fluids. The 18th International Symposium on Transports Phenomena, Korea, 2007: 1107-1110.

[96] X.H. Ma, F.M. Su, Z. Lan. Experimental study on the thermal Physical Properties of a CNTs-NH₃ binary nano-fluid. ASME Micro/Nanoscale Heat Transfer International Conference. Taiwan, 2008.

[97] C. Pang, W. Wu, W. Sheng, H. Zhang and Y.T. Kang. Mass transfer enhancement by binary nano-fluids (NH₃/H₂O+Ag nanoparticles) for bubble absorption process.

International Journal of Refrigeration 35 (2012): 2240-2247.

[98] T. Young. An essay on the cohesion of fluids, Philosophical Transactions of the Royal Society of London 95 (1805):65-87.

[99] R.N. Wenzel. Resistance of solid surface to wetting by water. Journal of Industrial & Engineering Chemistry 28(1936): 988-994.

[100] A.B.D. Cassie, S. Baxter. Wettability of porous surfaces. Transactions of the Faraday Society 40(1944): 546-551.

[101] A. Ulman, An introduction to ultrathin organic films: from Langmuir-Blodgett to Self-Assembly, Academic Press, Inc, Boston, 1991.

[102] D.L. Elbert, J.A. Hubbell. Surface treatments of polymers for biocompatibility. Annual Review of Materials Research 26(1996): 365-394.

[103] C. M. Chan, T. M. Ko, H. Hiraoka. Polymer surface modification by plasmas and photons. Surface Science Reports 24(1-2) (1996): 3-54.

[104] M. Ozdemir, C. U. Yurteri, H. Sadikoglu. Physical polymer surface modification methods and applications in food packaging polymers. Critical Reviews in Food Science and Nutrition 39(5) (1999): 457-477.

[105] K. S. Siow, L. Britcher, S. Kumar, H. J. Griesser. Plasma methods for the generation of chemically reactive surfaces for biomolecule immobilization and cell colonization-a review. Plasma Processes and Polymers 3(6-7) (2007): 392-418.

[106] S. Farris, S. Pozzoli, P. Biagioni, L. Duo, S. Mancinelli, L. Piergiovanni. The

fundamentals of flame treatment for the surface activation of polyolefin polymers-a review. *Polymer* 51(16) (2010): 3591-3605.

[107] C. Decker, K. Zahouily. Photodegradation and photooxidation of thermoset and UV-cured acrylate polymers. *Polymer Degradation and Stability* 64(2) (1999): 293-304.

[108] M. Nie, P. Patel, S. Kai, D.D. Meng. Superhydrophilic anti-fog polyester film by oxygen Plasma Treatment. 4th IEEE International Conference on Nano/Micro Engineered and Molecular Systems, Shenzhen, 2009, 1017-1020.

[109] E. B. Nauman. Chemical Reactor Design, Optimization, and Scaleup. McGraw-Hill Professional, 2002.

[110] A. Faghri, Y.W. Zhang. John Howell. Advanced Heat and Mass Transfer. Global Digital Press. 2010.

[111] C. Li, Z. Wang, P.I. Wang, Y. Peles, N. Koratkar and G.P. Peterson. Nanostructured copper interfaces for enhanced boiling. *Small*, 4(8) (2008): 1084-1088.

[112] Y. Im, Y. Joshi, C. Dietz and S. Lee. Enhanced boiling of a dielectric liquid on copper nanowire surfaces. *International Journal of Micro-Nano Scale Transport* 1(1) (2010): 79-96.

[113] R. Chen, M.C. Lu, V. Srinivasan, Z. Wang, H. H. Cho and A. Majumdar. Nanowires for enhanced boiling heat transfer, *Nano Letters*, 9(2) (2009): 548-553.

[114] P. Patel, C. K. Choi and D.D. Meng. Superhydrophilic surfaces for antifogging

and antifouling microfluidic devices. *Journal of Laboratory Automation*, 15(2) (2010): 114-119.

[115] H.W. Coleman, W.G. Steele, *Experimentation, Validation and Uncertainty Analysis for Engineers*, John Wiley & Sons, Inc., 2009.

[116] M. Żenkiewicz. Methods for the calculation of surface free energy of solids. *Journal of Achievements in Materials and Manufacturing Engineering* 24(1) (2007): 137-145.

[117] D.K. Owens, R.C. Wendt. Estimation of the surface free energy of polymers. *Journal of Applied Polymer Science* 13 (1969): 1741-1747

[118] N. Nusselt, Die Oberflächenkondensation des Wasserdampfes. *Zeit. Ver. D. Ing.* 60(1916) 541-569.

[119] B.G. Ganchev, V.M. Koglov, V.V. Lozovetskiy. A study of heat transfer to a falling film at a vertical surface. *Heat transfer-Soviet Research* (4) (1972): 102-110.

[120] G.J. Gambutis. Heat transfer in film heat exchangers. *Proceeding of 14th International Conference of Refrigeration. Moscow* 195 (2)1-7.

[121] H. Takahama, S. Kato. Longitudinal flow characteristics of vertically falling liquid film without concurrent gas flow. *International Journal of Multiphase Flow* 6(20) (1980) 203-215.

[122] T.D. Karapantsios, S.V. Paras, A.J. Karabelas. Statistical characteristics of free falling film at high Reynolds number. *International Journal of Multiphase Flow* 15 (1)

(1989): 1-21.

[123] Z. Jiang, W. Tyan. Experimental studies on surface wave characteristics of free-falling liquid films. Proceeding of 4th International Symposium on Heat Transfer. Beijing High Education Press, 1966, 200-205.

[124] R.H. Qi, L. Lu, H.X. Yang, F. Qin. Influence of plate surface temperature on the wetted area and system performance for falling film liquid desiccant regeneration system. International Journal of Heat and Mass Transfer 64 (2013): 1003-1013.

[125] L.A. Girifalco, R.J. Good. A theory for the estimation of surface and interfacial energies. I. Derivation and application to interfacial tension. The Journal of Physical Chemistry 61 (1957): 904-909.

[126] C.J. van Oss, M.K. Chaudhury, R.J. Good. Interfacial Lifshitz-van der Waals and polar interactions in macroscopic systems, Chemical Review 88 (1988): 927-940.

[127] Principles of Colloid and Surface Chemistry, Third Edition, Marcel Dekker, Inc. 1997.

[128] Y. Takata, S. Hidaka, M. Masuda and T. Ito. Pool boiling on a superhydrophilic surface. International Journal of Energy Research 27 (2003): 111-119

[129] J.R. Reker, C.A. Plank, E.R. Gerhard. Liquid surface area in wetted-wall column, AIChE Journal 12(5) (1966): 1008-1010.

[130] K. Onda, H. Takeuchi, Y. Kumoto. Mass transfer coefficients between gas and liquid phases in packed columns. Journal of Chemical Engineering of Japan 1(1)

(1968): 56-62.

[131] C.H.E. Nielsen, S. Kiil, H.W. Thomsen, K. Dam-Johansen. Mass transfer in wetted-wall columns: Correlations at high Reynolds numbers. *Chemical Engineering Science* 53 (3) (1998): 495-503.

[132] X. H. Liu, Y. Jiang, X.M. Chang, X.Q. Yi. Experimental investigation of the heat and mass transfer between air and liquid desiccant in a cross-flow regenerator. *Renewable Energy* 32 (10) (2007) 1623-1636.

[133] R.H. Qi. Study on Heat and mass transfer of internally heated liquid desiccant regeneration for solar-assisted air-conditioning system. Phd dissertation. The Hong Kong Polytechnic University, Hong Kong China, 2013.

[134] F. Zhang, Z.B. Zhang, J. Geng. Study on shrinkage characteristics of heated falling liquid films. *AIChE Journal* 51(11) (2005): 2899-2907.

[135] J. Benaman. A systematic approach to uncertainty analysis for a distributed watershed model. PhD dissertation, Cornell University, Ithaca, N.Y. 2002.

[136] Hong Kong Government. Code of practice for overall thermal transfer value in buildings. Hong Kong, 1995.

[137] EMSD. Performance-based Building Energy Code, 2003 edition. Electrical and Mechanical Services Department, Hong Kong, 2003.